DISSERTATIONES
NEUROSCIENTIAE
UNIVERSITATIS
TARTUENSIS
44

FANGLING XUAN

Regulation of stress response in first episode schizophrenia by monocytes and microglia

DISSERTATIONES NEUROSCIENTIAE UNIVERSITATIS TARTUENSIS
44

DISSERTATIONES NEUROSCIENTIAE UNIVERSITATIS TARTUENSIS
44

FANGLING XUAN

Regulation of stress response in first episode schizophrenia by monocytes and microglia

UNIVERSITY OF TARTU
Press
1632

Department of Physiology, Institute of Biomedicine and Translational Medicine, University of Tartu, Tartu, Estonia.

The dissertation was accepted for the commencement of the degree of Doctor of Philosophy in Neurosciences on March 6th, 2024 by the council for the Curriculum of Neurosciences.

Supervisors: Li Tian, PhD, Research Professor,
Department of Physiology, Institute of Biomedicine and Translational Medicine, University of Tartu, Estonia

Claudio Rivera Baeza, PhD, Professor,
Helsinki In Vivo Animal Imaging Platform, University of Helsinki, Finland

Eero Vasar, MD, PhD, Professor,
Department of Physiology, Institute of Biomedicine and Translational Medicine, University of Tartu, Estonia

Kersti Lilleväli, PhD, Associate Professor,
Department of Physiology, Institute of Biomedicine and Translational Medicine, University of Tartu, Estonia

Reviewers: Kalle Kilk, MD, PhD, Associate Professor,
Department of Medical Biochemistry, Institute of Biomedicine and Translational Medicine, University of Tartu, Estonia

Liina Haring, MD, PhD, Associate Professor,
Department of Psychiatry, Institute of Clinical Medicine,
University of Tartu, Estonia

Opponent: Pentti Tienari, MD, PhD, Professor,
Translational Immunology Research Program and Department of Neurosciences, Clinicum, Faculty of Medicine, University of Helsinki, Finland

Commencement: May 17th, 2024

This study was supported by the Mobilitas Pluss top researcher grant No. MOBTT77 by the European Union through the European Regional Development Fund, the personal research grant No. PRG878 from the Estonian Research Council, and National Natural Science Foundation of China (grant Nos.: 81761128021, 81771452, 82001415, and 82171507).

ISSN 1736-2792 (print)
ISBN 978-9916-27-490-3 (print)
ISSN 2806-2418 (pdf)
ISBN 978-9916-27-491-0 (pdf)

University of Tartu Press
www.tyk.ee

TABLE OF CONTENTS

LIST OF ORIGINAL PUBLICATIONS

The thesis is based on the following original papers, referred to in the text by Roman numerals I–III.

I. Chen S, Fan F, Xuan FL, Yan L, Xiu M, Fan H, Cui Y, Zhang P, Yu T, Yang F, Tian B, Hong LE, Tan Y, Tian L. Monocytic subsets impact cerebral cortex and cognition: differences between healthy subjects and patients with first-episode schizophrenia. Front Immunol. 2022 Jul 11;13: 900284. Doi: 10.3389/fimmu.2022.900284

II. Yan L*, Xuan FL*, Song C, Gou M, Chen W, Li Y, Wang Z, Wang L, Xie T, Fan F, Zharkovsky A, Tan Y, Tian L, Replenished microglia partially rescue schizophrenia-related stress response. Front. Cell. Neurosci. 2023 Sep 17; 1662; 5102. Doi: 10.3389/fncel.2023.1254923.

III. Xuan FL, Yan L, Li Y, Fan F, Deng H, Gou M, Chithanathan K, Heinla I, Yuan L, Seppa K, Zharkovsky A, Kalda A, Hong LE, Hu GF, Tan Y, Tian L. Glial receptor PLXNB2 regulates schizophrenia-related stress perception via the amygdala. Front Immunol. 2022 Oct 17;13:1005067. Doi: 10.3389/fimmu.2022.1005067.

Contribution of the author:

I. The author participated in RNA-seq data analysis, figure preparation, and manuscript revision.
II. The author participated in immunohistochemistry data analysis and manuscript writing.
III. The author participated in animal experimental design and performance, including amygdala microinjection and immunohistochemistry, data analysis, and manuscript writing.

* Shared first authorship.

ABBREVIATIONS

ANOVA	Analysis of variance
ANCOVA	Analysis of covariance
AMG	Amygdala
ANG	Angiogenin
BBB	Blood-brain barrier
BDNF	Brain-derived neurotrophic factor
BGI	Beijing Genomics Institute
BM	Bone marrow
BMI	Body mass index
BVMT	Brief Visuospatial Memory Test
CCL2	Chemokine (C-C motif) ligand 2
CCR2	C-C chemokine receptor 2
CD	Cluster of differentiation
CNS	Central nervous system
CR1	Complement receptor 1
CRP	C-reactive protein
CSF1	Colony-stimulating factor 1
CSF1R	Colony-stimulating factor 1 receptor
CSF1Ri	Colony-stimulating factor 1 receptor inhibitor
Ctr	Control
CPZ	Chlorpromazine
CTQ	Childhood Trauma Questionnaire
CUS	Chronic unpredictable stress
CX3CR1	CX3C motif chemokine receptor 1
DAPI	4',6-diamidino-2-phenylindole
DAMPs	Damage-associated molecular patterns
DAVID	Database for Annotation, Visualization and Integrated Discovery
DEGs	Differentially expressed genes
DSM-IV	Diagnostic and Statistical Manual of Mental Disorders Fourth Edition
E	Embryonic day
EMP	Erythron-myeloid progenitor
EPM	Elevated plus maze
FDR	False discovery rate
FES	First episode schizophrenia
FES-hs	High stress group of FES
FES-ls	Low stress group of FES
Fig.	Figure
GFAP	Glial fibrillary acidic protein
GnRH	Gonadotropin-releasing hormone
GO	Gene ontology

GO-BP	Gene ontology biological pathway
HC	Healthy control
HSC	Hematopoietic stem cell
HPC	Hippocampus
IBA1	Ionized calcium-binding adapter molecule 1
ICV	Intracranial volume
IHC	Immunohistochemistry
IL	Interleukin
immdev-DEGs	DEGs involved in immune system development
IRF3	Interferon regulatory factor 3
KEGG	Kyoto Encyclopedia of Genes and Genomes
Log_2FC	Log_2 of fold change
LPS	Lipopolysaccharide
mAb	Monoclonal antibody
MCCB	The MATRICS™ Consensus Cognitive Battery
MHC	Major histocompatibility complex
MRI	Magnetic resonance imaging
MS	Multiple sclerosis
NF-κB	Nuclear factor kappa light chain enhancer of activated B cells
NLRP3	Nucleotide-binding oligomerization domain like receptor pyrin domain-containing 3
NMDA	N-Methyl-D-Aspartate
NPR	Neuropilins
NSAIDs	Non-steroidal anti-inflammatory drugs
OFT	Open field test
OPC	Oligodendrocyte precursor cell
P2RY12	Purinergic Receptor P2Y12
PANSS	Positive and Negative Symptom Scale
PANSS-G	General subdomain of PANSS
PANSS-N	Negative subdomain of PANSS
PANSS-P	Positive subdomain of PANSS
PANSS-T	Total score of PANSS
PBS	Phosphate-buffered saline
PFA	Paraformaldehyde
PFC	Prefrontal cortex
PLXN	Plexin
PPI	Protein-protein interaction
PROK2	PROKINETICIN 2
PSS	Perceived Stress Scale
RNA-seq	RNA sequencing
RNASE2	Ribonuclease A family member 2
RSDS	Repeated social defeat stress
S	Supplementary
SCID	Structured clinical interview for DSM-IV

SD	Standard deviation
SEM	Standard error of mean
SEMA	Semaphorin
SYP	Synaptophysin
RepMg	Repopulation of microglia
TCT	Three-chamber test
TGF-β	Transforming growth factor beta
TLR	*toll*-like receptor
TMEM119	Transmembrane protein 119
TST	Tail suspension test
Veh	Vehicle
YS	Yolk sac

1 INTRODUCTION

Schizophrenia, a complex neuropsychiatric disorder, affects almost 1% of the global population with significant social and economic impacts, as patients often suffer from unemployment and homelessness. However, pathobiological mechanism of this disorder is not fully understood and current antipsychotics are characterized by severe limitations[1]. Thus, schizophrenia researchers have long sought to unveil its enigmatic etiology and pathophysiology.

Schizophrenia is believed to arise from a confluence of various interrelated factors. These factors span across genetic, biological, and environmental domains, creating a diverse landscape of potential triggers and influences. One of the central aspects of pathogenesis of schizophrenia involves dysfunctions in key neurotransmitter systems[1,2] – notably the dopaminergic, glutamatergic, and serotonergic systems, each playing a distinct yet interconnected role in the development of the disorder. Hence, current treatments for schizophrenia are based on the interaction between antipsychotics and various neurotransmitter receptors, which however are inefficient for up to 25% of patients and mainly target positive symptoms[2].

Among miscellaneous environmental risk factors that interact with genetic risks to shape schizophrenia, emerging evidence suggests the importance of stress[3,4] and inflammation[5] in its onset and progression. Abnormity of the immune system has been frequently found in schizophrenia patients[6,7], suggesting a deeper interrelationship between immune response and schizophrenia. Therefore, novel potential treatment targets including microglia were recently suggested for ameliorating cognitive impairments in schizophrenia[1,8].

This interrelationship is further illustrated by examining the roles of monocytes and microglia in the brain. Monocytes, as the major circulating myeloid immune cells, and microglia, as the major resident myeloid immune cells of the central nervous system, participate in not only immune defense but more importantly also modulation of developmental processes and homeostatic functions of the brain[9,10,11]. Accumulating evidence demonstrates that monocytes and microglia are key mediators of stress-induced neuroinflammatory processes in neuropsychiatric disorders[9,12]. However, how they regulate stress response in schizophrenia patients is still unclear.

Thus, this study aims to investigate molecular mechanisms mediated by monocytes and microglia in neuroinflammatory processes in the context of stress by studying first episode schizophrenia patients and animal stress models. Furthermore, our efforts are focused on identifying molecules specific to monocytic and microglial subtypes that may serve as novel candidates for the development of diagnostic biomarkers and therapeutic drugs for schizophrenia.

2 REVIEW OF LITERATURE

2.1 Clinical manifestation of schizophrenia

Schizophrenia is a neurodevelopmental disorder resulted from complex interactions between genetic predisposition and environmental risk factors[3–5]. Clinicians have recognized sets of clinical features constituting the disorder, covering positive, negative, and cognitive symptoms. Positive symptoms are presented as hallucinations, delusions, and disorganized thoughts and speech; negative symptoms include avolition, flat affect, anhedonia, and social withdrawal; and cognitive symptoms encompass multiple deficits in working memory, executive function, and processing speed[1]. While positive symptoms represent a characteristic feature of schizophrenia, negative and cognitive symptoms contribute substantially to long-term burden to persons with this disorder[1,13].

Individuals with schizophrenia consistently display alteration in brain structures, such as the lateral ventricular enlargement and brain volume reduction[13,14]. Magnetic resonance imaging (MRI) done by us and others has shown atrophy in specific brain regions including cortical, subcortical, and limbic structures, particularly dystrophy in the medial temporal limbic structures (e.g., the amygdala (AMG), caudate nucleus, hippocampus (HPC), and thalamus) and the white matter in schizophrenia patients[14–17]. Utilizing resting-state or task-performing functional MRI, numerous studies have noted altered connectivity between cortical and subcortical regions in schizophrenia, such as between the thalamus and the prefrontal cortex (PFC) or between the posterior cingulate cortex and the cerebellum, has been frequently found in patients with schizophrenia[18].

According to the latest multi-hit synaptic hypothesis, loss of synapses induced by stress and immune activation during neurodevelopment disrupts the balance of excitatory-inhibitory neurotransmission in pyramidal neurons in the frontal cerebral cortex, which contributes to negative and cognitive symptoms, whilst synaptic loss of interneurons disinhibits dopaminergic projection to subcortical mesostriatal regions, which contributes to psychotic symptoms[4].

2.2 Stress and schizophrenia

2.2.1 Psychosocial stress as a risk factor for schizophrenia

Stress has been a long-known environmental risk factor linked to the etiology of schizophrenia[4,5]. Childhood trauma, social isolation, low economic status, and urbanicity can trigger maladaptive stress response and lead to persistent stress sensitization in individuals with genetic susceptibility of psychiatric disorders[19]. In the brain neural circuits, stress can induce activation and epileptic-like brain synchronization of the mesolimbic and mesocortical systems, which affect consciousness and emotional arousal via altering dopaminergic and glutamatergic

neurotransmissions in schizophrenia[20,21]. We have also demonstrated that structural changes in the whiter matter and cerebral ventricles were associated with maladaptation of stress responses in patients with schizophrenia[22].

The dopamine hypothesis is the longest standing patho-etiologic theory on neurobiological mechanisms of schizophrenia[4]. Animal studies consistently show that stressors (psychosocial and physical) lead to dopamine release and behavioral deficits in animals[23]. In the stress-processing circuit, the basolateral AMG and the HPC mediate dopamine-dependent stress exaggeration and withdrawal response in opposite modes, respectively[24].

The glutamatergic theory of schizophrenia is formulated based on the detrimental effects of phencyclidine and ketamine, agents blocking the N-Methyl-D-Aspartate (NMDA) glutamate receptor[25] and hence exacerbating cognitive deficits in patients with schizophrenia[26,27]. Besides, elevated glutamate level in the anterior cingulate cortex in association with treatment resistance to antipsychotics is the most consistent neurochemical finding in patients of schizophrenia[28]. Regulation of stress response through the glutamatergic system was reported in schizophrenia[29], which is corroborated by animal studies on stress-induced psychiatric-like behaviors[30–32].

2.2.2 Chronic unpredictable stress (CUS) animal model

Chronic unpredictable stress (CUS) is currently one of the most commonly used and effective animal models to study psychiatric-like behaviors such as anxiety and anhedonia in rodents[33,34]. The model was firstly created by Katz et al. in 1980s[35] and has been modified with a variety of mild and unpredictable stressors by different laboratories and studies[34,36].

Animals can show behavioral phenotypes recapitulating schizophrenic symptoms[37]. For examples, positive symptoms and impaired sensory-motor gating in human patients can be translated into hyper-locomotion, anxiety, and reduced pre-pulse inhibition in rodents, while negative symptoms into anhedonia, learned hopelessness, and social behavioral withdrawal. Chronic stress such as CUS induces and exacerbates anxiety, depressive-like and schizophrenic-like behaviors, as well as cognitive impairments via remodeling of the limbic structures critical for these behaviors[38–40].

CUS-induced psychiatric-like behaviors are mediated by multiple neurobiological processes including, but not limited to, disturbances in mono-aminergic neurotransmission[41], glucocorticoid receptor activity[42,43] and brain-derived neurotrophic factor (BDNF)-mediated neurogenesis[44,45] and synaptic plasticity[46] in the limbic system.

Neuroinflammation mediated by glial cells, especially microglia, is also involved in regulating stress responses. For example, activation of the purinergic receptor P2X7 and nucleotide-binding oligomerization domain like receptor pyrin domain-containing 3 (NLRP3) inflammasome mediated CUS-induced depressive-like behaviors[47]. For more information, see also **section 2.4.2**.

2.3 Monocytes and microglia

2.3.1 Monocytes and monocytic signature genes

Monocytes belong to mononuclear phagocytes, a family of myeloid cells that comprise also dendritic cells and macrophages. Monocytes derive from hematopoietic precursors in the bone marrow and enter the blood circulation, constituting ~10% of total blood leukocytes in human beings and 2–4% in mice Monocytes have a very short lifespan with an average half-life of 3 days in human beings and 17 hours in mice. Via the blood circulation, monocytes are recruited into tissues throughout the body, where they differentiate into, and function as, macrophages[48].

Circulating human monocytes are a notably heterogeneous population, which is reflected for example by the relative expression levels of cluster of differentiation (CD) 14 and the low-affinity Fcγ-III receptor (CD16), which namely divide monocytes into classical ($CD14^{++}CD16^{-}$), intermediate ($CD14^{++}CD16^{+}$) and nonclassical ($CD14^{+}CD16^{++}$) subsets (**Fig. 1**). Classical, intermediate, and nonclassical monocytes account for ~85%, 5%, and 10% of circulating monocytes, respectively[49,50]. In humans, classical monocytes have a half-life of ~1.6 days, while intermediate and nonclassical monocytes have longer circulating lifespans (~4 and ~7 days, respectively)[48,51]. Each of these subsets is regarded as phenotypically distinct, carrying different signature genes. Classical monocytes express *CD14, CX3CR1, CCR2, CD163, SELL, S100A8, A9* and *A12*; intermediate monocytes exhibit *LHA, EGR1 and EGR2*; and nonclassical monocytes display *FCGR3A (CD16), CDKN1C, TCF7L2, C1A, QB, QC, IFITM1, IFITM2* and *ITGAL*[50,52].

In mice, classical monocytes show high Ly6C expression and low CD43 ($Ly6C^{++}CD43^{+}$), intermediate monocytes are high in both Ly6C and CD43 ($Ly6C^{++}CD43^{++}$), whilst nonclassical monocytes show low Ly6C and high CD43 ($Ly6C^{+}CD43^{++}$)[49]. The half-lives of classical and non-classical monocytes in mice are estimated to be ~20 hours and ~2.2 days, respectively[48].

Monocytic subsets play nonoverlapping roles in a myriad of chronic inflammatory and autoimmune conditions including neurological diseases[52–54]. Classical monocytes have the highest phagocytic capacity and a predominant antimicrobial function[50]. By contrast, nonclassical monocytes are generally viewed as anti-inflammatory and patrol along the vasculature, thereby playing a critical role in maintaining vascular homeostasis[54]. Nevertheless, as a highly complex functional subset, nonclassical monocytes can also be pro-inflammatory and sensitive to immune senescence after being stimulated[55]. Intermediate monocytes presumably represent a transitional stage between the classical and nonclassical monocytes, sharing some phenotypic and functional characteristics of both subsets[49], and are involved in antigen presentation to induce T-cell proliferation in infectious[50,56] and inflammatory conditions[57,58].

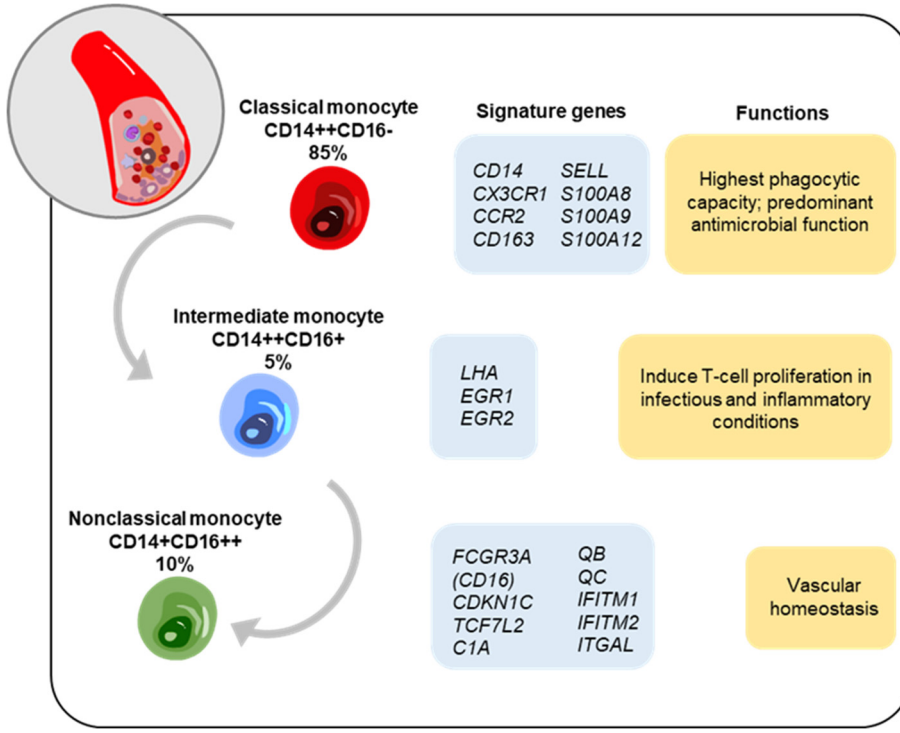

Fig. 1. Signature genes and functions of human monocytic subsets. Monocytes originate from hematopoietic stem cells within the bone marrow and subsequently enter the bloodstream. Based on the expressions of CD14 and CD16, human monocytes are divided into classical ($CD14^{++}CD16^{-}$), intermediate ($CD14^{++}CD16^{+}$) and nonclassical ($CD14^{+}CD16^{++}$) subsets. Both intermediate and non-classical monocytes putatively develop from the established reservoir of classical monocytes[49,50]. CD: cluster of differentiation.

2.3.2 Microglia and microglial signature genes

Microglia are the major myeloid immune cells residing in the central nervous system (CNS). Adult microglia are long living and self-renew themselves[59]. The complex microenvironment of the CNS, which is built up by miscellaneous cell types with neuronal connections projecting across various regions, shapes microglial characteristics *in situ*[59,60].

A precise distinction of specific phenotypes is nowadays essential to study microglial functions and tissue state in a quickly changing brain microenvironment[60]. Choosing appropriate microglial markers is a scientific challenge, however. In mice, similar to most tissue macrophages, microglia express colony stimulating factor 1 receptor (CSF1R, also called CD115), fractalkine receptor or CX3C motif chemokine receptor 1 (CX3CR1), glycoproteins F4/80 and CD68, and integrin CD11b[61]. Microglia can be distinguished from peripheral macrophages by the purinergic receptor P2ry12 (P2RY12), transmembrane

protein 119 (TMEM119), Hexb, Sall1, and Pu.1 markers[62,63] (**Fig. 2**). Another research depicted temporospatial heterogeneity of mouse and human microglia defining *TMEM119*, *SELPLG* and *SLC2A5* as microglial homeostatic genes postnatally, whereas microglia positively expressing ionized calcium-binding adapter molecule 1 (IBA1) together with apolipoprotein E or cathepsin B existed temporarily in embryonic stage[64]. However, microglia-like cells such as stromal cells in the choroid epiplexus or monocyte-derived macrophages in the cerebral ventricles were found to also express microglial signature genes such as *P2ry12* and *Slc2a5*[65].

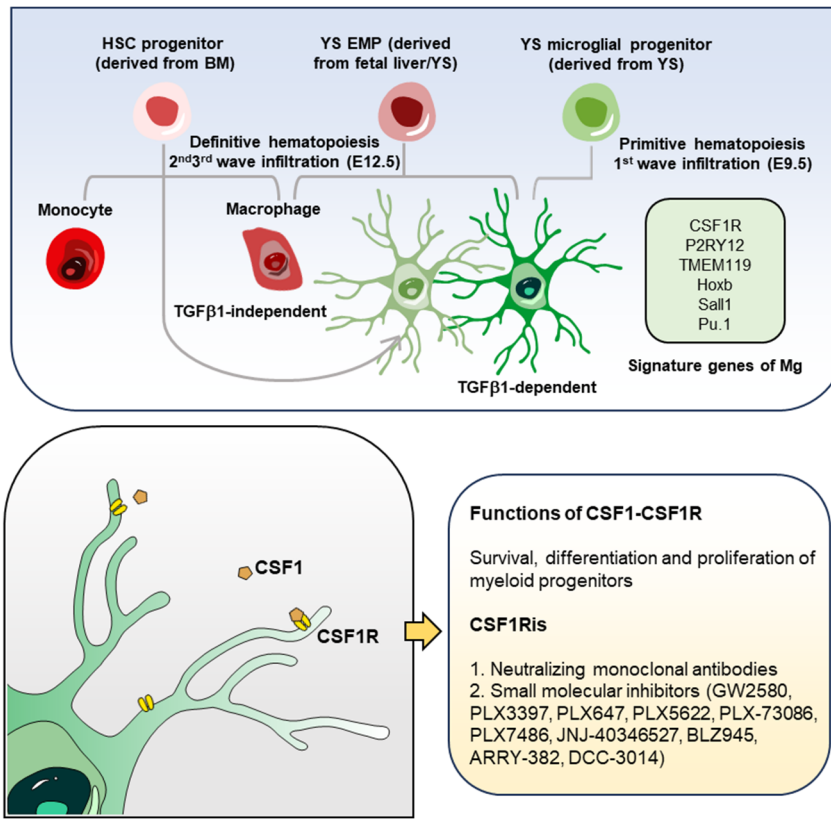

Fig. 2. Microglial origin, signature genes, and the CSF1R receptor. Microglia are derived from primitive hematopoiesis in the yolk sac at embryonic day E7.5 – E8.5 in mice[59,66]. Microglial progenitors comprise the first wave of infiltration to the embryonic brain at E9.5[66,67]. The second and third waves of infiltration occur at around E12.5, by microglia derived from erythron-myeloid progenitors in the YS or fetal liver and hemato-poietic stem cells from the bone marrow[68–70]. Microglia maturation is dependent on TGF-β1 signaling[71]. Microglia can be distinguished from brain macrophages, a heterogenous myeloid populations derived from putatively the same cell lineage as microglia, by expressions of P2RY12, TMEM119, Hoxb, Sall1 and Pu.1[62,63]. CSF1R regulates multiple processes of microglial development[72,73]. BM: bone marrow; E: embryonic day; EMP: erythron-myeloid progenitor; HSC: hematopoietic stem cell; Mg: microglia; YS: yolk sac.

2.3.3 Development of microglia in mice

Microglia are derived from yolk sac primitive macrophages and erythromyeloid progenitors (EMPs) at around embryonic day (E) 7.5 – E8.5 during primitive hematopoiesis in mice and enter the primitive blood vessels to colonize the neuroepithelium at around E9.5[59,66] (**Fig. 2**). Hence, the appearance of microglia in the murine embryonic brain occurs during E9.5 – E14.5 before the formation of the blood-brain barrier (BBB)[66,67]. Putatively, a second or even third wave of entry of peripheral microglial progenitors, derived from definitive hematopoiesis in the fetal liver, has been demonstrated, such as microglia expressing Hoxb8, a known important transcription factor for microglial development, which invade the murine brain by E12.5[68–70]. Unlike macrophages, microglial maturation in the brain is dependent on the transforming growth factor beta 1 (TGF-β1) signaling[71].

Compared to the adult murine brain, the embryonic brain hosts microglia unevenly and some microglia are located adjacent to hotspots such as the newly formed blood vessels[74,75], developing axons[74,76], and apoptotic neurons[77–79]. In these hotspots of the developing brain and later in the entire mature brain, microglia act as a regulator of brain development by controlling neurogenesis and gliogenesis, neuronal migration, angiogenesis, axonal outgrowth or fasciculation, axonal myelination, phagocytosis of neural progenitor cells or apoptotic neurons and clearance of their debris, as well as synaptic formation and pruning[11,68,80].

2.3.4 Microglial CSF1R and CSF1R inhibitor (CSF1Ri)

CSF1R is a 972-amino acid protein encoded on the long arm of chromosome 5 (5q32) and belongs to the class III family of receptor tyrosine kinases. It is activated by two ligands, CSF1 and interleukin (IL)-34[81]. In the brain CSF1R is restricted to microglia and perivascular macrophages at all developmental stages[81], whereas CSF1 and IL-34 are expressed by astrocytes and neurons, respectively[82].

CSF-1/CSF-1R signaling promotes survival of myeloid progenitors and their differentiation into monocytes, macrophages, dendritic cells, and osteoclasts, as well as microglia[72,73]. In humans, haploinsufficiency of *CSF1R* causes agenesis of microglia and the corpus callosum, among other maldevelopments in the brain, as well as maldevelopment of the bone[83] (**Fig. 2**).

CSF1R inhibitors (CSF1Ri) include two classes, neutralizing monoclonal antibodies (mAbs), which block the binding of CSF1 to CSF1R, and small molecular inhibitors, which target the cytosolic kinase domain of CSF1R, such as GW2580, PLX3397, PLX647, PLX5622, PLX-73086, PLX7486, JNJ-40346527, BLZ945, ARRY-382, DCC-3014[84,85]. These CSF1Ris have been used to treat cancers[84,86]. Among the small molecular inhibitors, PLX3397 and PLX5622 have been extensively utilized as they lead to >95 % elimination of microglia within 7–21 days, followed by a rapid microglial replenishment upon drug withdrawal[87]. Numerous studies have characterized CSF1Ris in modulation of animal behaviors. For details, see also **section 2.4.3**.

2.3.5 Plexins (PLXNs) and their ligands semaphorins (SEMAs)

Plexins (PLXNs) are a family of cell adhesion receptors with multiple important functions by binding to their ligands semaphorins (SEMAs)[88]. There are four subfamilies of vertebrate PLXNs and nine SEMAs in total: PLXN-A1 – A4, -B1 – B3, -C1, and -D[89]. In the CNS, PLXNs together with SEMAs and their coreceptors neuropilins (NPRs) regulate cell proliferation, migration, and differentiation, as well as axonal outgrowth and myelination during embryogenesis[88] (**Fig. 3**). For more information, see also **section 2.4.4**.

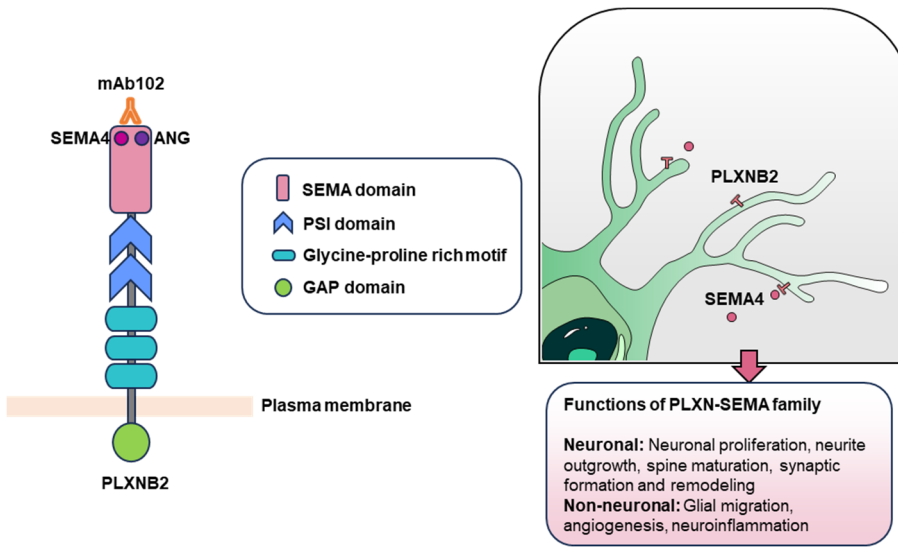

Fig. 3. Structure and ligands of PLXNB2. PLXNs are single-pass transmembrane receptors distinguished by the presence of a split cytoplasmic GAP domain that binds small GTPases. The extracellular domains of all plexins contain a SEMA domain, PSI motifs, and immunoglobulin-plexin-transcription glycine–proline (G–P)-rich motifs, which the Plxns share with the tyrosine kinase receptors[88,89]. Of the PLXNB family, PLXNB2 can be blocked by an mAb102, preventing its binding by the ligands SEMA4A, -4B and ANG[90]. PLXNBs are engaged in multiple processes of brain development[88] and also expressed by immune cells including microglia[91]. ANG: angiogenin; mAb102: monoclonal antibody 102; GAP: GTPase-activating protein; G-P: glycine–proline; PLXN: plexin; PSI: PLXN-SEMA-integrin; SEMA: semaphorin.

Neurodevelopmental processes mediated by PLXNs and their ligands include neuronal migration and lamination during corticogenesis[92,93], migration of glia such as the oligodendrocyte precursor cell (OPC)[94,95], neuronal proliferation[96–99], neurite outgrowth[100], spine and synaptic formation[101–104], synaptic remodeling[104–106], as well as angiogenesis[107].

Roles of PLXNs and SEMAs in the immune system have also been discovered[91]. For instances, PLXNA4 dampened anti-inflammatory polarization and lipid metabolism in macrophages[108]. PLXNB2 regulated inflammatory pain[109], guided T cell recruitment in the spleen[110], promoted inflammatory response in keratinocytes and participated in pathogenesis of psoriasis[111], and enhanced natural killer cell functions in patients with chronic hepatitis type C[112]. PLXNB2 also reduced the progression of leukemia[90]. Besides, PLXNB2 promoted angiogenesis via angiogenin (Ang)[90], a process that immune cells closely monitor as well[113]. Furthermore, SEMA7A and its receptors (PLXNC1 and beta-1 integrin) contributed to TGF-β1-induced pulmonary fibrosis[114]. PLXND1-SEMA3E was involved in migration of thymocytes[115].

2.4 Mechanisms of microglia and microglia-like cells in regulating stress response and schizophrenia

2.4.1 Monocytes and microglia in schizophrenia

Increasing evidence suggests immunological and inflammatory dysfunctions play an important role in schizophrenia[6,7,116,117]. For instances, a hypothesis on dormant viral infection as a risk for schizophrenia has been persisted for decades and is supported by epidemiological evidence on perinatal immune activation models[118,119]. On average about 30% of patients with schizophrenia show dysregulated peripheral biomarkers of inflammation, which are associated with the severity of some psychotic or cognitive symptoms[120–123]. Numerous inflammatory biomarkers such as C-reactive protein (CRP) and IL-6 are altered in the peripheral blood of patients with schizophrenia[124]. Immune genes are also shown to be changed with expressions in the peripheral blood or the postmortem brains of individuals with schizophrenia[125–127], such as *IFITM*s[126,128–131], *S100A8/S100A9/S100A12*[126,132,133], and various cytokines, etc.[134,135].

Various studies have demonstrated changes in blood monocytes from patients with schizophrenia, including increased monocytic numbers[136–139] and enhanced release of proinflammatory factors from monocytes[140–143]. Lowered expression of the monocytic receptor *CSF1R* was also observed in the corpus callosum of individuals with schizophrenia[144]. By contrast, expressions of *toll*-like receptor (TLR) 3 and TLR4, which are pattern recognition receptors for damage-associated molecular patterns (DAMPs) and mediate activation of monocytes[145], were significantly upregulated in patients with schizophrenia[146,147]. A recent study analyzed monocytic genes in schizophrenia and found their involvement in pathways mediated by the nuclear factor kappa light chain enhancer of activated B cells (NF-κB), lipopolysaccharide (LPS), and glucocorticoid receptor[143]. Notably, monocytic count can be considered as an indirect marker of microglial activation in schizophrenia[137] (**Fig. 4**).

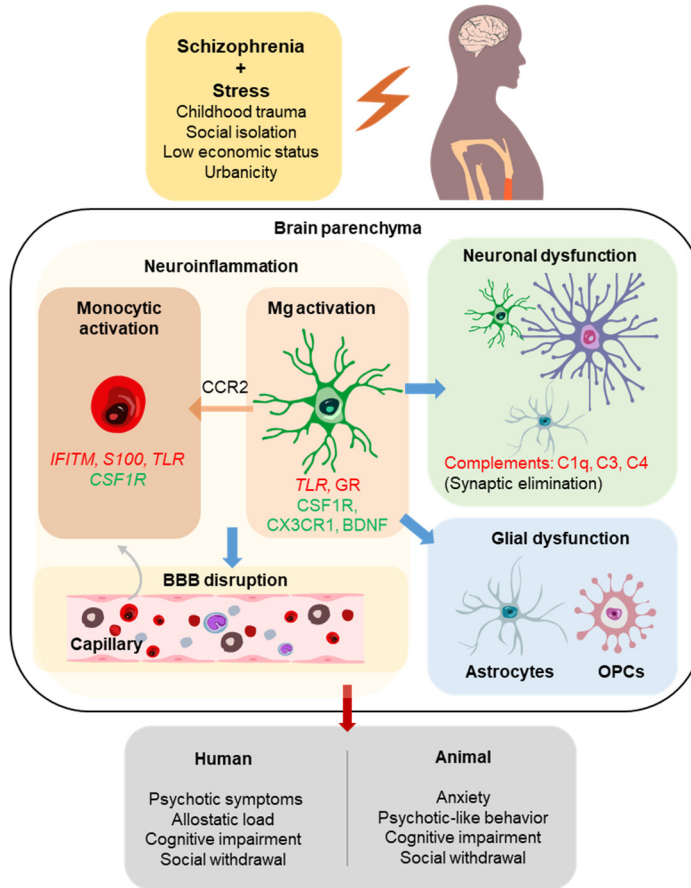

Fig. 4. Mechanisms underlying stress-induced activation of monocytes/microglia in schizophrenia. In schizophrenia patients, monocyte/microglia activation, represented by alteration of expressions of specific inflammatory genes, could trigger BBB disruption and neuroinflammation[6,7,116,117]. Microglial activation could also induce monocytic recruitment through CCR2[148]. In turn, microglial activation could directly affect neuronal development such as synaptic formation and development of astrocytes and OPCs, therefore inducing synaptic elimination and hypomyelination in schizophrenia[149–151]. Stress exaggerates monocyte- and microglia-induced neuroinflammation and results in enhanced anxiety, depressive- and schizophrenic-like behaviors in animals[152]. BBB: blood-brain barrier; Mg: microglia; OPC: oligodendrocyte.

Microglia[153] and the related synaptic disconnection[154] hypotheses of schizophrenia were dated back to as early as 1990s. As microglia are pivotal in regulating brain development, a unified gliocentric model of schizophrenia has been proposed[149,150], e.g., an untimely activation of microglia during fetal development suppresses the differentiation of glial progenitor cells, resulting in delayed maturation and abnormal functions of oligodendrocytes and astrocytes. As such,

hypomyelination and compromised integrity of the white matter, as well as reduced synaptic coverage and abnormal buffering of glutamate and potassium may occur in schizophrenia (**Fig. 4**).

Clinical research has observed elevated microglial markers, such as the major histocompatibility complex (MHC) class II and CD68 and increased microglial number along with infiltrated monocytes in the postmortem brains of patients with schizophrenia[155–158]. Microglial polygenic score was associated with cognitive performance in a manner comparable to the neuronal polygenic score for schizophrenia[159]. Morphological changes of microglia in patients with schizophrenia were also reported, accompanied by release of cytokines and free radicals[155,160]. Some, but not all, positron emission tomography studies have confirmed *in vivo* microglial activation in schizophrenia patients as well[161–164].

Anomalous microglial activity during neurodevelopment may result in excessive synaptic elimination or pruning during adolescence and early adulthood in association with schizophrenia[149,150]. For instances, microglial depletion induced significant reduction in hippocampal spine density and glutamatergic activity, which recovered after microglial repopulation[165]. Particularly, the classical complement (C) activation pathway, e.g., the C1q-triggerred accumulation of the C3, which is recognized by the microglial C3 receptor – the integrin CD11b, has been found to contribute to schizophrenia[166]. The C4 component was overexpressed in the cerebral cortex and the associative striatum of patients with schizophrenia[167,168]. Overexpression of the *C4A* promoted excessive synaptic loss[169,170] and led to behavioral changes in mice[170]. Moreover, astrocyte-derived signaling was found to be important in regulating the human neural C4 expression[169]. Besides, KCNH2-3.1, an isoform of the KCNH2 potassium channel, mediated aberrant complement activation and impaired hippocampal-medial prefrontal circuitry associated with working memory deficits[171].

2.4.2 Stress and microglia/monocytes-mediated neuroinflammation

Psychosocial stressors have been profoundly demonstrated to cause the onset and development of psychiatric disorders while inducing inflammation in humans[172,173] (**Fig. 4**). In humans, for instances, acute stress increased monocytic level and modulated expression of monocytic receptors (CSF1R and CD29) in healthy subjects[174]. Increased blood IL-6 and blunted glucocorticoid receptor signaling in monocytes were found in chronically stressed caregivers[175]. Norepinephrine induced immediate increases in neutrophils and monocytes, which resembled the effects of psychosocial stress[176,177]. Enhanced perceived stress was also associated with age-related monocyte/macrophage cytokine production in clinically healthy aging adults[178].

Stress-induced priming of monocytes and microglia leads to aberrant peripheral and central inflammation and sensitization of stress responses[152]. In numerous animal stress models, such as prenatal maternal stress, chronic restraint stress, repeated social defeat stress (RSDS), and CUS, stress has been

shown to induce remarkable depressive-like and anxiety behaviors, simultaneously causing monocyte-mediated inflammation. For instances, reduced blood monocytic count was reported in CUS-subjected mice[179] and in male offspring undergoing maternal social stress[180]. Such reduction may be possibly due to the relocation of circulating monocytes into the brain. Indeed, monocytic trafficking from the spleen to the brain contributed to vulnerability and re-establishment of anxiety in stress-sensitized mice[181–183], and knockout of the microRNA106b~25 cluster in monocytes promoted behavioral resilience to RSDS[183]. The monocyte chemotactic protein-1 was also regarded as a marker of prolonged psychosocial stress[184].

Mechanistically, RSDS-induced behavioral changes were caused by impairment of the BBB due to for example a reduced expression of the tight junction protein – claudin-5, thereby leading to an IL-6 leakage into the brain[152]. IL-6 induced by RSDS promoted a unique transcriptional signature in monocytes that facilitated anxiety, including *Il1 , Cd14, Mmp9, Myd88, Ager*, and *Stat3*[12]. Alternatively, RSDS selectively induced microglial expression of chemokine (C-C motif) ligand 2 (CCL2), a monocytic chemoattractant that recruited blood-borne monocytes into the brain[152]. Treatment with C-C chemokine receptor 2 (CCR2) antagonist suppressed recruitment of bone marrow-derived monocytes into the HPC and alleviated depressive-like behaviors induced by stress induced by electric foot shock[148].

Stress induces remarkable microglial activation as well[185]. Mechanisms underlying microglial activation in response to stress involve activations of the hypothalamic-pituitary gland-adrenal gland axis[186] and the sympathetic nervous system[187–189], the BBB disruption[190,191], resulting in cytokine production[185,192] and mitochondrial dysfunction in microglia[192]. Microglial activation induced by stress is typically characterized by morphological hyper-ramification, indicating enhanced surveillance[193,194], and is accompanied by exaggerated immune responses[195,196] and synaptic loss[197]. By contrast, hypo-ramification usually implies surveillant deficits, which was for instances found in aged microglia[198,199] and long-term high fat diet-conditioned mice[200].

In return, dysfunctions of microglia and microglial receptors can exacerbate stress response to accelerate psychiatric-like behaviors, as demonstrated by us and others in several animal stress models[193,201,202]. For instances, microglia recruited IL-1β-producing monocytes causing stress-enhanced anxiety[203]. Early life stress induced impairment in microglial pruning of excitatory synapses and provoked aberrant stress responses in adult mice[204]. Deficiency of the microglial receptor CX3CR1 resulted in resilience to stress-induced depressive-likes behavior[205], impaired cognitive and synaptic functions[206], and alterations in hippocampal gene transcription[207] in mice. Moreover, ablation of *Hoxb8* in microglia also modulated stress-associated behaviors such as severe over-grooming and anxiety in mice[208,209], whereas optogenetic stimulation of *Hoxb8* in microglia in the ventral CA1 region of the HPC induced anxiety and freezing[210].

In CUS models, contribution of heightened microglia-mediated neuroinflammation to anxiety or depression has also been demonstrated[211,212], via for

example microglial fractalkine[213,214], glucocorticoid receptor[215,216], and BDNF[217]. CUS-exposed microglia showed increased phagocytosis of neuronal elements, leading to reduced density of dendritic spines in pyramidal neurons[218]. Furthermore, in our latest study, CSF1R was shown to regulate schizophrenia-related stress response and cerebral vascular association of microglia/macrophages, which was also impacted by CUS[219].

2.4.3 Microglial ablation and replenishment in animal stress models

Microglial ablation and repopulation have been tested in several animal models of neurological diseases, in which repopulated microglia can improve behavioral and neurobiological outcomes[87,220]. For psychiatric disorders, the role of microglial ablation and replenishment has also been pursued, but its beneficial or harmful effect remains complicated. For instances, some studies have demonstrated that microglial elimination does not affect or even alleviates anxiety, depressive behavior, social withdrawal, and memory deficit in animal stress models[203,221–225], Nevertheless, others have observed harmful effect of microglial elimination on psychiatric-like behaviors[226–228], highlighting beneficial functions of microglia.

On the one hand, ablation of microglia by PLX3397 treatment ameliorated depressive-like endophenotypic behaviors in mice subjected to social isolation[229] or deficient for dopamine receptor 3[230]. Enhanced fear acquisition and impaired fear memory extinction in stress-subjected male rats were also prevented by PLX3397[231]. Moreover, PLX3397 attenuated locomotor hyperactivity induced by dizocilpine, an NMDA receptor antagonist used for establishing animal models of schizophrenia[232]. PLX3397 did not affect acute locomotor response to cocaine or cocaine sensitization after repeated dosing in mice, however[233]. Likewise, PLX5622 treatment restored learning and memory[228,234] and ameliorated anxiety and depressive-like behaviors[203,222,223,225] impacted by chronic stressors in mice. Besides, PLX5622 corrected maternal inflammation-induced synaptic dysfunction and autistic-like behaviors[224]. These demonstrate the detrimental role of microglia in psychiatric-like behaviors.

On the other hand, PLX3397 was reported to abrogate antidepressants' effects[235–237] and tolerance to RSDS[238] or CUS[239] after an LPS-induced preconditioning in several animal studies. PLX5622 also failed to rescue sickness behaviors induced by LPS[240] or RSDS[241] and completely abrogated therapeutic effects of electroconvulsive stimulation on depressive-like behaviors and neurogenesis in CUS-subjected mice[242]. Furthermore, PLX5622 treatment at embryonic stage enhanced locomotor hyperactivity and anxiety in juvenile and adult female mice[227]. These highlight the beneficial role of microglia in psychiatric-like behaviors.

The role of microglial replenishment in psychiatric conditions remains more obscure with limited studies[221–223,227]. For instances, mice with repopulated microglia performed similarly to controls in cognitive functions in both sex,

including novel object recognition and spatial memory[221], and microglial replenishment did not influence social interaction and anxiety impacted by RSDS[222,223].

2.4.4 PLXNs-SEMAs in regulation of psychiatric-like behaviors

Numerous studies have shown that PLXNs-SEMAs play an important role in neurological and mental illnesses, such as the Alzheimer's disease[243], autism[244], bipolar disorder[245,246], and schizophrenia[247–251].

In PLXNA family, genetic variations in *PLXNAs* and its ligands *SEMA3A* were linked to autism[244] and *PLXNA2* was a candidate gene for anxiety[252] and schizophrenia[248,251] in human subjects. *SEMA3D* was identified as a susceptibility gene for schizophrenia[248,249] and elevated level of *SEMA3A* was observed in the postmortem brains of individuals with schizophrenia[247]. In mice, Plxna1 was involved in controlling self-grooming and sensorimotor gating[253]. Behavioral studies with *Plxna2*-deficient mice showed impaired associative learning, sociability, and sensorimotor gating[251]. In PLXNB family, *PLXNB1* mutation induced deficits in neurite outgrowth and functional brain connectivity in pediatric bipolar disorder[245,246]. In mice, Plxnb2 played a crucial role in forming fear memory and its recall[105].

Regarding neuroinflammation-related processes in the CNS, heightened SEMA3A in human microglia initiated harmful inflammatory responses damaging both microglia and neural progenitors[254]. Expressions of SEMA3A, SEMA7A and their receptors in multiple sclerosis (MS) lesions were found, among which SEMA3A and its receptor NPR1 were expressed by reactive astrocytes[255]. Nevertheless, in animals, double knockout of *Sema3f-Npr2* in mice resulted in BBB leakage, neuroinflammation, and microglial activation, along with autistic-like phenotypes[256]. Plxnb2 regulated the development of peripheral somatosensory neurons and their nociceptive function in persistent inflammatory pain in mice[257]. Besides, Plxnb2 was depicted in interactions of microglia with fibroblasts and astrocytes during glial scar formation in response to spinal cord injury[258].

2.5 Anti-inflammatory treatments for schizophrenia

Several anti-inflammatory treatments as a supplementary therapy for schizophrenia have been proposed and tested[259,260]. Primary anti-inflammatory drugs, such as non-steroidal anti-inflammatory drugs (NSAIDs), minocycline, and cytokine mAbs, or drugs with potential anti-inflammatory properties, e.g. neurosteroids, N-acetyl cysteine, estrogens, fatty acids, statins, and glitazones (for type 2 diabetes), had small to median therapeutic effects and the trials on schizophrenia showed greater improvement than other psychotic disorders[259]. Particularly, some studies showed promising effects of hormonal therapies,

antioxidants, omega 3 fatty acids, and minocycline on reducing total, positive, and negative symptoms and general functioning in schizophrenia[260].

Appropriate control for microglial activation may also be a promising therapeutic strategy for schizophrenia, for instances by minocycline[261,262] and cannabinoid type-2 receptor antagonist[263]. Clozapine, an effective antipsychotic for treatment-resistant schizophrenia, might exhibit anti-inflammatory effects by inhibiting NLRP3 inflammasome under the condition of strong microglial activation[264]. Fingolimod (for MS) ameliorates schizophrenia-like cognitive impairments induced by phencyclidine in male rats by inhibiting microglial activation and IL-6 and IL-1β pro-inflammatory cytokines[265]. Besides these antipsychotic or anti-inflammatory drugs, electroconvulsive shock could also attenuate microgliosis and astrogliosis in the HPC and ameliorated schizophrenia-like behavior in rats[266].

3 AIM OF STUDY

Based on the above demonstrations, the current study aims to explore the complex interplay between stress, immune responses, and schizophrenia, particularly focusing on the correlation of brain structures with the disorder's clinical manifestations and the significant impact of psychosocial stress as a risk factor. Recognizing the pivotal role of monocytes and microglia, including their signature genes, in developmental processes in the context of schizophrenia, the current study concentrates on elucidating the underlying mechanisms mediated by monocytes and microglia as well as their effector molecules in stress response. By studying patients with first episode schizophrenia (FES) and employing CUS and microglial replenishment in animal models, we aim to advance our understanding of schizophrenia and to reveal new diagnostic and therapeutic pathways. More specific objectives were as followings:

1. To understand monocytic subsets and their genes in association with brain structure and cognition in FES patients: the role of peripheral immune components in schizophrenia (paper I).
2. To characterize mechanisms of microglial/immune developmental genes in stress regulation relevant to FES: the role of immune components in the brain in schizophrenia (paper II).
3. To characterize roles of microglial receptor PLXNB2 in stress regulation relevant to FES patients: a specific molecular mechanism underlying microglial activation in schizophrenia (paper III).

4 MATERIALS AND METHODS

4.1 Participants' demographic and clinical measures (papers I, II, III)

The study used a cross-sectional research design. This study complied with the Declaration of Helsinki regarding an investigation in humans, and the study protocol was approved by the Medical Ethical Committee of Beijing Huilongguan Hospital (No.2017-49). All participants gave written informed consent before the initiation of study procedures.

FES patients (n = 128) were enrolled in Beijing Huilongguan Hospital from 2016 to 2018, and the inclusion criteria were: 1) diagnosis of schizophrenia based on the Structured Clinical Interview for the Diagnostic and Statistical Manual, Fourth edition (DSM-IV) Axis I disorders (SCID)[267,268] , which was administered independently by two experienced psychiatrists; 2) Han Chineses and aged 18–55 years old; 3) illness duration ≤ 36 months; 4) education equal or greater than 8 years; 5) right handedness, and physically healthy in the past; 6) un-medicated or < 14 days of antipsychotic medication at the time of blood draw; 7) receiving no immunomodulators, immune-suppressive or anti-inflammatory agents in the past 6 months; 8) no substance and alcohol abuse/dependence. Candidates who unmet recruitment criteria were excluded. Additional exclusion criteria included: (1) other psychiatric disorders diagnosed according to the DSM-IV Axis I disorders[267,268]; (2) severe physical illness; (3) recent infection or treatment with physiotherapy or psychotherapy; (4) mental retardation or serious nervous system disease; and (5) lactation or pregnancy. Healthy controls (HCs, n = 111) were recruited from the local community simultaneously. Complete medical histories of HCs were collected, and physical examinations were conducted for all participants to identify those with chronic medical or psychiatric conditions. Potential control participants who had previously been diagnosed with an Axis I psychiatric disorder based on SCID criteria or had experienced substance abuse or dependence within the previous six months, and those who had a history of autoimmune disorders or other significant medical conditions or received anti-inflammatory medications were excluded. The other general criteria were the same as for FES patients.

The MATRICS™ consensus cognitive battery (MCCB) test was applied to assess the cognitive functioning for the subjects. It consists of ten tests encompassing seven cognitive domains, and domain scores as well as a composite score were computed using the MCCB scoring program. The clinical validity and reliability of Chinese version of MCCB had been previously established in both healthy volunteers and schizophrenia patients[269,270]

Past traumatic experiences were evaluated by Childhood Trauma Questionnaire (CTQ, short form) constituting retrospectively measured 28 items encompassing five factors: physical abuse, emotional abuse, sexual abuse, physical neglect, and emotional neglect[271,272]. Participants' stress levels were evaluated

based on Perceived Stress Scale (PSS) constituting 14 items measuring feelings and thoughts during the past month[273,274]. Positive and negative syndrome scale scores (PANSS)[275] consisting of positive (PANSS-P), negative (PANSS-N), and general (PANSS-G) subdomains and total scores (PANSS-T) were measured independently by two psychiatrists.

In paper II, FES patients (n = 74) and age- and sex-matched HCs (n = 68) were recruited.

In paper III, FES patients (n = 101) and age- and sex-matched HCs (n = 49) were recruited. Based on mean value of PSS score, patients were divided into two groups: high stress (FES-hs, PSS ≥ 24) and low stress (FES-ls, PSS < 24).

4.2 Human brain magnetic resonance imaging (MRI) (papers I, II, III)

Brain structural MRI data were acquired using a Siemens Prisma 3.0T MRI scanner with a 64-channel head coil, located at the Beijing Huilongguan Hospital Magnetic Resonance Scanner Center. Foam pads were used to minimize head motions. Sagittal three-dimensional magnetization prepared rapid acquisition gradient echo (MPRAGE) was used to collect each participant's anatomical data: repetition time (TR)/echo time (TE)/inversion time (TI)=2530/2.98/1100 ms, flip angle (FA)=7º, field of view (FOV)=256 × 224 mm^2, Pixel/gap size=1/0 mm, matrix size=256 × 224 bit. After scanning, two radiologists evaluated image quality and if there were significant artefacts, images were recollected. After imputing corresponding internal anatomical instructions, 70 Desikan-Killiany atlas-based cortical and subcortical regions were extracted and data were processed with FreeSurfer software (http://surfer.nmr.mgh.harvard.edu)[276] following the ENIGMA pipeline, e.g., region-by-region visual checking and removal of incorrect values for brain segmentations (http://enigma.usc.edu/protocols/imaging-protocols). Bi-hemispheric regional areas and thicknesses were measured, and regional and intracranial volumes (ICV, mm^3) were calculated.

4.3 Human blood collection and RNA-sequencing (RNA-seq) (papers I, II, III)

Whole blood (5 ml) was collected at 7–9 am after overnight fasting using PAXgene™ blood RNA tubes (Applied Biosystems). Tubes were shaken vigorously for at least 10 seconds after sampling and immediately stored at -80 °C. Total RNAs were extracted using Mag-MAX™ RNA Isolation Kit (Applied Biosystems) by following the manufacturers' instructions. RNAs were quantified and assessed for purity by optical density ratios of 260 nm/280 nm and 260 nm/230 nm using NanoDrop spectrophotometry (ThermoFisher), and samples (1 μg) were immediately shipped on dry ice to the laboratory of the

Beijing Genomics Institute (BGI) for sequencing on the BGIseq-500 platform. Quality controls (QCs) on RNA samples (RIN/RQN ≥ 7.0, 28S/18S ≥ 1.0) were confirmed by BGI, followed by globin mRNA removal and cDNA library construction. Clean data of at least 4 Gb (20 M clean reads) per sample were collected.

After QC of fastq files, an mRNA-seq count table was obtained from bam files. Gene expression analysis was done on the NetworkAnalyst platform using DESeq2[277]. Counts with variance percentile rank < 15 % and counts < 4 were filtered out, data were transformed and normalized to logarithmic values of reads per million values. Logarithmic fold changes (Log_2FC) were calculated for differentially expressed genes (DEGs) between FES patients and HCs, and *p* values were adjusted to Benjamini-Hochberg's false discovery rate (FDR).

DEGs according to the relevant literatures of monocytic transcriptomic profiling[53,278–281] were further selected for subsequent analyses of gene ontology-based biological processes (GO-BP) by the Database for Annotation, Visualization and Integrated Discovery (DAVID), Kyoto Encyclopedia of Genes and Genomes (KEGG), and protein-protein interaction (PPI) in the Search Tool for the Retrieval of Interacting Genes (STRING), respectively, with FDR < 0.05 as the cut-off for significantly enriched gene ontology (GO) terms and KEGG pathways. PPI network was set at a high confidence threshold of 0.7 and clustered with k-means method. Plots of DEGs were made using GraphPad (https://www.graphpad.com/), and online Morpheus (https://software.broadinstitute.org/morpheus).

4.4 Human blood flow cytometry (paper I)

Five ml of fresh heparin lithium-anticoagulated peripheral blood samples were collected from 29 FES patients and 27 HC subjects of the above participants after overnight fast and processed within half an hour for fluorescent staining of cell surface receptors as described previously[147]. The fluorochrome-conjugated antibodies used were 10 µl FITC-labeled mouse anti-human CD14 (Clone M5E2; #555397; BD Biosciences) and 3 µl PerCP-Cy™5.5-labeled mouse anti-human CD16 (Clone B73.1; #565421; BD Biosciences). The percentages of classical ($CD14^{++}CD16^{-}$), intermediate ($CD14^{++}CD16^{+}$) and non-classical ($CD14^{+}CD16^{++}$) subsets among the total monocyte population were determined based on corresponding gatings. Single cells were filtered through cell strainers, carefully suspended, and immediately acquired by a BD FACSCalibur flow cytometer and the analyses were performed with FlowJo V10 software (BD Bioscience, https://www.flowjo.com/).

4.5 Experimental animals (papers II, III)

4.5.1 Mice breeding

Wild-type C57BL/6NTac male mice (3–4-months-old, Taconic) were bred in laboratory animal facility at the Institute of Biomedicine and Translational Medicine, University of Tartu. Mice from different litters were housed in 1264C Euro standard type II cages (Tecniplast) measuring 268 × 215 × 141 mm. Cages containing aspen chips and wools for bedding and nesting were replaced once a week. Each cage contained 9–10 animals based on allocation after weaning. Mice were kept under standard conditions with unlimited access to food and water on a 12/12 hours light/dark cycle (light on 7am – 7pm). All experimental protocols were approved by the Estonian Authorization Committee for Animal Experiments (No. 171 and No. 227), and all experiments were performed in accordance with the European Communities Directive of September 2010 (2010/63/EU).

4.5.2 CUS procedure (papers II, III)

After a week of transfer adaptation, mice were exposed to a variable sequence of 7 mild and unpredictable stressors once per day for 5–8 consecutive weeks[34]. The 7 stressors were: stroboscopic light overnight 1 /s; rat odor and isolation overnight exposure; restraint for 2 hours; wet bedding and cage tilting at 45° overnight; food and water deprivation overnight; flipped light/dark exposure; and forced swimming at 18 °C for 10 minutes. All stressors were randomly scheduled and changed daily to sustain an unpredictable procedure.

In paper II, mice were randomly assigned into 4 groups: Control (Ctr) (n = 9), CUS (n = 9), microglial repopulation after CSF1Ri (repMg) (n = 10), and CUS+repMg (n = 10), and subjected to CUS treatment for 8 consecutive weeks. In paper III, mice were randomly assigned into two groups (Ctr and CUS, n = 7 per group) and subjected to CUS for 5 consecutive weeks.

4.5.3 CSF1Ri PLX3397 treatment procedures (paper II)

PLX3397 (# HY-16749/CS-4256, MedChemExpress) was dissolved at 200 mg/ml in DMSO (D8418, Sigma-Aldrich) solution and an aliquot was freshly diluted with corn oil (# 8267, Sigma-Aldrich) by 1: 6.5 before using. Drug-treated mice were individually fed with vehicle (Veh, 100 µl 15 % DMSO/85 % corn oil + 0.5 g Nutella/mouse/day) or PLX3397 (120 mg/kg bodyweight, e.g., 3 mg/ mouse in Veh) [87] for voluntary ingestion for 7 consecutive days after 5 weeks of CUS, followed by a 2-week recovery.

4.5.4 Intra-amygdaloid stereotaxic microinjection (paper III)

Mice were deeply anesthetized with ketamine/xylazine (10 mg/1.6 mg/ml, 0.1 ml/10 g bodyweight, i.p.), the skulls were measured for amygdaloid

coordinates (from Bregma: AP = -1.5 mm, L = ± 3.0 mm) and drilled open. Then, 0.5 µl saline (n = 10) or 10 ng mAb102 in 0.5 µl saline (n = 10) was injected at each amygdaloid site with microinjection syringes that penetrated the brain at -4.5 mm in depth. After surgery, animals were kept on a heating pad until fully awakened. Two or three animals were group-housed per cage after the operation.

4.6 Behavioral experiments (papers II, III)

4.6.1 Open field test (OFT)

Mice were habituated to ~250 lux room light for 1 hour. Individual mouse was measured for distance and time travelled in different zones of a digital box (44.8 × 44.8 × 45 cm) via a software (Technical & Scientific Equipment GmbH) for 30 minutes. The floor of the box was cleaned with 70 % ethanol and dried thoroughly after each mouse.

4.6.2 Elevated plus maze (EPM)

EPM consisted of open and closed arms (30 × 5 cm each) intersected at a central 5 × 5 cm square platform elevated to a height of 80 cm. Mice were habituated to ~ 40 lux room light for 1 hour. Each mouse was placed on the central platform facing the open arm and recorded for time spent on open/close arms by a software (EthoVision XT, Noduls) for 5 minutes. The arms were cleaned with 70 % ethanol and dried thoroughly after each mouse.

4.6.3 Three-chamber test (TCT)

Mice were habituated to ~ 40 lux room light for 1 hour. A rectangular three-chamber box made from clear Plexiglas was divided into three identical sections, each side one accommodating a lid-covered and wire-structured cup-like container large enough to enclose a single mouse, allowing free exchange of air but not direct physical contacts between mice on both sides. A test mouse was first habituated in the central chamber for 5 minutes, then introduced to a stranger mouse located in a container and left to freely explore the three chambers for the next 10 minutes. All stranger mice were at the same age as test mice and habituated to the apparatus in advance. The box and wire containers were cleaned with 70 % ethanol and dried thoroughly after each test. Social preference was defined as time spent with the stranger mouse and social contacts were counted when the head and front paws of a test mouse were within 3 cm vicinity of the container wall as recorded by a camera (Noldus).

4.6.4 Tail suspension test (TST)

Mice were habituated to ~ 40 lux room light for 1 hour. An animal was hung on a wooden bar at the tip of the tail by adhesive tape and recorded with a camera for 5 minutes. A complete lack of movement or small movements of forefeet and body swinging was counted as immobility, and time (seconds) of immobility was measured.

4.7 Mouse brain MRI (paper III)

Scanning was conducted in the University of Tartu Laboratory Animal Centre with 94/20 Bruker BioSpec small animal MRI. Microinjected mice (n = 4 + 5) were anesthetized with 4 % isoflurane (in medical air at 1.5 l/min). During scanning body temperature and breathing rate were monitored and kept stable (around 36 °C and 80 – 100 bpm) using an animal bed integrated with circulating warm water and inhalation anesthetic of 1.5–2.5 % isoflurane. Thirty-four coronal slices were obtained using a T2-weighted high-resolution sequence with the following scanning parameters: FoV = 20 × 20 mm, TR = 3585 ms, TE = 33 ms, Image size = 250 × 250 pixels, slice distance = 0.25 mm, imaging time = 12 minutes (total time approximately 30 minutes per animal).

The amygdaloid width was measured from the tip of the substantia nigra to the cortical edge at ~140° of angle from the horizontal line on slices of ca. -3 mm – +2.75 mm of the anterior commissure and normalized against the broadest brain width at ca. -2.97 mm of the anterior commissure per animal using ImageJ [282].

4.8 Mouse brain RNA-seq (paper II)

Mice were euthanized with CO_2 and the PFC tissues were dissected and immediately stored at - 80 °C. Total RNAs were extracted (Molecular Research Center), quantified assessed for purity using a spectrophotometry (ThermoFisher), and immediately sent to the Beijing Genomics Institution (BGI) for messenger RNA-seq on the BGIseq-500 platform. RNA-seq data QC, collection, and analysis procedures were performed as already described above.

4.9 Mouse brain flow cytometry (papers II, III)

Mice were sacrificed with CO_2. Tissues were minced and filtered through 70 μm cell strainers (# 352350, BD Biosciences) on ice. Homogenates were blocked in phosphate-buffered saline (PBS) + 10 % rat serum for 1 hour with gentle rotation at 4 °C. Fluorescent antibody markers (0.5 μl/marker, mostly from Biolegend) diluted in 200 μl PBS + 1 % fetal bovine serum were added and

incubated for 1 hour on ice with light protection as previously described [193,283]. In paper II, after surface marker staining, cells were washed by PBS+1 % fetal bovine serum, further fixed by 4 % paraformaldehyde (PFA) and then permeabilized by 0.05 % Triton-X100 in PBS, before being stained with intracellular Vglut2 marker. Samples were washed, resuspended in PBS, and filtered through 35 μm cell strainers into flow tubes (# 08-771-23, BD Biosciences).

In paper II, permeabilized hippocampal cells were stained with 0.5 μl anti-mouse Vglut2-Alexa488 (# MAB5504A4, Millipore), CD11b-BV421 (# 101251, BioLegend), CD45-BV650 (# 103151, BioLegend), Glast-APC (# 130-123-555, Miltenyi), O4-PE (# 130-117-357, Miltenyi) were used. Corresponding isotype control antibodies (all BioLegend) were: rat IgG2a-Alexa488 (# 400525), IgG2b-BV421 (# 400639), IgG2b-BV650 (# 400651), IgG2b-APC (# 400219), and IgM-PE (# 401611).

In paper III, for the CUS experiment, Plxnb2-PE (# 145903), CD11b-BV421 (# 101251), CD45-BV650 (# 103151), and Glast-APC (# 130-123-555) were used. Corresponding isotype control antibodies were: IgG2b-PE (# 400907), IgG2b-BV421 (#4 00639), IgG2a-BV650 (# 400265), and IgG2b-APC (# 400611); for the microinjection experiment, CD11b-FITC (# 101206), CD45-PE/Cy7 (# 103114), Glast-PE (# 130-118-344, Miltenyi), and MHCII-BV711 (# 107643) were used. Corresponding isotype control antibodies were: IgG2b-AlexaFluor488 (# 400625), IgG2b-PE/Cy7 (# 400617), IgG2a-PE (# 400211), and IgG2b-BV711 (# 400653).

Cell acquisition was made with BD LSR FortessaTM (BD Biosciences). Data were analyzed using Kaluza (Beckman Coulter). Astrocytes were defined as $Glast^+$ cells, OPCs as $O4^+$ cells, microglia as $CD45^{low}CD11b^{hi}$ cells. $Vglut2^+$ and $Plxnb2^+$ cells among glial populations were quantified. Cell populations were calculated as % among total brain cells or glial populations as previously described [193,283].

4.10 Immunohistochemistry (IHC, papers II, III)

Mice were anesthetized with intraperitoneal injection of end-dose of ketamine/xylazine mixture and transcardially perfused with PBS and 4 % PFA. Dissected brains were post-fixed in the 4 % PFA at 4 °C for 1 day, dehydrated by 30 % sucrose and stored at -80 °C. The brains were taken to -20 °C 1 day before cryosectioning. Coronal sections of 40 μm-thickness were washed in PBS and permeabilized in 0.5 % Triton-X100.

In paper II, washed brain slices were incubated with primary antibodies including rabbit anti-ionized calcium-binding adapter molecule 1(IBA1) (# SKL6615, Wako, diluted 1:500) and mouse anti-synaptophysin (SYP, sc-17750, Santa Cruz, diluted 1:250) in blocking buffer (10 % goat serum + 1 % BSA + 0.3 M Glycine) overnight at 4 °C, followed by PBS washing and incubation with the secondary antibodies goat anti-rabbit IgG H&L-Alexa568 (# ab175471, Abcam) and goat anti-mouse IgG H&L-PECy7 (# D2110, Sant

Cruz, diluted 1:500) and 0.1 μg/ml 4',6-diamidino-2-phenylindole (DAPI) (# ACRO202710100, VWR) for 2 hours at room temperature. After PBS washing, slices were mounted onto glass slides with Fluoromount™ Aqueous Mounting Medium (# F4680-25ML, Sigma-Aldrich).

In paper III, washed brain slices were incubated with primary antibodies including rabbit anti-IBA1 (# SKL6615, Wako, 1:500) and mouse anti-glial fibrillary acidic protein (GFAP) conjugated with AlexaFluor488 (# 53-9892-82, eBioscience, 1:500) overnight at 4 °C, followed by goat anti-rabbit IgG H&L-AlexaFluor568 antibody (# ab175471, Abcam, 1:500) and 0.1 μg/ml DAPI (# ACRO202710100, VWR) .

A FV1200MPE laser scanning microscope (Olympus) was used to image $IBA1^+$ and $GFAP^+$ cells with 10 × and 60 × objective lenses. In paper II, images of 512 × 512 pixels were taken at 60 × magnification with scanning velocity of 12.5 pixel/μm. Z-stacks (step: 0.5 μm, depth: 30 μm) were taken to analyze morphology of $IBA1^+$ cells and puncta of SYP. In paper III, images of 800 × 800 pixels were taken with a scanning velocity of 8.0 pixel/μm. For quantification of cell number and fluorescent intensity, images were taken with 2-fold zoom-in through a 10 × objective lens.

For cell number and fluorescent intensity, steps of "Image -> Adjust -> Threshold" in ImageJ were used to highlight all cells to be counted. After binary images were obtained, "Analyze particles" of ImageJ was used for counting.

For cell morphology, an "SNT" package in ImageJ was used to reconstruct cells in 3D and "Sholl analysis" was used to acquire the ramification index, while the other parameters were acquired through the "Quick measurements" of SNT, including total branches, average branch length, number and length of primary branches, inner branches, and tips. A total of ~33 microglia and ~12 astrocytes per group were measured.

For SYP^+ puncta in microglia, region of interest defined via cell skeleton were obtained by "Analyze particles" and SYP density was calculated as SYP^+ area (μm^2) per image area ($3.03 \times 103\ \mu m^2$) or per microglial area. 3D images segregating $IBA1^+$ microglia, nuclei, SYP^+ puncta were obtained with "Surface" and "Spots" functions, and videos were created by "Animation" in Bitplane software (Imaris, http://www.bitplane.com/imaris/imaris).

4.11 Data analysis (papers I, II, III)

Statistical procedures were performed with the IBM SPSS Statistics v27.0. Normality of data distribution was checked through Shapiro-Wilk's test.

Demographic and clinical data were compared between groups by Student's t-test, Mann-Whitney U test, or Chi-Square test, where appropriate. Pearson's or Spearman's correlation test was used to determine associations between variables. For analysis of covariance (ANCOVA) and partial correlation analyses, age and sex in papers I-III, body mass index (BMI) in paper II, as well as education years and ICV in paper III were taken as covariates.

In papers I and II, for partial correlations among normalized RNA-seq counts of DEGs, cortical thicknesses or volumes, and cognitive abilities or PSS scores, all coefficients were transformed into Fisher Zr values ($Zr = \ln((1+r) / (1-r)) / 2$), which were then compared between the FES and HC groups by t-test, respectively.

For mediation analyses, the PROCESS v3.3 plugin for SPSS was used, with age, gender, and education years as covariates. In paper I, *Ribonuclease A family member 2* (*RNASE2)* expression level was used as the independent variable, while the Brief Visual-Spatial Memory Test (BVMT) as the dependent variable, and lateral occipital cortex as the mediator. In paper III, AMG volume was used as the independent variable, expression level of *PLXNB2* as the dependent variable, and PSS score as the mediator.

For animal data, two-way analysis of variance (ANOVA) was used to examine interaction between CUS and repMg and their main effects. Tukey's or Bonferroni's correction method was used for post hoc pairwise comparisons and multiparameter comparisons were corrected by FDR. All figures were prepared in GraphPad Prism v8.0.1 and online (http://www.bioinformatics.com.cn/). Data were presented as mean ± standard deviation (SD) or standard error of mean (SEM), and p or FDR < 0.05 was considered statistically significant.

5 RESULTS

5.1 Paper I

5.1.1 Demographic and clinical data on first episode schizophrenia (FES) patients and healthy controls (HCs)

A total of 128 FES patients and 111 healthy subjects were recruited according to the inclusion and exclusion criteria. No differences were observed between the groups for age, sex and smoking status (all $p > 0.05$) (**Table 1**). Average years of education was significantly less in FES patients than that in HCs ($p < 0.01$) (**Table 1**). In the patient group, 18 patients were drug-naïve, and 110 patients had been exposed to antipsychotics for 1 – 14 days (median 4 days) at the time of blood drawing. Most patients took risperidone ($n = 48$), aripiprazole ($n = 16$), risperidone combined with haloperidol injection ($n = 15$), and olanzapine ($n = 14$) (**Table supplementary (S)1** of paper I).

Table 1. Participants' demographic and clinical characteristics.

Characteristics	FES (n=128)	HC (n=111)	Z/X2	*p*
Age (years)	30.64 ± 9.53	32.99 ± 9.57	-1.937	0.053
Males/females	55/73	56/55	1.338	0.247
Education (years)	12.76 ± 3.41	13.79 ± 2.59	-2.612	**0.009****
Smoker/Non-smoker	18/110	23/88	1.854	0.173
Illness duration (months)	12.28 ± 12.25	NA	NA	NA
PANSS total	76.45 ± 12.94	NA	NA	NA
P subscore	22.21 ± 5.10	NA	NA	NA
N subscore	17.41 ± 6.22	NA	NA	NA
G subscore	36.85 ± 7.17	NA	NA	NA

**$p < 0.01$. The bold values indicate statistically significant differences.

5.1.2 Monocytic subset signature genes were differentially expressed in the blood of FES patients

We first studied molecular signatures of circulating leukocytes and identified 9062 DEGs (FDR < 0.05) between FES patients and HCs, including 4479 upregulated and 4583 downregulated genes (**Fig. 5**). To get a better insight into gene expressions among CD14/CD16-subsets of monocytes in schizophrenia, seventy-nine subset-specific signature genes were chosen based on recent monocytic transcriptomic profiling works[53,278–281], among which 54 were found to have FDR < 0.05 in our RNA-seq datasets (**Fig. 5A; Table S2** of paper I). Among the 54 DEGs, four were expressed in all monocytes, nine in classical monocytes, twenty in intermediate monocytes, and twenty-one in nonclassical monocytes (**Table S2** of paper I). Most upregulated DEGs (*LIRPB2, IFITM2, IFITM3, SIRPA, POU2F, HCK*) belong to nonclassical monocytes, while downregulated DEGs (*S100A8, S100A9, SRGN, HLA-DRA, CD86, CCR3*) to classical/intermediate monocytes (**Fig. 5A; Table S2**).

Based on GO-BP terms in DAVID, the most significant and nonoverlapping functional clusters of the 54 DEGs are involved in leukocyte migration, regulation of inflammatory response, myeloid leukocyte activation, innate immune response, and defense response, etc. (**Fig. 5B**). Similarly, KEGG analysis revealed that the most significantly enriched pathways were infectious and autoimmune diseases (**Table S3** of paper I). PPI analysis further revealed a network containing 53 nodes and 75 edges, with enrichment $p < 1.0 \times 10^{-16}$ (**Fig. 5C**). Under the clustering criterium of k-means = 3, the three interconnected clusters include genes such as the S100A family members, the IFITM family members, and the complement receptor 1 (CR1)-integrin (ITG) family members, respectively (**Fig. 5C**).

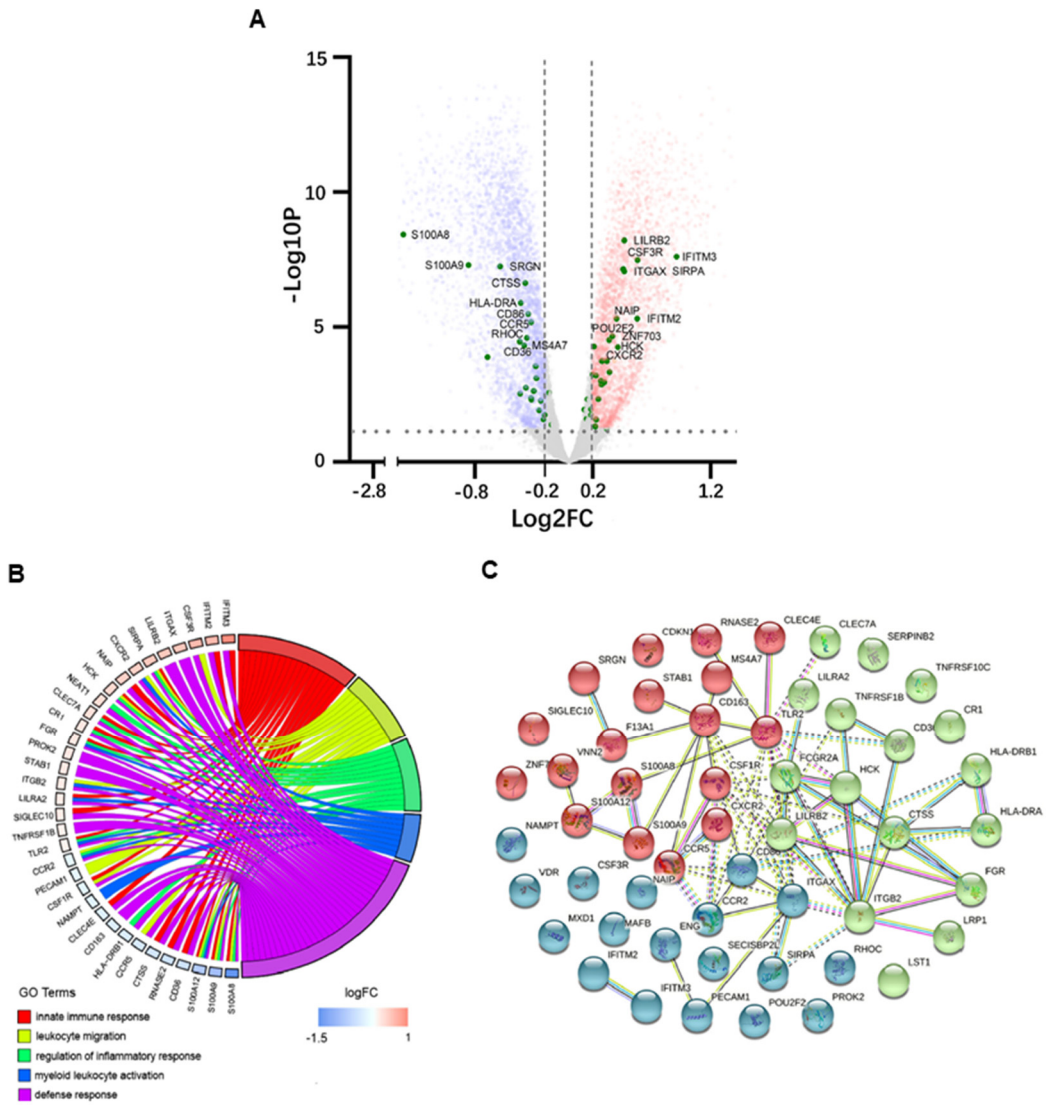

Fig. 5. Comparison of blood DEGs between FES patients and HCs. (A) Volcano plot indicates DEGs (FDR < 0.05, $Log_2FC > |0.2|$), depicted as upregulated (red) or downregulated (blue), in FES patients (n = 128) compared to HCs (n = 111). Fifty-four monocyte subset-specific DEGs are highlighted (green) and those with $-Log_{10}FDR > 3$ are nominated. **(B)** Chord plot shows most of the 54 DEGs in association with the top nonoverlapping GO-BP subontology terms, as analyzed in DAVID. Genes are ordered according to the observed Log_2FC and linked to their assigned terms via colored ribbons. **(C)** PPI analysis shows the interactions of DEGs set at a high confidence threshold of 0.7 and clustered into 3 color-coded sets with k-means = 3. Line between nodes features the type/strength of an interaction according to annotations in String. See also **Tables S2 & S3** of paper I.

5.1.3 FES patients showed reduced brain cortical thickness and declined cognition

A subset of 60 FES patients and 54 HCs from the total cohort underwent further MRI and MCCB tests (two patients and two controls did not complete the MCCB assessment). There were no significant differences in age, sex, education years, or smoking status between the FES and the HCs in this subset, and their clinical characteristics are displayed in **Table S6** of paper I.

For MRI structural imaging, the whole-brain average cortical thickness was reduced in the FES patients after controlling for age and sex (2.54 ± 0.08 vs. 2.59 ± 0.09, $F = 10.078$, $p = 1.946 \times 10^{-3}$). As illustrated in exemplary MRI images in **Fig. 6A**, among the 34 cortical regions defined by the Desikan-Killiany atlas, 8 regions, i.e. the supramarginal gyrus, the inferior parietal cortex, the superior parietal gyrus, the lateral occipital cortex, the inferior temporal gyrus, the precuneus, the fusiform gyrus, and the superior temporal gyrus were all remarkably thinner in the FES individuals, while their pericalcarine and lingual gyri were statistically thicker than those of the HCs (all FDR < 0.05) (**Fig. 6B; Table S7** of paper I).

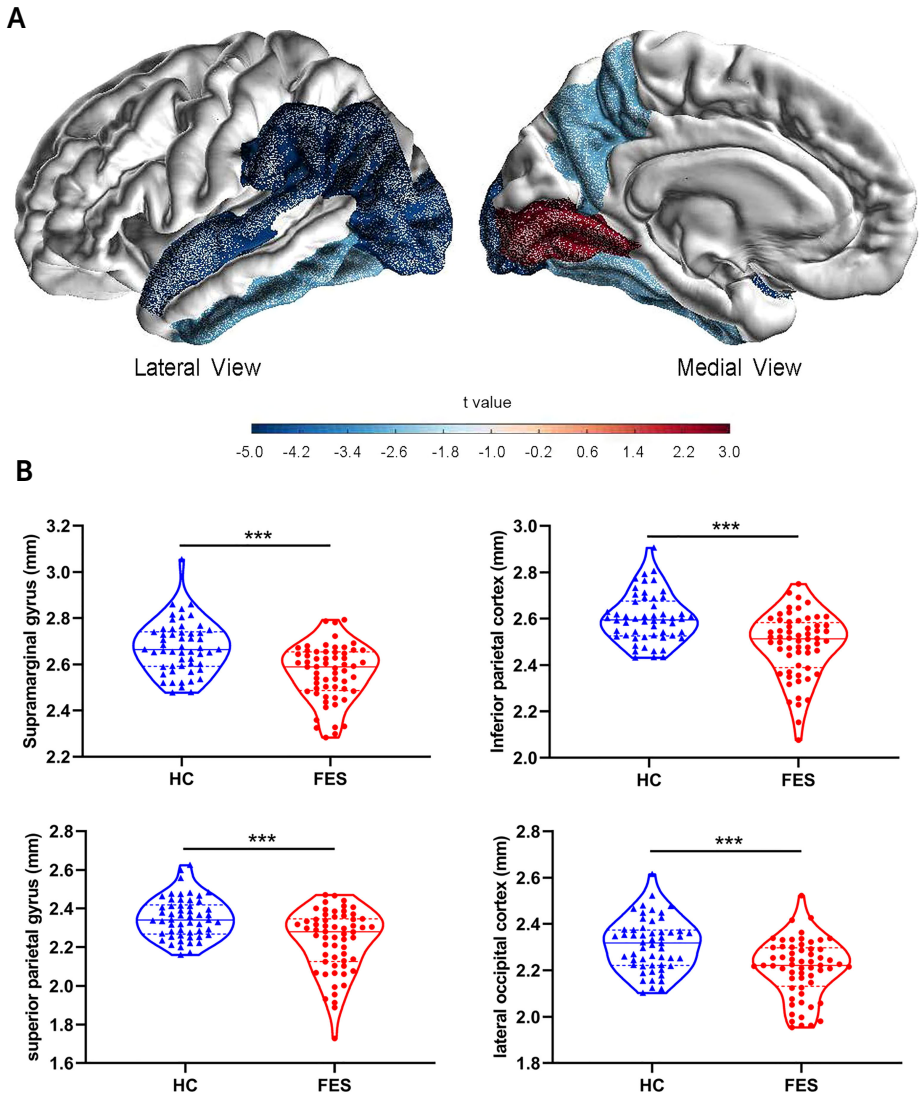

Fig. 6. Brain cortical thicknesses were different between FES patients and HCs. **(A)** Thirty-four distinct gyrus-defined regions per hemisphere were extracted according to the Desikan-Killiany atlas and averaged for both hemispheres in HCs (n = 54) and FES patients (n = 60). Exemplary MRI images show the cortical regions with significant group differences in thickness, with blue and red colors encoding cortical thinning and thickening in FES patients as compared to HCs, respectively, after FDR correction and controlling for age and sex. Color gradient is based on the statistical t values of group comparison. **(B)** Brain regions with the most significant reduction in cortical thickness of FES patients are shown, with median and upper or lower quartile drawn in violin plots, respectively. *** FDR < 0.001. See also **Table S7** of paper I.

As expected for MCCB test, the FES patients also showed significantly lower total MCCB score and the seven domain subscores compared to the HCs after controlling for age, sex, and education years (all FDR < 0.001) (**Table 2**).

Table 2. Comparison of the MCCB scores between FES and HCs.

MCCB domains	**FES (n=58)**	**HC (n=52)**	**F**	***p***	**FDR**
Composite score	44.93±9.30	58.69±6.98	76.397	4.047×10^{-14}	**NA**
Processing speed	44.32±11.05	57.50±8.73	42.368	2.383×10^{-9}	$\mathbf{8.341\times10^{-9}}^{***}$
Attention/ vigilance	40.50±11.91	57.17±10.83	49.714	1.707×10^{-10}	$\mathbf{1.195\times10^{-9}}^{***}$
Working memory	46.00±10.94	57.55±7.17	37.923	1.284×10^{-8}	$\mathbf{2.996\times10^{-8}}^{***}$
Verbal learning	48.72±10.98	57.37±7.78	17.237	6.572×10^{-5}	$\mathbf{7.667\times10^{-5}}^{***}$
Visual learning	45.53±9.78	55.02±7.22	28.969	4.258×10^{-7}	$\mathbf{5.961\times10^{-7}}^{***}$
Reasoning/ problem solving	46.98±10.33	56.63±7.40	32.037	1.238×10^{-7}	$\mathbf{2.167\times10^{-7}}^{***}$
Social cognition	46.32±11.16	54.46±10.08	12.409	6.253×10^{-4}	$\mathbf{6.253\times10^{-4}}^{***}$

Analysis of covariance with age, sex and education years as covariates. ***FDR < 0.001. The bold values indicate statistically significant differences. NA, Not Applicable.

5.1.4 Associations among monocytic subset signature genes, cortical thickness, and cognition

To explore relationships of monocytic DEGs with brain structure and cognition, we performed partial correlational analyses of the three modules, e.g., 54 DEGs' RNA-seq counts, averaged thicknesses of the 34 brain cortical regions, and MCCB subscores, controlled for age, sex, and education years in FES and HC groups, respectively (**Fig. 7; Fig. S1** of paper I). Correlational matrices of these three modules showed main differences between the two groups, including two aspects.

Firstly, internal positive correlations among 54 DEGs inside the gene module and among 34 brain regions inside the cortex module were both significantly attenuated in the FES group as compared to those in the HCs (Zr-mean within DEGs: 0.388 vs 0.335, t = -8.319, $p = 2.052 \times 10^{-16}$; Zr-mean within brain regions: 0.449 vs 0.346, t = -10.576, $p = 5.886 \times 10^{-24}$) (**Fig. 7A; Fig. S3A, B** of paper I). As for a whole profile of inter-relationships among the three modules, in the HC group, mono-DEGs counts were in strikingly inverse correlations with both the cortical thicknesses and the MCCB scores, which were positively associated with each other (**Fig. 7B**). By contrast, in the FES group, such negative correlation of the mono-DEGs with the cortical thicknesses was markedly weakened (Zr-mean: -0.116 vs -0.025, t = 21.555, FDR = 1.447×10^{-91}), and even reversed to a positive correlation with the cognitive scores (Zr-mean: -0.088 vs 0.085, t = 17.188, FDR = 3.956×10^{-49}), respectively (**Fig. 7B**). A positive correlation between the cortical thicknesses and the cognitive scores was also trendily weakened in the FES patients (Zr-mean: 0.091 vs 0.070, t = -1.955, FDR = 0.052) (**Fig. 7B, Fig. S1A, B** of paper I).

Secondly, when comparing the subset-specific mono-DEGs, we found that the negative correlations between them and the cortical regions were also remarkably weakened in the FES group, especially for the nonclassical mono-DEGs, showing the greatest statistical significance (Classical mono-DEGs: Zr-mean: -0.089 vs -0.005, t = 8.383, FDR = 2.697×10^{-15}; intermediate mono-DEGs: Zr-mean: -0.134 vs -0.054, t = 11.737, FDR = 1.511×10^{-28}; nonclassical mono-DEGs: Zr-mean: -0.111 vs -0.010, t = 15.236, FDR = 9.638×10^{-45}) (**Fig. 7C**).

Furthermore, compared to the HC group, the correlations between the subset-specific mono-DEGs and the MCCB subscores were reversed in the FES group, and likewise, with the nonclassical mono-DEGs showing the greatest statistical significance (Classical mono-DEGs: Zr-mean: -0.095 vs 0.161, t = 10.949, FDR = 6.997×10^{-16}; intermediate mono-DEGs: Zr-mean: -0.081 vs 0.042, t = 7.939, FDR = 7.195×10^{-13}; nonclassical mono-DEGs: Zr-mean: -0.081 vs 0.086, t = 10.114, FDR = 3.482×10^{-18}) (**Fig. 7C**).

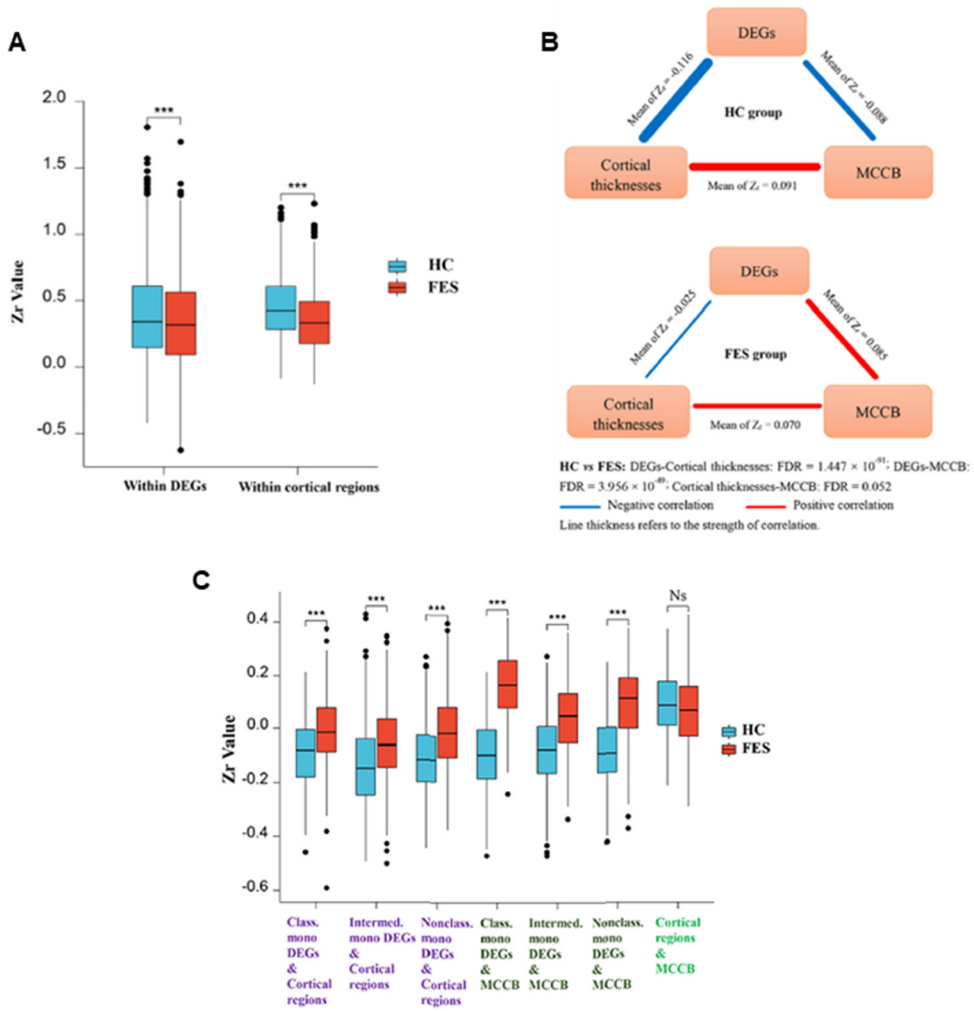

Fig. 7. Monocytic DEG mRNAs, cortical thicknesses, and cognition showed differential correlations among each other in FES patients and HCs. Partial correlational analyses of three modules comprising 54 monocytic DEGs' normalized RNAseq counts, averaged thicknesses of the bi-hemispheric 34 brain cortical regions, and MCCB scores in HCs and FES patients, respectively, controlled for age, sex, and education years. All partial correlation coefficients were then transformed into Fisher Zr. **(A)** Zr scores of intra-associations within the monocytic DEGs module and the brain regions module were compared between the two groups. **(B & C)** Zr scores of inter-relationships among the three modules **(B)**, including DEGs refined to different monocytic subsets **(C)**, were compared between the two groups. mean ± SD; *** FDR or $p < 0.001$. See also **Fig. S1A, B** of paper I.

Next, we checked detailed correlations between individual DEGs and each cortical region, controlling for age, sex, and education years and setting the significant level at $p < 0.01$, as visualized in **Fig. 8**. In the HC group, numerous negative correlations appeared, with the top outstanding ones coming from genes that were all upregulated in the FES patients compared to the HCs, such as an intermediate monocytic gene *PROKINETICIN 2* (*PROK2*) (**Fig. 8A**).

In the FES group, the most highly significant correlation came from a classical monocytic gene *RNASE2*, which was downregulated in the FES patients compared to the HCs ($Log_2FC = -0.41$, FDR = 0.003, **Table S2**) and was inversely correlated with the lateral occipital cortical thickness (**Fig. 8B**). Besides, the intermediate monocytic genes of the S100A family members were inversely associated with the thicknesses of the precentral, middle temporal and paracentral cortices in the FES group (**Fig. 8B**). Among all the correlations in both groups, only the negative relationship between the RNASE2 and the thickness of the lateral occipital cortex in the patient group survived multiple comparison correction for 54 × 34 tests (partial $r = -0.531$, FDR = 0.040).

Additionally, negative associations existed between expressions of a variety of the monocytic genes and the MCCB subscores in the HC group (**Fig. 8C**), among which some were reverted to positive relationships in the FES group, especially the *CR1*, *ITG*, and *CSF1R* genes that belong to the classical-intermediate monocytes (**Fig. 8D**), but none of these correlations passed FDR correction.

We also explored whether the percentage of nonclassical monocytes was associated with cortical thicknesses. The results showed that among the FES patients, after adjustment for age, sex, and education years, the percentage of nonclassical monocytes was inversely correlated with the cortical thicknesses of seven anatomic regions, including the paracentral lobule, the entorhinal cortex, the fusiform gyrus, the middle temporal gyrus, the pars opercularis of the inferior frontal gyrus, the superior temporal gyrus, and the temporal pole (partial r within the range of -0.5 ~ -0.7, all FDR < 0.05) (**Fig. S2A** of paper I). No significant correlations between the percentage of nonclassical monocytes and the thicknesses of cortical regions in the HC group (**Fig. S2B** of paper I) and between classical or intermediate monocytes and cortical regions in both groups were detected (all FDR > 0.05). Furthermore, there were no significant correlations between the percentage of nonclassical monocytes and all the MCCB domains in both groups even at nominal levels (all $p > 0.05$).

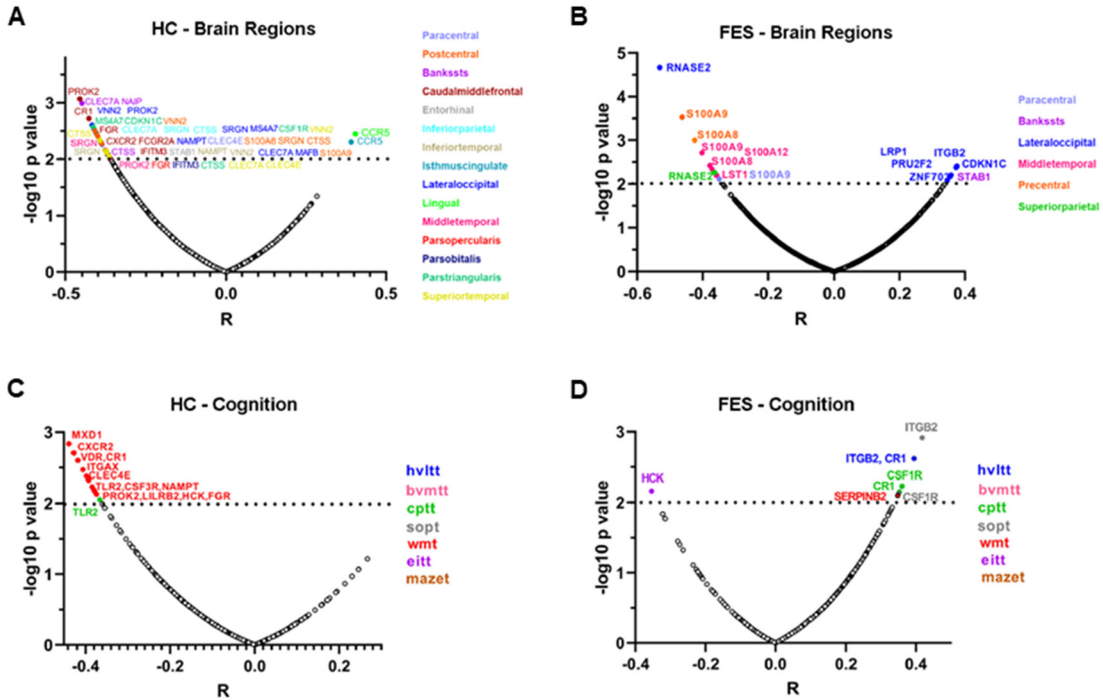

Fig. 8. Correlations of individual monocytic DEG mRNAs with cortical thicknesses and MCCB scores highlighted more extensive negative features in HCs compared to FES patients. (A-D) Partial correlational analyses of the mRNA levels of 54 monocytic DEGs with the averaged thicknesses of bi-hemispheric 34 cortical regions, after controlling age, sex, and education years, in HC **(A)** and FES **(B)** groups, respectively; and with the 7 MCCB subscale scores in HC **(C)** and FES **(D)** groups, respectively. The abscissa represents partial correlation coefficient. The significant level was set at $p < 0.01$. Among all the correlations, only the inverse relationship between the classical monocytic gene *RNASE2* and lateral occipital cortical thickness in FES patients passed the FDR (54 × 34) correction. HVLT, Hopkins verbal learning test; CPT, continuous performance test; SOPT, speed of processing test; WMT, working memory test; EIT, emotion intelligence test; MAZET, mazes test.

5.1.5 Mediation effect of the cortical thickness on the association of monocytic gene and cognition

Finally, considering the overt relationship between the gene *RNASE2* and the lateral occipital cortical thickness in FES group (**Fig. 9B**), we further explored whether the lateral occipital cortex may mediate the *RNASE2*-cognition relationship in the FES patients. Because the thickness of the lateral occipital cortex was associated with only BVMT subscore of MCCB scores at nominal level (partial r = 0.370, nominal p = 0.005), the BVMT score was used as the dependent variable the lateral occipital cortical thickness as the mediator in the mediation analysis. We observed that the indirect path (path ab) from expression level of RNASE2 to the BVMT score was significant (β = -0.156, 95 % CI, -0.359 to -0.003), while the direct effect (path c') between them was insignificant (β = -0.047, t = -0.367, p = 0.715), implying that the effect of *RNASE2* on the BVMT score was fully mediated by the lateral occipital cortex (**Fig. 9**).

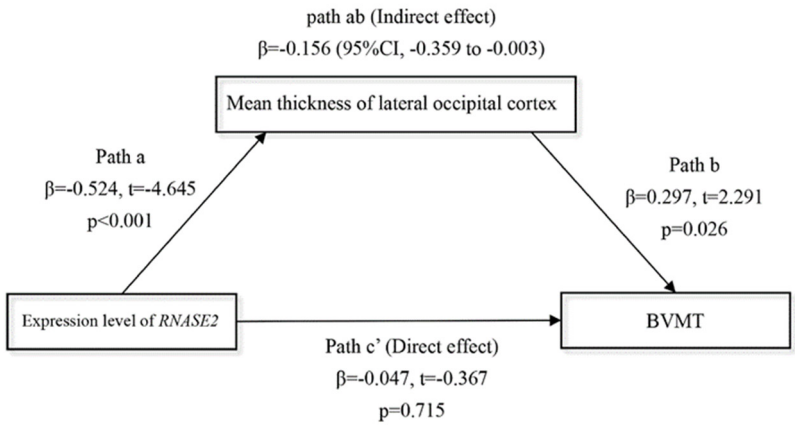

Fig. 9. Full mediation effect of the lateral occipital cortex between gene *RNASE2* and visual memory. Independent variable = RNASE2 expression level; Dependent variable = BVMT score; Mediator = lateral occipital cortex. Age, sex, and education years were included as covariates.

5.2 Paper II

5.2.1 Demographic and clinical characteristics of a sub-cohort of FES patients and HCs

As schizophrenia is a stress-vulnerable disorder, to better characterize stress effect on patients with schizophrenia, we further selected a sub-cohort of FES patients who showed higher PSS scores than HCs. No differences in age, sex, and education years between the two groups were found (**Table 3**). However, the FES patients had lower BMI ($p < 0.001$) as well as higher CTQ ($p = 0.002$, **Table 3**) and PSS ($p = 0.001$, **Table 3**) scores than the HCs.

Table 3. Demographic and clinical characteristics of FES patients and HCs

Demographics	**FES (n=74)**	**HC (n=68)**	**F or $\chi 2$**	***p***
Sex (M/F)	44/30	31/37	2.736	0.098
Age (years)	31.30 (1.20)	33.77 (1.27)	2915.500	0.102
Education (years)	12.67 (0.45)	13.37 (0.31)	2847.000	0.167
BMI (kg/m^2)	21.48 (0.400)	23.38 (0.39)	3382.500	**2.892E-5**
CTQsum	86.84 (4.59)	66.00 (3.62)	1336.500	**0.002**
PSS score	26.93 (0.50)	23.19 (0.79)	1554.000	**0.001**
Age of illness onset (years)	29.90 (1.09)			
Illness duration (months)	14.89 (2.30)			
PANSS-P	21.68 (0.59)			
PANSS-N	17.72 (0.73)			
PANSS-G	37.72 (0.97)			
PANSS-T	77.10 (1.64)			

Abbreviations: CTQsum, Childhood Trauma Scale summation (short form).

5.2.2 Hippocampal fimbria were smaller in FES patients and negatively correlated with stress perception and psychopathological symptoms

Interestingly, MRI data showed alterations of the hippocampal subregions (**Fig. 10A, Table 4**), but not the PFC structures (data not shown), in the FES patients, with significantly smaller hippocampal fimbria (left: $p = 7.213\times10$, right: $p = 1.041e^{-9}$, **Fig. 10B & 10C**), but larger tails (left: $p < 0.05$, right: $p < 0.0001$), left presubiculum ($p < 0.01$), and right fissure ($p < 0.05$).

Table 4. Hippocampal volumes (mm^3) in FES patients and HCs

Cortical regions	**FES** (*n*=56)	**HC** (*n*=64)	***F***	***p***
HPC	8134.16 ± 85.18	8155.13 ± 90.73	0.168	0.683
Left_Whole HPC	3443.81 ± 32.83	3438.20 ± 37.16	0.516	0.474
Right_Whole HPC	3514.50 ± 36.04	3530.10 ± 34.99	0.130	0.719
Left_CA1	611.59 ± 7.86	610.02 ± 7.90	0.427	0.515
Left_CA3	185.54 ± 2.87	186.60 ± 3.23	0.037	0.849
Left_CA4	245.40 ± 2.95	250.59 ± 3.21	0.765	0.384
Left_DG	288.00 ± 3.34	294.15 ± 3.77	0.826	0.365
Left_Fimbria	86.62 ± 2.69	110.68 ±2.43	33.152	**7.213×10^{-8}**
Left_Fissure	151.17 ± 2.80	146.53 ± 2.52	2.133	0.147
Left_HATA	55.01 ± 1.01	57.29 ± 1.05	1.089	0.299
Left_Molecular layer	563.52 ± 6.14	564.39 ± 6.24	0.204	0.652
Left_Parasubiculum	63.43 ± 1.71	61.50 ± 1.54	1.423	0.235
Left_Presubiculum	338.81 ± 5.75	320.17 ± 4.50	8.068	**0.005**
Left_Subiculum	447.56 ± 4.75	453.87 ± 5.55	0.025	0.875
Left_Tail	558.32 ± 8.80	528.93 ± 7.99	6.317	**0.013**
Right_CA1	628.94 ± 8.68	645.05 ± 7.34	0.755	0.387
Right_CA3	201.32 ± 3.45	201.26 ± 3.70	0.031	0.860
Right_CA4	253.29 ± 3.09	256.56 ± 3.23	0.152	0.697
Right_DG	296.09 ± 3.57	301.50 ± 3.67	0.438	0.509
Right_Fimbria	79.27 ± 2.58	104.78 ± 2.14	44.204	**1.041×10^{-9}**
Right_Fissure	155.84 ± 2.99	147.90 ± 2.55	6.664	**0.011**
Right_HATA	55.92 ± 1.00	58.31 ± 0,89	1.192	0.277
Right_Molecular layer	575.82 ± 6.84	585.05 ± 5.94	0.275	0.601
Right_Parasubiculum	57.46 ± 1.23	57.20 ± 1.47	0.080	0.777
Right_Presubiculum	319.92 ± 5.48	308.15 ± 3.90	3.811	0.053
Right_Subiculum	449.87 ± 5.71	461.16 ± 4.50	0.370	0.544
Right_Tail	596.61 ± 8.98	551.08 ± 7.83	16.520	**8.800×10^{-5}**

ANCOVA with age, sex and BMI as covariates; Abbreviations: dentate gyrus (DG), hippocampal amygdala transition area (HATA).

While no correlations with the PSS scores were found for the left hippocampal fimbria in both groups (**Fig. 10D**), volumes of the right hippocampal fimbria were negatively correlated with the PSS scores in the FES patients (r = -0.397, p = 0.003, **Fig. 10E, Table S4** of paper II), but not in the HCs.Furthermore, the volumes of the left hippocampal fimbria were negatively associated with PANSS scores (PANSS-N: r = -0.388, p = 0.004; PANSS-T: r = -0.339, p = 0.013; **Fig. 10F & 10G, Table S5** of paper II). No correlations were found between the CTQ scores and hippocampal volumes (**Table S6** of paper II).

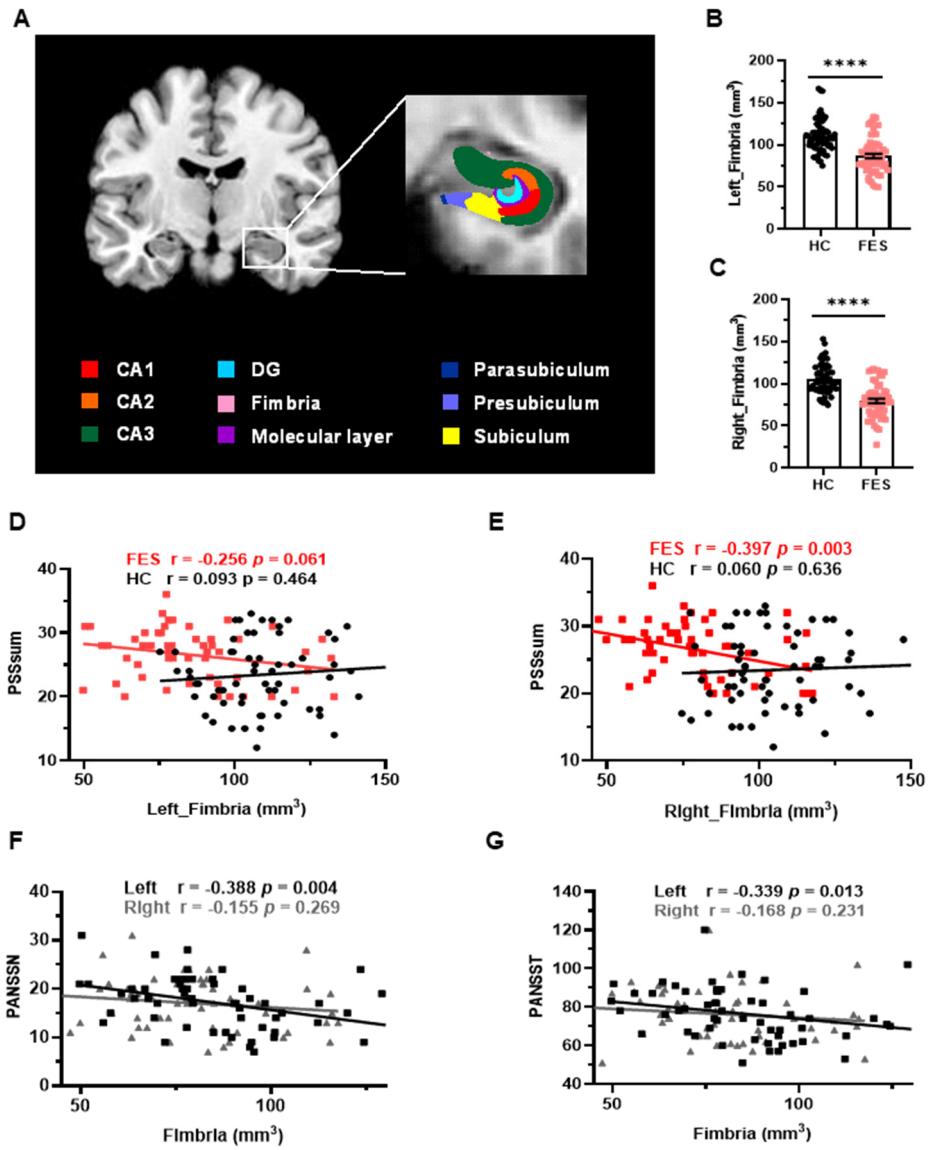

Fig. 10. **Hippocampal fimbria were smaller in FES patients and negatively correlated with PSS and PANSS scores. (A)** A representative T1 MRI image with colored hippocampal subregions. **(B & C)** The bilateral fimbria were significantly reduced in FES (n = 59) compared to HC (n = 64). Data are plotted as mean±SEM. **** $p <$ 0.0001. ANCOVA with age, sex, and BMI as covariates. **(D & E)** Volumes of the right fimbria were negatively correlated with PSS scores in FES patients but not HCs (Spearman's). **(F & G)** Volumes of the left fimbria were negatively correlated with both PANSS-N and PANSS-T scores (Pearson's partial correlation controlled for age, sex, and BMI). See also **Tables S4-S6** of paper II.

5.2.3 Blood immune DEGs are correlated negatively with PSS score and positively with the right hippocampal fimbria volume in FES patients but not HCs

As implied in paper I, reduced amount of nonclassical monocytes along with altered signature gene expressions in FES patients compared to HCs may be due to deficits in myeloid development or reprograming in the FES patients. Assuming this, we explored blood RNA-seq data on the FES patients and HCs. The top GO-BP pathway of human blood DEGs involved nucleotide metabolism and transcription regulation (**Table S7** of paper II). Furthermore, we found 181 DEGs involved in immune system development (immdev-DEGs) (**Fig. 11A, Table S7 of** paper II), such as hematopoiesis and leukocyte differentiation (**Fig. 11B).** Compared to the HCs, these 181 immdev-DEGs overall showed a negative correlation with the PSS scores ($p < 0.0001$, **Fig. 11C, S3B of** paper II) and a positive correlation with the hippocampal fimbria volumes, particularly on the right side ($p < 0.0001$, **Fig. 11D, S3B** of paper II) in the FES patients. Among these immdev-DEGs, 18 genes with the most significant correlational coefficients (Zr) kept such trends in the FES patients, which were reversed in the HCs in most cases (**Fig. 11C & 11D**). We further made mediator analysis assuming stress negatively affected hippocampal structures via certain immdev-DEGs. Notably, *KCNQ1*, encoding a voltage-gated potassium channel, was upregulated in the FES patients (FDR < 0.01, **Fig. 11E**), and partially mediated the negative regulation of the right fimbria volume by the PSS score ($\beta = -0.442$, 95 % CI: -1.326 – -0.087, **Fig. 11E**).

These data overall marked the hippocampal fimbria as an important stress-sensitive subregion of which immune genes may engage in regulation in FES.

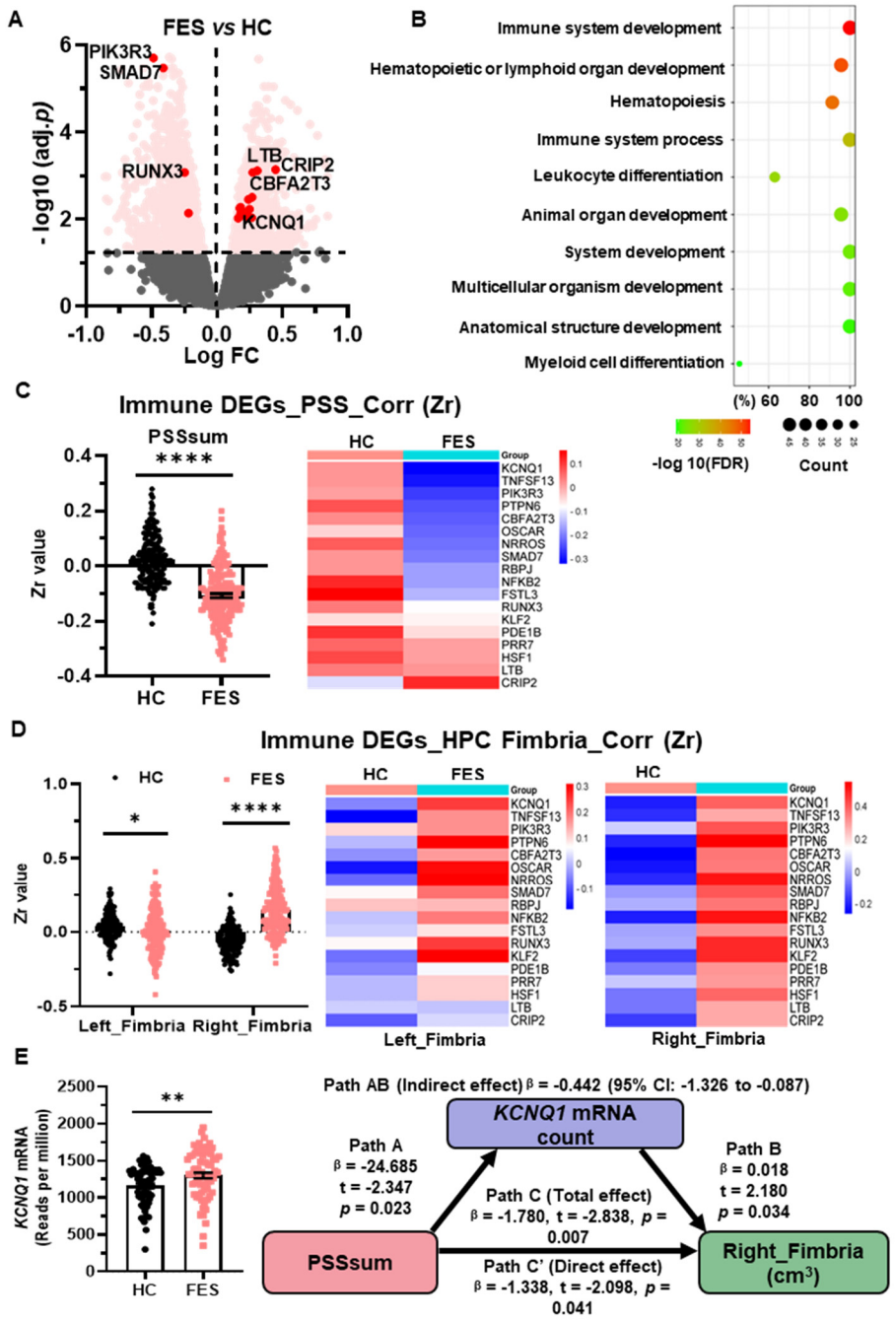

Fig. 11. Blood immdev-DEGs were correlated negatively with PSS score and positively with the right hippocampal fimbria volume in FES. (A) Volcano plot showing expressions of blood DEGs between FES patients (n = 74) and HCs (n = 68) after bulk RNA-seq. Pink dots indicate 181 significant DEGs involved in immune system development. Those with values of -Log_{10}(FDR) ≥ 2 and also correlated with PSS are

highlighted in red dots. **(B)** GO-BP enrichment analysis of the 181 immdev-DEGs showing top 10 pathways based on -Log_{10}(FDR) clustering values and gene counts. See also **Table S7** of paper II. **(C & D)** These 181 immdev-DEGs differed between HC and FES in correlations of their RNAseq counts with PSS scores **(C**, Spearman's**)** and right fimbria volumes **(D**, Pearson's partial correlation controlled for age, sex, and BMI**)**, as represented in dot charts. Correlational coefficients were transformed into Fisher Zr values before comparisons. Top 18 immdev-DEGs with the most significant correlational differences are shown in heatmaps. Mean±SEM; * $p < 0.05$, **** $p < 0.0001$. **(E)** *KCNQ1* mRNA count was elevated in FES compared to HC (** FDR < 0.01), and partially mediated a negative regulation of PSS score on right fimbria volume (Path AB, controlled by age, sex, and BMI). PSS score was negatively correlated wtih *KCNQ1* (Path A, $p < 0.05$), which *KCNQ1* was positively correlated with the right fimbria volume (Path B, $p < 0.05$). While PSS score directly impacted the right fimbria volume (Path C', $p < 0.05$), this effect was stronger when *KCNQ1* was considered as a mediator (Path C, $p < 0.01$). See also **Fig. S3** of paper II**.**

5.2.4 Replenished microglia rescued CUS-triggered learned hopelessness and social deficit but not anxiety

As psychosocial stress promotes inflammation and microglial activation, we further explored how microglia and repMg affected stress behaviors in a CUS animal model. We performed a battery of behavioral tests on mice of Ctr, CUS, repMg, and CUS+repMg groups (**Fig. 12A**). The CUS induced anxiety as shown by decreased ratio of central versus total travel distance ($p < 0.01$, **Fig. 12B**) in OFT and increased time in EPM closed arms ($p < 0.05$, **Fig. 12C**). In the repMg and CUS+repMg groups, mice showed similar anxiogenic effects in the OFT (both $p < 0.05$, **Fig. 12B**) and the EPM ($p < 0.05/0.01$, **Fig. 12C**). CUS × repMg interactions were found in the OFT ($F(1,35) = 7.545$, $p < 0.01$) and the EPM ($F(1,35) = 4.489$, $p < 0.05$). Overall, these suggest that microglial replenishment causes anxiety itself and cannot ameliorate CUS-induced anxiety. A CUS × repMg interactive effect on sociability was also found in TCT ($F(1,35) = 9.623$, $p < 0.01$). CUS-subjected mice displayed less preferential entry into the social chamber and time spent there than in the empty chamber (**Fig. 12D & 12E**). Mice in the repMg group also entered less into the social chamber (**Fig. 12D**) but spent longer time once there than in the empty chamber ($p < 0.001$, **Fig. 12E**). However, mice of the CUS+repMg group showed normal sociability similarly as the Ctr mice ($p < 0.01$, **Fig. 12D & 12E**), indicating that microglial replenishment can partially rescue CUS-triggered social deficit.

For depressive-like behavior, the CUS also interacted with the repMg ($F(1,35) = 12.180$, $p < 0.01$). Mice in the CUS but not the repMg group showed longer immobility time than the Ctr mice ($p < 0.05$, **Fig. 12F**). Furthermore, CUS+repMg-subjected mice showed significantly less immobility time than the CUS-subjected mice ($p < 0.05$, **Fig. 12F**), demonstrating ameliorative effect of microglial replenishment on CUS-induced learned helplessness.

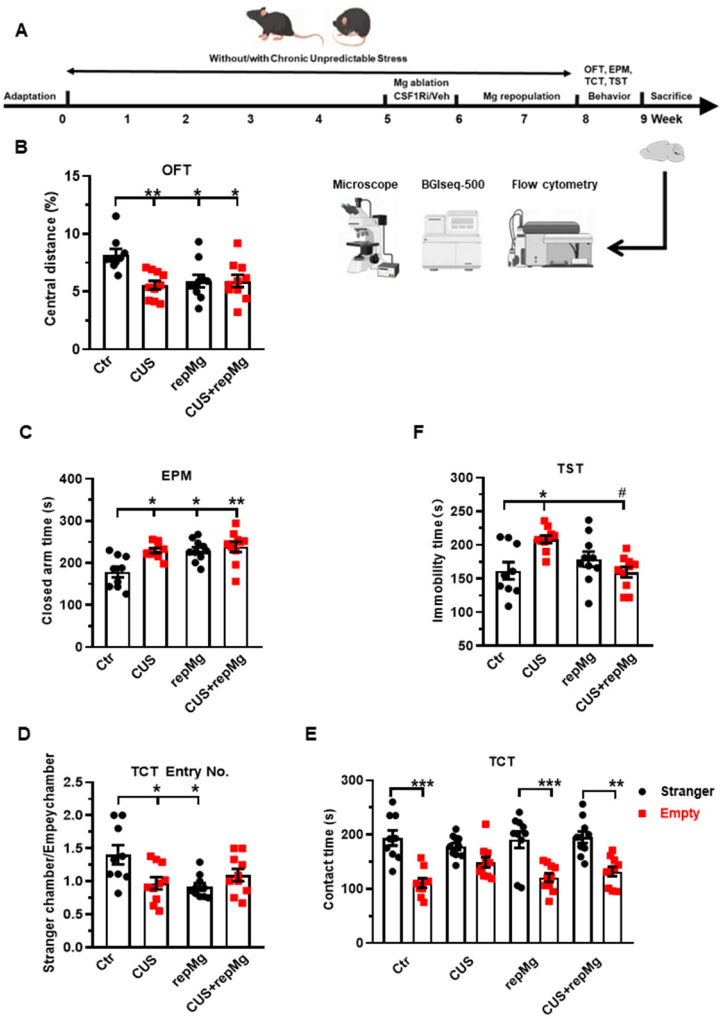

Fig. 12. RepMg rescued CUS-induced learned helplessness and social deficit but not anxiety. (A) Schematic diagram of experimental design. Mice were separated into 4 groups (Ctr, CUS, repMg, and CUS+repMg; n = 9/9/10/10 mice per group) and underwent CUS and/or CSF1Ri (PLX3397) treatment. Afterwards, behavioral tests were conducted, followed by flow cytometry and IHC. **(B)** Treated mice showed decreased central versus total distance (%) than Ctr mice in OFT. **(C)** In EPM test, time spent in closed arms were significantly increased in CUS, repMg and CUS+repMg. **(D & E)** In TCT, ratios of frequencies of entry into a stranger mouse chamber versus an empty container chamber were declined by CUS or repMg treatment, but not CUS+repMg **(D)**; moreover, except for CUS, the other groups showed similarly longer stay with the stranger mice than with the empty container (**E**). **(F)** In TST, CUS induced elongated immobility time compared to Ctr, which was reduced by CUS+repMg. Mean±SEM; * or # $p < 0.05$, ** $p < 0.01$ (* compared to Ctr; # compared to CUS); Two-way ANOVA with Tukey's corrections.

5.2.5 CUS and microglial replenishment affected brain developmental transcriptomics in the mouse prefrontal cortex (PFC)

To further investigate the underlying mechanisms of behavioral changes and microglial function on phagocytosis, we run an RNA-seq analysis using the PFC samples from 4 groups of mice. Among the 4 groups, 502 upregulated and 577 downregulated DEGs were identified, involving nervous system development and axon guidance among the top 10 GO-BP pathways (**Fig. 13A-13D, Table S1** of paper II). Notably, expressions of the DEGs in these 2 pathways were generally recovered in CUS+repMg group (**Fig. 13C & 13D**). Furthermore, compared to Ctr, DEGs affected particularly by repMg were involved in rhythmic process and regulation of synaptic plasticity, with most synaptic DEGs down-regulated (**Fig. S1, Table S2** of paper II), whereas those affected by CUS were a small group of angiogenic DEGs (**Table S3** of paper II). These results uncovered that CUS and microglial replenishment both affectted brain structural remodeling, but microglial replenishment can partially restore brain developmental processes altered by CUS.

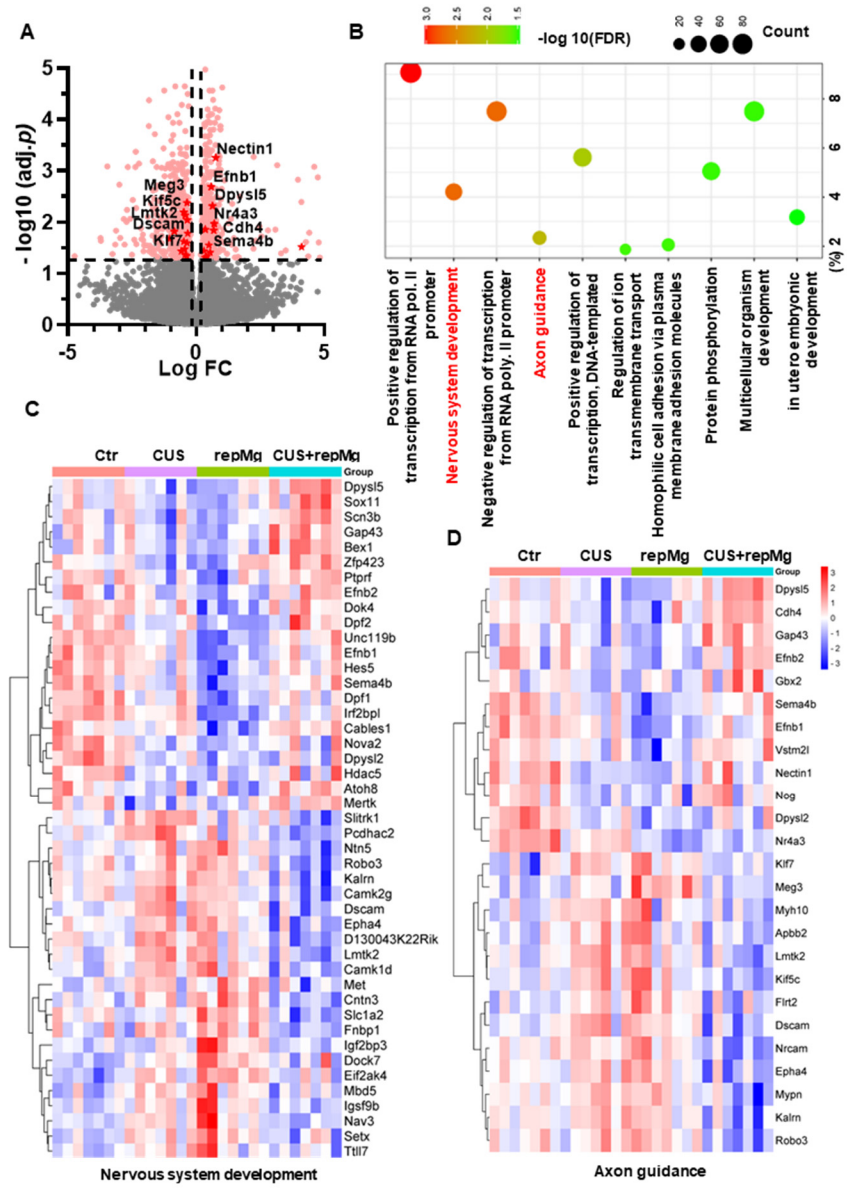

Fig. 13. CUS and repMg changed DEGs involved in nervous system development and axonal guidance in the mouse PFC. (A) Volcano plot showing expressions of DEGs compared among the four groups (Ctr, CUS, repMg, and CUS+repMg; n = 7 mice pergroup) after bulk RNA-seq. Pink dots indicate significant DEGs. Those involved in axon guidance and with values of -Log_{10}(FDR)>1.3 are highlighted in red dots. **(B)** GO-BP enrichment analysis of the DEGs showing top 10 pathways based on -Log_{10}(FDR) clustering values and gene counts. **(C & D)** Heatmaps showing expressions of DEGs involved in nervous system development and axon guidance, which were changed in CUS and repMg compared to Ctr, but partially recovered in CUS+repMg. Two-way ANOVA with FDR. See also **Tables S1-S3** and **Fig. S1** of paper II.

5.2.6 Replenished microglia corrected CUS-triggered pre-synaptic endocytosis by glial cells in the PFC and hippocampus (HPC).

To check synaptic remodeling function of replenished microglia, we studied the mouse PFC and HPC regions. We first co-stained mouse PFC sections by IHC for SYP, a presynaptic marker, and IBA1 (**Fig. 14A**). CUS × repMg interactions were found on SYP puncta number ($F(1,44) = 5.229$, $p < 0.05$), SYP density ($F(1,44) = 11.480$, $p < 0.01$), and SYP-density per microglia ($F(1,76) = 7.469$, $p < 0.01$). CUS induced loss of the SYP puncta ($p < 0.05$, **Fig. 14B**) and SYP density ($p < 0.01$, **Fig. 14C**) compared to Ctr, and repMg rescued CUS-triggered decrease in SYP ($p < 0.05$, **Fig. 14C**). Importantly, the SYP density inside microglia was higher in the CUS than the Ctr group ($p < 0.05$, **Fig. 14D**). The CUS and repMg also interacted on microglial ramification index ($F(1,76) = 7.963$, $p < 0.01$) and total branch length ($F(1,76) = 5.089$, $p < 0.05$). Compared to Ctr microglia, CUS-conditioned microglia had a larger ramification index ($p < 0.05$, **Fig. 14E**) and a longer total branch length ($p < 0.01$, **Fig. 14F**). In contrast, the repMg corrected CUS-triggered increases in these parameters (both $p < 0.01$, **Fig. 14E & 14F**). No differences were found on the number of branches among the groups (**Fig. 14**).

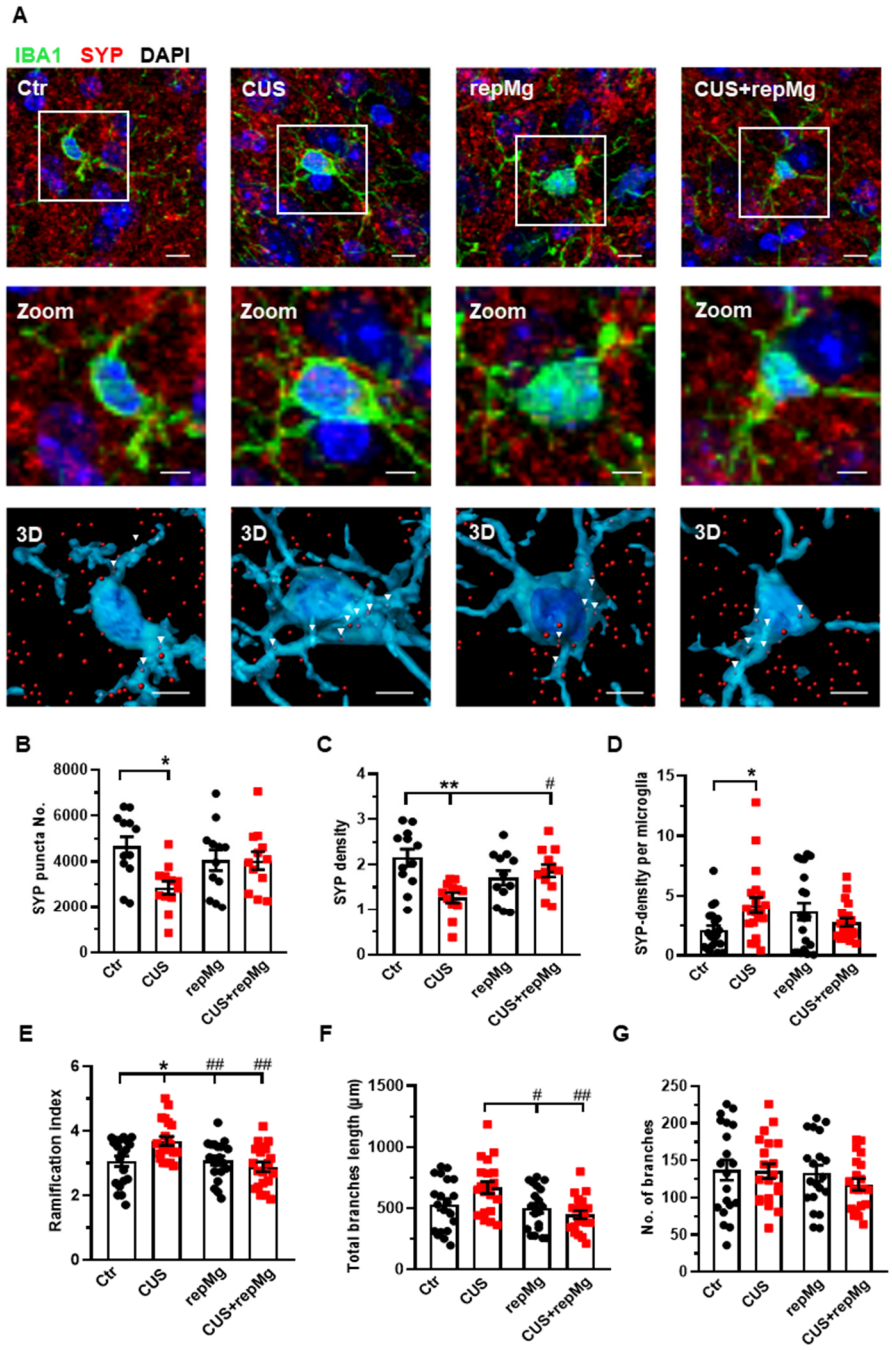

Fig. 14. RepMg rescued CUS-triggered loss of SYP and microglial over-ramification in the mouse PFC. (A) Representative images of microglia (IBA1, green), synaptophysin (SYP, red) and nucleus (DAPI, blue), with zoomed and 3D images showing SYP puncta in microglia. Arrowheads indicate SYP puncta engulfed by microglia. Scale

bar = 1μm. **(B)** CUS decreased SYP puncta compared to Ctr. **(C)** CUS reduced SYP density, which was recovered in CUS+repMg. **(D)** CUS enhanced SYP density in microglia. **(E)** CUS enhanced microglial ramification compared to Ctr, which was dampened in repMg and CUS+repMg. **(F)** Microglial total branch length was shorter in repMg and CUS+repMg than in CUS. **(G)** Number of microglial branches did not change. $N = 3$ mice/6–7 slices per group; Mean±SEM; * or # $p < 0.05$, ** or ## $p < 0.01$ (* compared to Ctr; # compared to CUS); Two-way ANOVA with Tukey's corrections.

We also quantified glial cells by flow cytometry with hippocampal tissues, another important region for stress regulation (**Fig. 15A, Fig. S2A** of paper II). The CUS and repMg interacted on microglia % ($F(1,24) = 10.680$, $p < 0.01$). The CUS did not significantly affect microglia % (**Fig. 15B**). Although microglial abundancy did not fully recover in the repMg as compared to the Ctr group ($p < 0.01$, **Fig. 15B**), the recovery was better in the CUS+repMg group compared to the repMg group alone ($p < 0.01$, **Fig. 15B**). No changes in other glial populations were found (**Fig. 15C & 15D**), demonstrating the microglia-specific effect of CSF1Ri.

We further quantified glial engulfment of Vglut2, a glutamatergic presynaptic marker. CUS × repMg interactions existed on $Vglut2^+$ microglia ($F(1,24) = 10.250$, $p < 0.01$), $Vglut2^+$ astrocytes ($F(1,24) = 7.024$, $p < 0.05$), and $Vglut2^+$ OPCs ($F(1,24) = 9.100$, $p < 0.01$). Compared to the Ctr, the CUS elevated Vglut2 engulfment in microglia ($p < 0.05$, **Fig. 15E**), astrocytes ($p < 0.01$**, Fig. 15F**), and OPCs ($p < 0.05$, **Fig. 15G**).

Compared to Ctr microglia, replenished microglia were not over-pruning but led to elevated Vglut2 engulfment by the OPCs ($p < 0.05$, **Fig. 15G**). Notably, the repMg treatment normalized the Vglut2 engulfment by stressed microglia ($p < 0.001$, **Fig. 15E**) and astrocytes ($p < 0.01$, **Fig. 15F**), thereby supporting the RNA-seq and IHC results and strengthening the idea that microglial replenishment can partially rescue CUS-induced synaptic remodeling.

These data overall suggest that CUS-conditioned microglia are over-ramified and more phagocytic on pre-synaptic components, which can be corrected by microglial replenishment.

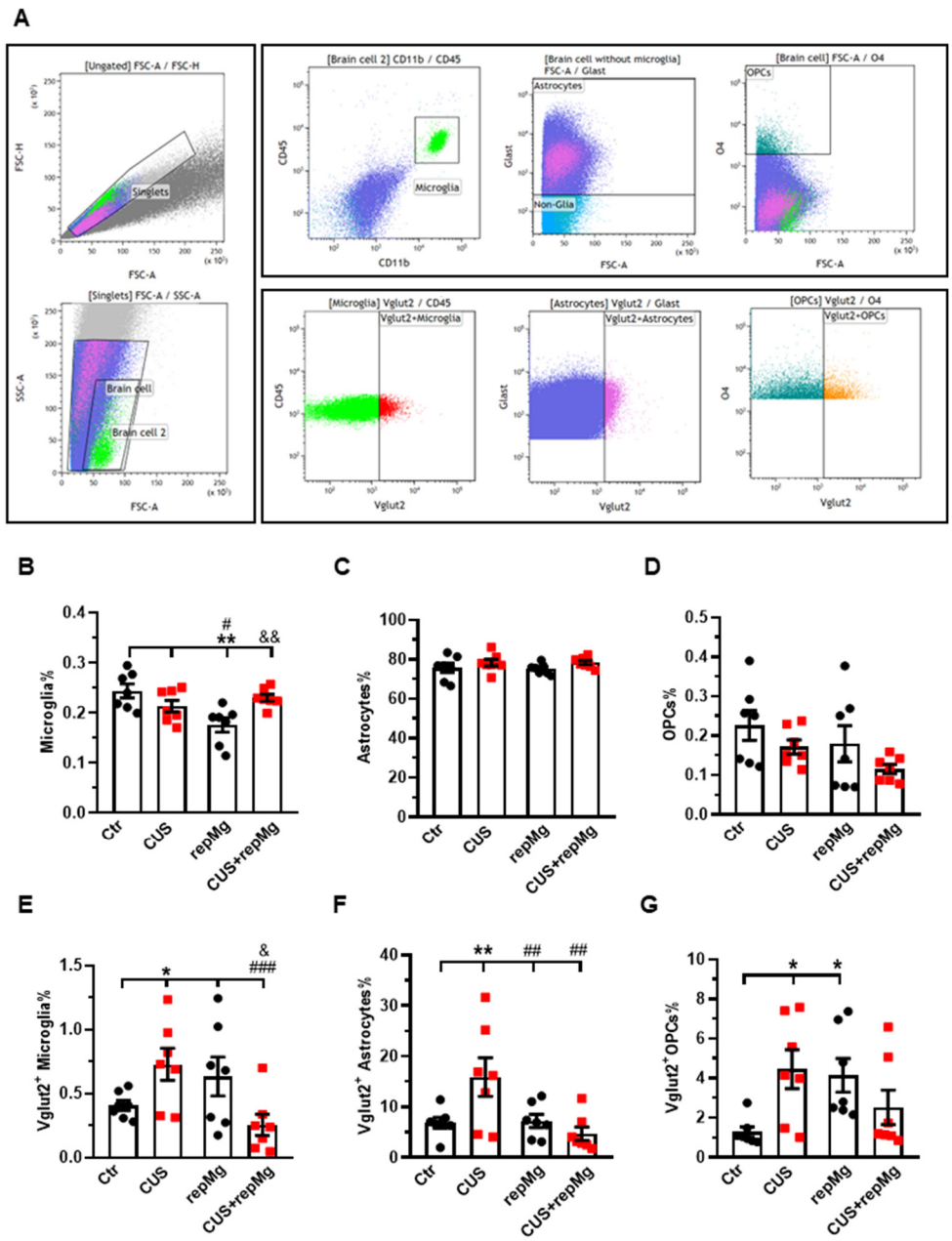

Fig. 15. CUS and repMg enhanced endocytosis of VGLUT2⁺ by hippocampal microglia, astrocytes or OPCs. (A) Dot plots represent gating strategy of flow cytometric analysis. **(B)** Compared to Ctr and CUS, microglia in repMg were still less abundant, but recovered better in CUS+repMg. **(C & D)** Abundancies of astrocytes and OPCs did not change. **(E-G)** CUS induced universal VGLUT2 engulfment by all the 3 glial subtypes compared to Ctr, which was ameliorated in repopulated microglia **(E)** and

astrocytes **(F)** in CUS+repMg. Furthermore, repMg had more abundant VGLUT2$^+$ microglia than CUS+repMg **(E)**, VGLUT2$^+$ astrocytes than CUS group **(F)**, and VGLUT2$^+$ OPCs than Ctr **(G)**. $N = 7$ mice per group; Mean ± SEM; * or # or & $p < 0.05$, ** or ## or && $p < 0.01$, ### $p < 0.001$ (* compared to Ctr; # compared to CUS; & compared to repMg); Two-way ANOVA with LSD corrections. See also **Fig. S2** of paper II.

5.3 Paper III

5.3.1 Perceived stress differed among FES patients and HCs

Intriguingly, we also observed that some FES patients had lower PSS scores than HCs. Since FES patients showed bimodular distribution in their PSS scores, to better understand potential biological differences among them, we divided them into two groups that had PSS scores above and below the average value of 24 derived from the whole patient cohort: i.e., FES-hs and FES-ls, respectively. Specifically, the FES-hs patients showed a higher PSS average score than both the FES-ls patients and the HCs (both FDR < 0.001; **Table 5**), whereas the FES-ls patients showed a lower PSS average score than the HCs (FDR = 0.03; **Table 5**). Gender distribution, age, and years of education did not significantly differ among patients and HCs (**Table 5**). Among patient groups, the age of illness onset, illness duration, and antipsychotic treatment did not differ (**Table 5**).

Table 5. Demographic and clinical characteristics of FES patients and HCs

Demographics	**Mean (SEM)**			**F/χ^2**	***p* (FDR)**	**FDR**	**FDR**	**FDR**
	FES-hs (1) (*n*=51)	**FES-ls (2) (*n*=50)**	**HC (3) (*n* =49)**			**1 vs 2**	**1 vs 3**	**2 vs 3**
Gender (M/F)	17/34	24/26	25/24	3.66	0.16			
Age (years)	30.1 (1.51)	28.8 (1.07)	33.7 (1.40)	5.81	0.06			
Education (years)	12.7 (0.49)	12.7 (0.45)	13.2 (0.33)	1.72	0.42			
CTQsum	86.3 (5.36)	88.5 (5.11)	68.5 (4.54)	7.91	**0.02**	0.68	**0.03**	**0.04**
PSS	28.8 (0.31)	17.7 (0.91)	21.3 (0.64)	93.03	**< 0.001**	**< 0.001**	**< 0.001**	**0.03**
Age of illness onset (years)	28.4 (1.46)	28.0 (1.08)	NA	0.001	0.97			
Illness duration (months)	16.0 (2.92)	10.0 (1.72)	NA	3.05	0.08			
Antipsychotic duration (days)	5.4 (0.78)	4.0 (0.44)	NA	3.17	0.14			
Antipsychotic dosage (CPZ equivalent mg/day)	232.8 (27.44)	271.6 (24.08)	NA	1.33	0.29			
Suicidality	1.2 (0.08)	1.3 (0.09)	NA	0.59	0.44			
PANSS-P	21.8 (0.74)	22.2 (0.89)	NA	0.50	0.48			
PANSS-N	18.2 (0.90)	15.8 (0.79)	NA	2.74	0.10			
PANSS-G	39.9 (1.16)	35.1 (0.86)	NA	7.33	**0.01 (0.03)**			
PANSS-T	80.1 (1.94)	73.2 (1.66)	NA	4.13	0.05 (0.09)			

All data were reported as mean (SEM); CPZ: Chlorpromazine; Bold text indicates those with significant *p* or FDR value.

Notably, CTQsum scores were higher in both patient groups compared to the HCs (both FDR < 0.05; **Table 5**), indicating more early life adverse experiences in patients. Furthermore, PANSS-G was scored higher in the FES-hs patients than the FES-ls patients (FDR = 0.03; **Table 5**), and difference in PANSS-T was marginally significant (p = 0.05; **Table 5**), while no differences were found for PANSS-P and PANSS-N symptoms. The PSS scores were nominally correlated positively with the PANSS-G scores in all FES patients (Spearman's r = 0.240, p = 0.023, FDR > 0.05) but not in separate patient groups. Suicidality records did not differ among patient groups, and no significant correlations between the CTQsum and the PSS or the PANSS scores were found.

5.3.2 Brain limbic structures differed in sizes among FES patients and HCs

Next, we measured the total brain ICV and volumes of subcortical limbic structures of FES patients and HCs by MRI (**Fig. 16A)**. The ICV did not differ among patients and HCs after controlling age, gender, and education (**Table 6**). The AMG, caudate, HPC and thalamus exhibited significant group differences (**Fig. 16B**; **Table 6**). Specifically, the FES-hs patients had the largest volumes of caudate and thalamus, particularly compared to the HCs (FDR = 0.02 & 0.001, respectively; **Fig. 16B**) and a larger hippocampal volume than the FES-ls patients (FDR = 0.01; **Fig. 16B**). In contrast, smaller AMG was found in the FES patients, particularly in the FES-ls patients (FDR = 0.002; **Fig. 16B**) and marginally so in the FES-hs patients (p = 0.07; **Table 6**) compared with HCs. No significant group differences were found in other subcortical limbic structures (**Table 6**). Antipsychotic dosages were not correlated with brain volumes in both patient groups.

Table 6. Volumes of brain limbic structures of FES patients and HCs

Brain structure (mm^3)	**Mean (SEM)**			***F***	***p* (FDR)**	**FDR**	**FDR**	**FDR**
	FES-hs (1) (*n*=35)	**FES-ls (2) (*n*=36)**	**HC (3) (*n*=47)**			**1 vs 2**	**1 vs 3**	**2 vs 3**
Accumbens	935.1 (18.86)	929.8 (28.79)	965.9 (25.73)	1.93	0.15			
AMG	3234.0 (56.22)	3180.6 (62.71)	3446.8 (51.98)	7.77	**0.001 (0.002)**	0.50	0.13	**0.002**
Caudate	7582.5 (150.95)	7023.4 (142.19)	7023.4 (974.84)	4.71	**0.01 (0.02)**	0.05	**0.02**	1.12
HPC	8229.4 (102.55)	8014.5 (102.01)	8088.7 (96.45)	5.13	**0.007 (0.02)**	**0.01**	0.11	0.64
Pallidum	4194.5 (62.48)	4137.8 (98.36)	4150.2 (70.64)	1.13	0.33			
Putamen	10351.0 (158.35)	10494.4 (235.37)	10290.1 (200.17)	0.56	0.57			
Thalamus	18067.2 (502.66)	17449.9 (528.13)	15843.6 (259.93)	9.16	**< 0.001 (0.001)**	0.59	**0.001**	0.14
ICV	1534285.7 (23565.70)	1548888.9 (27581.85)	1549787.2 (24917.05)	0.26	0.77			

All data were reported as mean (SEM); ANCOVA was controlled by age, sex, education, and ICV and corrected for multiple comparisons among 7 regions; Bold text indicates those with significant FDR value.

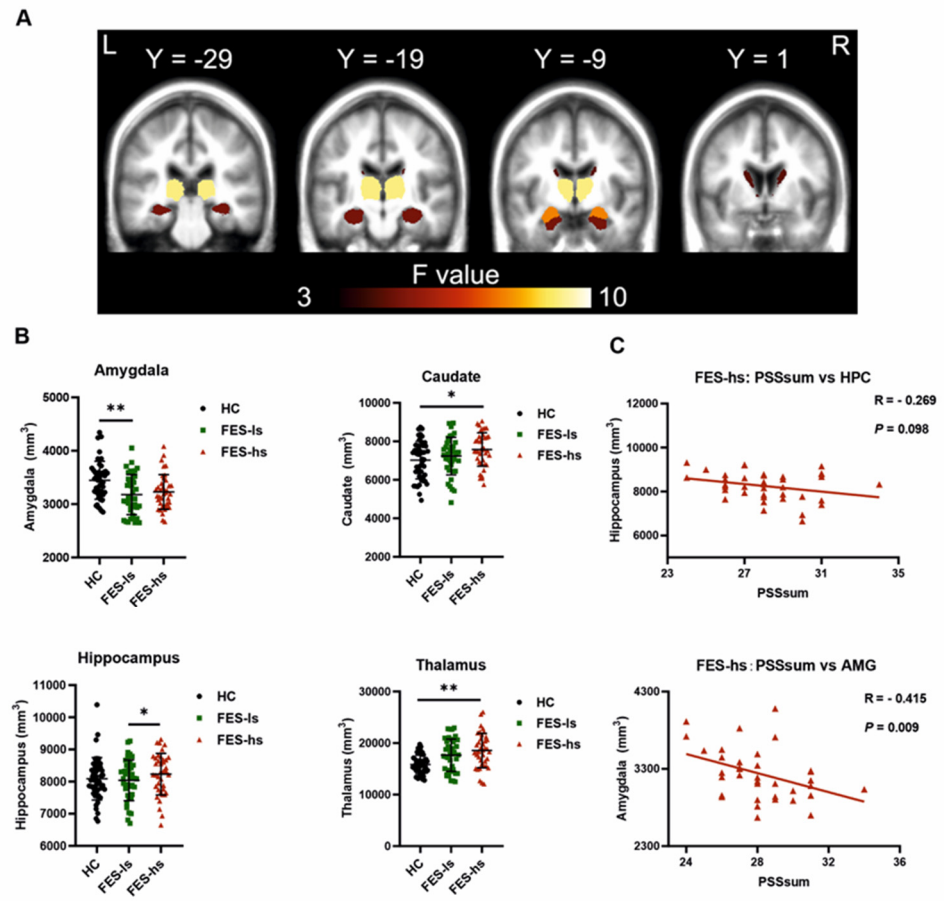

Fig. 16. Brain subcortical limbic structures among FES patients and HCs. (A) Colors in MRI image represent ANCOVA *F* value of group differences. Yellow = thalamus, orange =HPC, red = AMG, dark brown = caudate. **(B)** Volumes of the AMG, caudate, thalamus and HPC were different among FES-hs (n = 35) and FES-ls (n = 36) patients and HCs (n = 47), controlled by age, sex, education years, and ICV. * FDR < 0.05, ** FDR < 0.01 (ANCOVA). **(C)** Correlations of sizes of AMG and HPC with PSS scores in FES-hs patients (n = 35, Spearman's correlation). See also **Table S1.1** and **Fig. S1** of paper III.

5.3.3 Negative correlations of amygdaloid size with perceived stress in FES-hs patients

We further assessed correlations of the limbic structures with PSS scores and noted a negative relationship of amygdaloid size with PSS score in FES-hs patients (r = -0.415, p = 0.009, FDR = 0.04; **Fig. 16C, Table S1.1** of paper III) but not in other groups (**Fig. S1B & S1C** of paper III). There was a trend of

negative correlation between the hippocampal volume and the PSS score in the FES-hs group (r = -0.269, p = 0.098). In contrast, both amygdaloid (r = 0.31, p = 0.03, FDR > 0.05; **Fig. S1C** of paper III) and hippocampal (r = 0.419, p = 0.003, FDR = 0.01; **Fig. S1C** of paper III) volumes were positively correlated with the PSS score in HCs.

Thalamic sizes were negatively correlated with PANSS-G scores in the FES-hs patients while hippocampal sizes positively with PANSS-N scores in the FES-ls patients (FDR = 0.001 & 0.032, respectively; **Table S1.4** of paper III). No other significant correlations were found.

5.3.4 Blood *SEMA4s* and *PLXNB2* mRNA levels were higher in FES-ls patients

To figure out what target immune genes may contribute to the limbic structural changes in FES-hs and FES-ls patients, we first explored the peripheral blood cell RNA-seq data of the FES patients and HCs as described in Paper I. Interestingly, out of the clustered DEGs with GO terms for molecular functions, PLXNs and SEMAs stood out as the top-ranking clustered protein domain with transmembrane signaling receptor activity (GO:0004888) (**Table S2.1 & S2.2** of paper III). Notably, among the *PLXN/SEMA* family, *PLXNB2* and its ligands *SEMA4A/4B* were the most abundantly expressed members in the peripheral blood cells (**Table S2.3** of paper III).

We further repeated DEG analysis on the available RNA-seq counts of subjects in our current cohort (FES-hs = 44, FES-ls = 37, HC = 48), which showed in total 1247 DEGs with the upregulated SEMA4A and SEMA4B among them in the FES-ls and FES-hs groups (**Fig. 17A; Table S3.1** of paper III). Compared to the HCs, 1184 (472 up-regulated and 712 down-regulated) and 836 (405 up-regulated and 431 down-regulated) DEGs were obtained in the FES-ls and the FES-hs patients, respectively, while only 16 DEGs were differentiated between the two patient groups (**Fig. 17B**). Group-wise comparisons also noted 500 overlapping DEGs including the *SEMA4B* shared by both the FES-hs and the FES-ls patients as compared to the HCs, whereas the *SEMA4A* was upregulated only in the FES-ls patients (**Fig. 17B**). Pathway analysis showed that the 500 overlapping DEGs were mostly related to cancer biology and cell proliferation, while the FES-hs-specific 329 DEGs involved a small group of cytokine signaling genes and the FES-ls-specific 681 DEGs were engaged with leukocyte activation and innate immune response (**Table S3.2** of paper III). Between the two patient groups, the 16 nonoverlapping DEGs were related to *hemoglobin* and *glycophorin A* (**Table S3.2** of paper III). Although the *PLXNB2* did not show up in the 3 clusters of DEGs, it was differentially expressed between the FES and HC groups in the bigger cohort (FDR = 0.007, **Table S2.3** of paper III).

To exclude confounding effects of age, gender and education on gene expression, we further controlled these factors in group-wise comparisons and observed consistent upregulations of the *SEMA4A* and *SEMA4B* (**Fig. 17C**). It is noteworthy that their receptor *PLXNB2* was also upregulated in the FES-ls

patients compared with the FES-hs patients (FDR = 0.046; **Fig. 17C**). No significant changes in other *SEMA* and *PLXN* receptors were observed (**Table S3.1** of paper III). We next pursued the associations of *PLXN/SEMA* expressions with PSS scores and brain volumes.

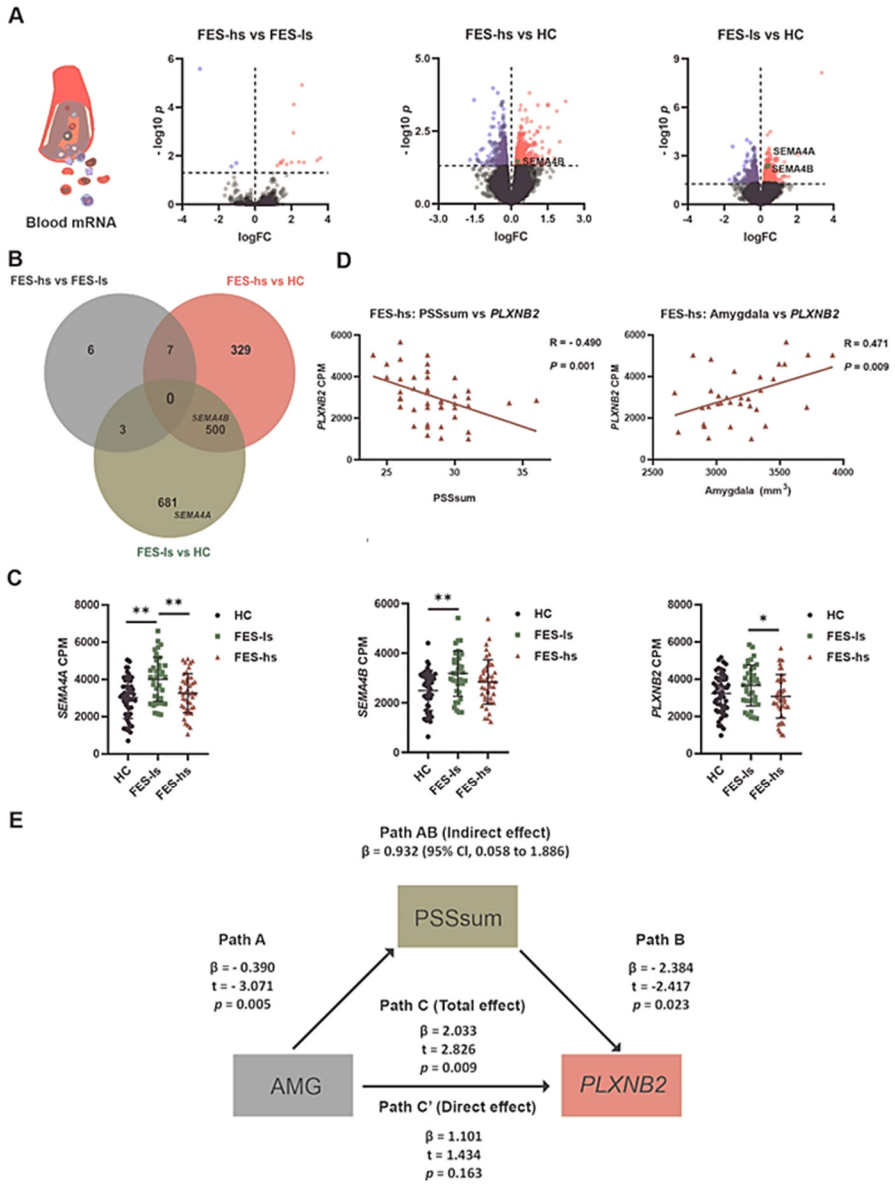

Fig. 17. Increased *SEMA4A*, *4B* and *PLXNB2* mRNA levels in FES-ls patients and amygdaloid association with *PLXNB2* expression mediated by stress perception in FES-hs patients. (A) Volcano plots represent pairwise comparisons for RNA-seq DEGs in peripheral blood of FES-hs (n = 44) and FES-ls (n = 37) patients versus HC (n = 48) individuals. Genes with FDR < 0.05 are colored (red: up-regulation; blue dots:

down-regulation). *SEMA4A* and *SEMA4B* are highlighted. **(B)** Venn diagram illustrates overlapping and group-specific DEGs. Circles denote genes, overlapping regions between circles denote respective shared genes among the groups. The upper histogram chart represents numbers of pairwise DEGs and the lower histogram chart represents numbers of overlapping and nonoverlapping DEGs. **(C)** Blood mRNA levels of *SEMA4A*, *SEMA4B* and *PLXNB2* in HCs, FES-ls and FES-hs patients, controlled by age, sex, and education. **(D)** Correlations of *PLXNB2* with PSS (Spearman's, $n = 44$) and with amygdaloid size (Pearson's, $n = 28$) in FES-hs patients, controlled by age, sex, and education. **(E)** PSS score mediated positive association between amygdaloid volume and *PLXNB2* in high-stress FES patients (Path AB), controlled by age, sex, and education. Path A represents a direct negative relationship of amygdaloid relationship with PSS. Path B represents a direct negative relationship of PSS score with *PLXNB2*. A path C' represents a direct relationship of amygdaloid volume with *PLXNB2*, while a path C represents a positive relationship of amygdaloid volume with *PLXNB2* when PSS score was considered, indicating a full mediation effect of PSS score. * FDR < 0.05, ** FDR < 0.01 (ANCOVA). See also **Tables S1.2 & S1.3** and **Fig. S1** of paper III.

5.3.5 Perceived stress mediated positive association between amgdaloid volume and blood *PLXNB2* expression in FES-hs patients

By incorporating the RNA-seq, MRI, and symptom data, we found that blood mRNA level of *PLXNB2* was negatively correlated to PSS score in FES patients groups ($r = -0.337$, $p = 0.002$; **Fig. S2A** of paper III), especially in FES-hs patients ($r = -0.490$, $p = 0.001$, FDR = 0.003; **Fig.17D; Table S1.2** of paper III), but not FES-ls and HCs (**Fig. S2B & S2C**). Conversely, there was a significant positive correlation between the *PLXNB2* and the amygdaloid volume in all the FES patients ($r = 0.228$, $p = 0.035$; **Fig. S2E** of paper III) and in the FES-hs patients (partial $r = 0.471$, $p = 0.009$, FDR = 0.04; **Fig. 17D, Table S1.3** of paper III), after controlling age, gender, and education, but not in the FES-ls patients and HCs (**Fig. S2F & S2G ; Table S1.3** of paper III). Antipsychotic dosages were not correlated with the *PLXNB2* levels in both patient groups and no significant correlations with the PSS and PANSS scores were found on *SEMA4A* and *SEMA4B* (**Table S1.2 & S1.5** of paper III).

As blood *PLXNB2* expression could be a sensitive molecular substrate of stress, which is regulated by the AMG, we performed a mediation analysis predicting that brain structural deficit underlies the stress-induced *PLXNB2* expressional changes in the FES patients, i.e., the amygdaloid volume as the independent variable, the *PLXNB2* mRNA level as the dependent variable, and the PSS score as the mediator, controlled by age, gender, and education (**Fig. 17E**). The direct effect on the association of the amygdaloid volume with the *PLXNB2* as denoted by a Path C' was insignificant, whereas the total effect on the association as denoted by a Path C, when the PSS score was introduced as a mediator (path AB: $\beta = 0.9318$, 95 % CI: 0.058 – 1.886), was significant ($p = 0.009$, **Fig. 17E**). The model hence suggested a positive effect of the AMG on the PLXNB2, which was fully mediated by the PSS score in the FES-hs

patients. However, no such effects existed in the FES-ls or HCs and neither for the *SEMA4A* and *SEMA4B*.

5.3.6 Plxnb2 was enriched in glial cells and decreased by CUS in mice

To further understand the role of Plxnb2 in stress response and the underlying brain mechanism, we next investigated animal CUS models. We first explored available online brain RNA-seq databases, showing enrichment of the *PLXNB2* in human/murine microglia as compared to the other brain cell types (**Fig. S3A** of paper III). We also explored a GEO dataset on isolated murine microglia from different developmental stages [284], showing that the *Plxnb2* was stably expressed in microglia from E16.5 onward (**Fig. S3B** of paper III). Besides, murine astrocytes also highly expressed the *Plxnb2* (**Fig. S3C** of paper III). To confirm this and to understand the stress effect, we next studied Plxnb2 expression using the CUS mouse model in flow cytometry (**Fig. 18A**). The Plxnb2 was enriched in hippocampal glial cells, especially in astrocytes and microglia (**Fig. 18A & 18B**), but much less so in nonglial cells (e.g., neurons).

In the CUS condition, no significant interaction between the CUS and the cell type was observed (data not shown), but there was a main effect of the CUS ($p = 0.004$) ($n = 7 + 7$). The Plxnb2 expressions in the astrocytes ($p = 0.020$; **Fig. 18B**) and nonglial ($p = 0.004$; **Fig. 18B**) were decreased after the CUS compared to the Ctr, whereas no changes were observed in the microglia and macrophages (**Fig. 18B**). Considering that astrocytes and nonglia represent the great majority of adult brain cells, this result indicates that Plxnb2 was overall downregulated in the brain by the CUS. We also measured *Sema4a* and *Sema4b* mRNA levels in the CUS model but did not find significant changes in them (data not shown).

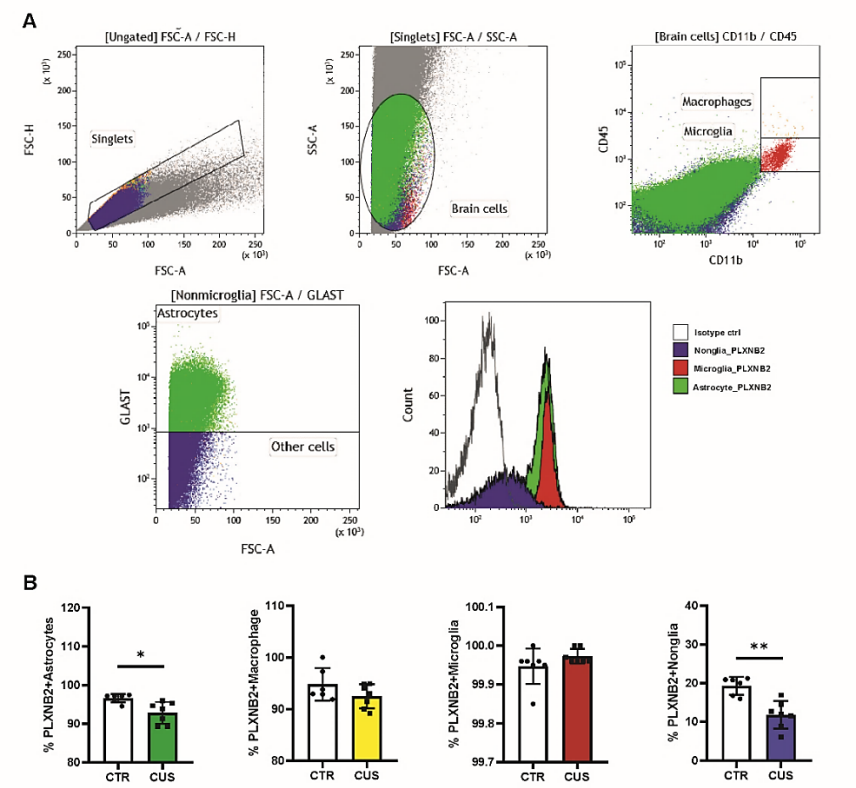

Fig. 18. Mouse Plxnb2 expression in glial and nonglial cells after chronic unpredictable stress (CUS). (A) Flow cytometric staining of brain cells in the HPC are illustrated in representative gating dot plots. Cell populations stained by Plxnb2-specific antibody and isotype antibody are shown in overlaid histograms. **(B)** Population of Plxnb2-expressing astrocytes, macrophage, microglia and nonglial cells were compared. Plxnb2 was enriched in glia and showed decrease in CUS group (n = 7 mice) compared to the control (CTR) group. * $p < 0.05$; ** $p < 0.01$ (Student's t-test). See also **Fig. S3** of paper III.

5.3.7 Plxnb2 blocking in the amygdala (AMG) induced anxiety behavior in mice

Based on the above data, we postulated that Plxnb2 in the AMG may regulate stress response or anxiety. To test this, we selected a blocking antibody (mAb102) that targets extracellular epitope of both the human and mouse PLXNB2 with high affinity. The half-maximal effective concentrations of (EC50s) for the mAb102's binding to CHOK1 cells expressing the human and mouse PLXNB2 were 1.0 nM and 2.2 nM, respectively (**Fig. S4A** of paper III). Functionally, the mAb102 was able to inhibit the binding of ANG and SEMA4C, two ligands of the PLXNB2, to CHOK1-PLXNB2 cells, with the half-maximal inhibitory

concentrations (IC50s) of 10.6 nM and 13.2 nM, respectively (**Fig. S4B** of paper III).

We injected 10 ng of the mAb102 or saline into each AMG per mouse (n = 8 + 9). Five days later, we studied anxiety behaviors in OFT and EPM, followed by alive animal brain MRI scan, and by flow cytometry and IHC upon animal sacrifice (**Fig. 19A**).

In the OFT, total travel distance showed no group difference, indicating equivalent locomotor activity among treated animals (**Fig. 19B**). While time spent in the central zone had no group difference (**Fig. 19C**), time spent in rearing was longer in mAb102-treated mice than in saline-treated mice (p = 0.04; **Fig. 19D**). Moreover, the mAb102 group showed shorter time spent on open arms in the EPM test (p = 0.039; **Fig. 19E**).

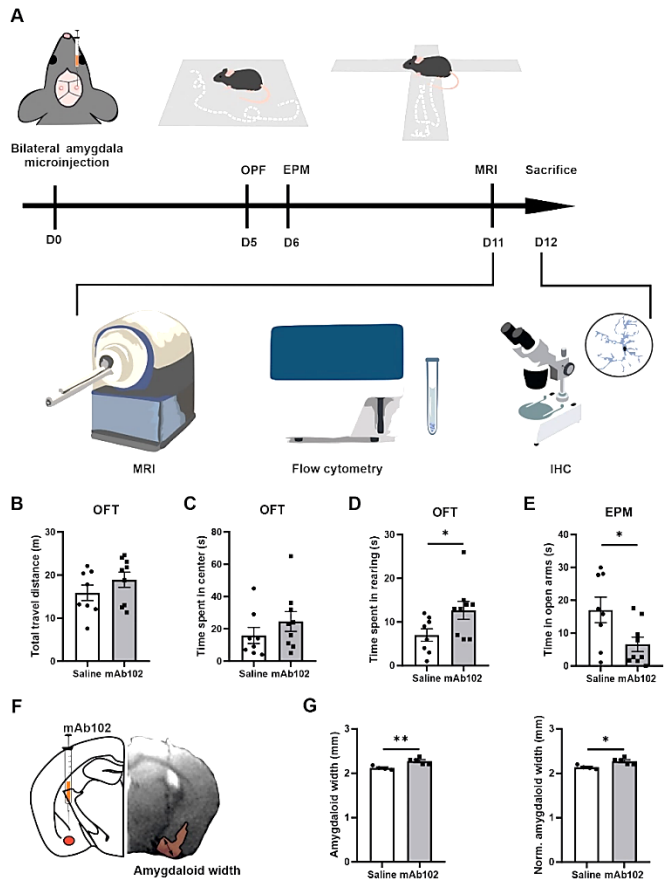

Fig. 19. Anxiety-like behaviors in mice and quantification of amygdaloid width. (A) Schematic diagram of experimental design. 0.5 µl mAb102 (10 ng, n = 9 mice) or saline (n = 8 mice) was injected in each AMG of mice bilaterally and OFT and EPM test were conducted on the 5th and 6th day after the operation, respectively. Mice were later sent

for MRI scan. The brains were collected for flow cytometry and IHC. **(B-D)** In OFT, total travel distance, time spent in the central zone and in rearing by mice highlighted anxiety-related exploration of mAb102-treated mice. **(E)** Time spent in EPM open arms indicated enhanced anxiety in mAb102-treated mice. See also **Fig. S4** of paper III. **(F)** Intra-AMG injection site is illustrated in representative brain coronal diagram and the corresponding MRI image of injection is shown, with the measured amygdaloid width indicated. **(G)** Amygdaloid width before and after normalization with the maximal brain width showed increase in mAb102 group (n = 5 mice) compared to saline group (n = 4 mice). * $p < 0.05$; ** $p < 0.01$ (Student's t-test).

5.3.8 Plxnb2 blocking in the AMG resulted in amygdaloid enlargement and glial activation

Measuring amygdaloid size in MRI images (**Fig. 19F**), we found theamygdaloid width was increased in mAb102 group compared to saline group (p = 0.006; **Fig. 19G**) (n = 4 + 5), which stayed significant after normalization with the brain width (p = 0.011; **Fig. 19G**). Staining of brain sections with IBA1 and GFAP (**Fig. 20A**) (n = 3 + 3) showed that although the number of IBA1$^+$-microglia had no group difference (**Fig. 20B**), the average IBA1 intensity was higher in the mAb102 group ($p < 0.05$; **Fig. 20C**). In comparison, the number of GFAP$^+$-astrocytes was decreased in the mAb102 group ($p < 0.05$; **Fig. 20D**), while the average GFAP intensity showed no group difference (**Fig. 20E**).

Interestingly, microglia in the mAb102-treated mice were over-ramified, showing longer total branch length, shorter average branch length and more tips (all $p < 0.001$**; Fig. 20F–H; Table S4** of paper III). Astrocytic morphology didn't show striking differences in these parameters (**Fig. 20I–K**) but displayed shorter length of inner branches in the mAb102 group (p = 0.034; **Table S4** of paper III), hence a tendency of de-ramification.

Moreover, flow cytometric analysis of amygdaloid tissues (**Fig. 20L**) (n = 7 + 7) showed that in microglia, while the total population did not differ (**Fig. 20M**), the percentage of MHCII$^+$-microglia was decreased in the mAb102 group (p = 0.026; **Fig. 20N**). By contrast, total astrocytes and MHCII$^+$ astrocytes did not change in the mAb102 group (**Fig. 20O & 20P**). We also measured cytokines *Il1b*, *Il6*, and *Il10* mRNA levels but did not find significant differences in them between the mAb102 and saline groups (data not shown).

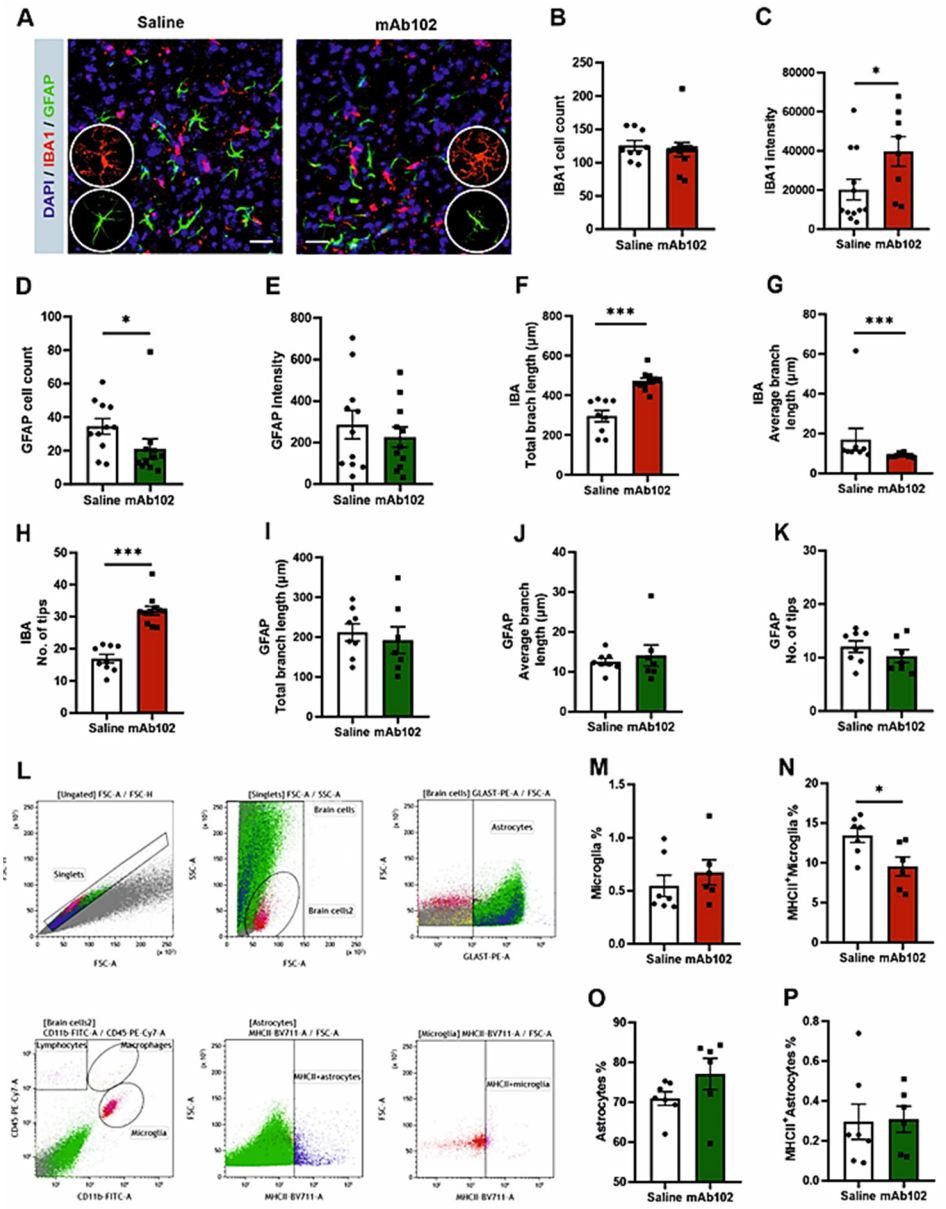

Fig. 20. Quantification of amygdaloid width and glial responses in saline- and mAb102-injected mice. (A) IBA1 and GFAP immunostainings for microglia and astrocytes, respectively, are shown in immunohistochemical images. Scale bar = 10 µm. Zoomed images showing morphologies of microglia and astrocytes are inserted. **(B–E)** $IBA1^+$ and $GFAP^+$ cell number and intensity were quantified (n = 11 + 11 slices from 3 + 3 mice). **(F–K)** Morphological parameters of $IBA1^+$ (n = 9 + 11 slices from 3 + 3 mice) and $GFAP^+$ (n = 8 + 7 slices from 3 + 3 mice) cells were quantified, including total branch length, average branch length, and number of tips. Microglia were more ramified and had increased IBA1 whereas astrocytes were less responsive in mAb102

group than their counterparts in saline group. See also **Table S4** of paper III. **(L)** Gating strategy for flow cytometry is shown. Debris and cell aggregates were excluded using correlation of FSC area vs height. For visual comparison, astrocytes and microglia were colored and identified as $GLAST^+$ and $CD45^+CD11b^+$ cells, respectively. **(M-P)** The main populations of astrocytes, $MCHII^+$ astrocytes, microglia and $MCHII^+$ microglia are shown, from which the population of $MCHII^+$ microglia underwent significant reduction in mAb102 group (n = 7 mice) compared to saline group (n = 6 mice). * $p < 0.05$; *** $p < 0.001$ (Student's t-test or Mann-Whitney U test).

6 DISCUSSION

6.1 Monocyte/microglia-associated immune genes in schizophrenia

6.1.1 Monocytic differentially expressed genes (DEGs) in FES (paper I)

We studied peripheral blood by flow cytometry and RNA-seq to probe monocytic functions in FES patients, providing the first evidence to our knowledge that altered monocytic functions may be implicated in the pathogenesis at early stage of schizophrenia. Recent transcriptomic studies using the blood, postmortem brains, and patient-derived cerebral organoids generated from induced pluripotent stem cells have also demonstrated dysregulated inflammation and immune functions in FES[125–127,140–143,146,147]. Particularly, a recent study on monocytic genes found involvement of multiple innate immune pathways in schizophrenia[143].

To scrutinize specific monocytic functions with higher detail, we categorized the DEGs according to different monocytic subtypes. We found that more DEGs fell into the intermediate and nonclassical monocytes compared to the classical subset in the patients, suggesting that biological functions of these two subpopulations may be more affected. We speculate that the aberrant expressions of the candidate intermediate and nonclassical mono-DEGs and the looser intra-correlations among these monocytic DEGs in the patients may be due to maladapted monocytic subset functions in FES patients, as discussed below.

Nonclassical monocytes play an important role in maintaining vascular homeostasis[54] and earlier studies demonstrated that patients with schizophrenia had vascular endothelial pathologies due to chronic low-grade systemic inflammation[285,286]. This possibly leads to recruitment of nonclassical monocytes into the brain to repair parenchymal vascular endothelium, resulting in nonclassical monocytopenia in the peripheral blood along with altered mono-DEGs involved in leukocyte migration, as we found in the FES patients. Similar observation was reported in patients with severe forms of lupus nephritis, showing that lower levels of nonclassical monocytes in the peripheral blood were accompanied by a higher degree of infiltrates of $CD16^+$ cells in the glomerulus[285].

Alternatively, accelerated monocytic immune senescence or inflammation may occur, similarly as the coexistence of myeloid functional deficiencies and increased myelopoiesis during aging[287]. Indeed, nonclassical monocytes were found in a pro-inflammatory state of senescence after stimulation by a recent study[55], while Uranova et al.[142] found that the area and number of lysosomes of monocytes were significantly increased in patients with schizophrenia as compared to HCs. This postulates a provocative concept that schizophrenia may be an inflammaging disorder, as supported by our finding that proinflammatory nonclassical monocytic genes, such as the IFITM family members, were up-

regulated in FES patients. Upregulation of IFITM family members is corroborated by earlier studies of the blood and postmortem brains of patients with schizophrenia, especially in the PFC, HPC, and cortical blood vessels, independent of antipsychotic use[126,128–131]. IFITM2/3 proteins, which are mainly localized to late endosomal/lysosomal membranes, have been shown to restrict a broad range of viral entry and replication, such as the influenza A virus and cytomegalovirus[288,289], it is therefore plausible that dormant or reminiscent viral infection may be associated with schizophrenia pathogenesis[118,119,290].

Recent genetic research has highlighted contribution of CpG epigenetic changes in inflammatory genes to psychotic conversion in young adults[291]. Interestingly, among the DEGs belonging to classical monocytes, most were downregulated in our FES patients. Likewise, in intermediate monocytes, downregulations of the myeloid alarmin-related S100A genes (S100A8, S100A9, and S100A12) in patients were the most notable changes. Previous studies have reported increased S100A8/9/12 gene expression in the peripheral blood cells, PFC, and HPC of individuals with schizophrenia[126,132,133]. The inconsistency with our results is possibly due to chronicity of the disease and antipsychotic medication in those studies.

Taken together, our results highlight that not only global monocytic functions but also their subtypes may be more specifically affected in schizophrenia, which should not be neglected in this field of research.

6.1.2 Immune system developmental DEGs changed in FES (papers II, III)

Molecules belonging to immune signaling pathways have been extensively shown to be involved in neurodevelopment and neuronal functioning in association with schizophrenia[6,7].

We found 181 human blood DEGs involved in immune system development, including those expressed in microglia, such as *SPI1, PTPRC, TLR3, TLR9, HSPD1, SOD2, PML, REST* (**Table S7** of paper III). *SPI1*, also known as PU.1, regulates development of B lymphocytes, macrophages, and monocytes[292,293]. Point mutation in *PTPRC*, encoding altered CD45, is associated with MS[294]. *TLRs* are important in maturation of dendritic cells, which play a central role in bridging the innate and adaptive immune responses[295]. *HSPD1* is a novel interferon regulatory factor 3 (IRF3)-interacting protein involved in pathogenesis of a variety of autoimmune diseases and schizophrenia[296,297]. *SOD2* is associated with mitochondrial functions and affects hematopoietic stem cells[298]. *PML* is primarily known for its involvement in acute promyelocytic leukemia[299] and regulation of hematopoiesis[300]. *REST* helps maintain genes involved in immune system homeostasis[301].

To our particular interest, the immune developmental DEGs also included *PLXNB2,* which is expressed in various immune cells and participates in immune developmental processes such as T cell recruitment in the germinal center of the spleen[110]. In addition, some other PLXNs and SEMAs have been

implicated in schizophrenia previously[247–251]. In our results (paper III), we demonstrated that blood mRNA levels of *PLXNB2* along with its ligands *SEMA4A* and *SEMA4B* were upregulated in FES patients with lower perceived stress (FES-ls), and *PLXNB2* showed the lowest level in FES patients with higher perceived stress (FES-hs) compared to FES-ls patients and HCs. Our result is the first clinical study demonstrating the importance of *PLXNB2* with its ligands *SEMA4A* and *SEMA4B* in stress perception of schizophrenia patients.

6.2 Association of immune DEGs with cognition and stress in schizophrenia

6.2.1 Associations of monocytic subset DEGs with cortical thickness and cognition in FES (paper I)

Our further finding was that FES patients exhibited widespread cortical thinning, primarily in the parietal, occipital and temporal cortices, which agrees with previous studies in FES patients and suggests that extensive cortical gray matter loss has taken place in the early phase of illness. Cortical thickness reduction, which reflects neuronal/glial dystrophy and/or loss of synapses, is a consistent structural MRI finding in schizophrenia congruently shown by others and us[22,302,303]. However, unlike prior studies, we did not detect differences in the frontal and cingulate regions, possibly because we averaged the left and right hemispheres in our study.

We found inverse correlations of the percentage of the blood nonclassical monocytes with the cortical thickness especially in the temporal lobe of the patients but not healthy participants, implying that the patients' cortical dystrophy may require more infiltration of nonclassical monocytes for tissue repair. However, since the temporal lobe is a significant part of the limbic system that is known to regulate genesis and mobilization of myeloid cells[176], temporal cortical dystrophy may cause disturbance in this process in patients, causing nonclassical monocytes lingered in the blood of those patients with severe cortical dystrophy. It may also be possible that these negative correlations are attributed to the pro-inflammatory side of the nonclassical monocytic features, as mentioned above. These speculative accounts deserve further investigation.

Little is known about the monocytic effect on the schizophrenic brain currently. Nevertheless, as mentioned before, lowered expressions of *IFITM3* in the PFC[6] and *CSF1R* in the corpus callosum[144] were observed in individuals with schizophrenia. By contrast, IRF genes that affect monocytic activity were observed to be upregulated in the HPC of individuals with schizophrenia[128].

Research findings in other fields may also be enlightening. A recent study reported that higher plasma monocyte activation markers sCD14 and sCD163 were associated with smaller frontal and temporal cortical volumes among women with HIV[304]. Moreover, chemokine receptor CCR2 on intermediate monocytes was correlated with disturbances of neuro-metabolites in the right

and left caudate nucleus, contributing to HIV-associated neurocognitive disorders[305]. Another related important research field is Alzheimer's disease. Recently, disease-associated microglial subset implied in amyloidosis and cognitive impairment have been depicted in Alzheimer's disease patients through single-cell RNA-seq[306,307]. Several highly significant monocytic DEGs found in our current study, such as *CCR5, CLEC7A, CTSS, IFITM3,* and *ITGAX*, are associated with such microglial subtype. Also, a relationship between monocyte-derived inflammation and hippocampal atrophy as well as cognitive decline in Alzheimer's disease had been reported[308].

Intriguingly, with a data-driven approach here, we detected negative inter-relationships existing between monocytic DEGs and cortical thicknesses as well as between monocytic DEGs and cognition in the HCs. Furthermore, the negative inter-relationships were weakened in schizophrenia patients as compared to the HCs. These indicate that firstly, monocytic subsets in the peripheral blood may negatively impact brain and cognition in the HCs; secondly, a functional alteration of some subsets of monocytes (e.g., inflammaging of non-classical monocytes) with a compensatory mechanism of some other subsets of monocytes (e.g., down-regulation of genes in classical and intermediate monocytes) may occur in the FES patients in the early stage of the disease.

Notably, among the DEGs associated with cortical thinning in both study groups, the classical monocytic gene *RNASE2* was the most striking one. The protein encoded by *RNASE2* is a cytotoxic protein that can induce proinflammatory cytokine production in monocytes/macrophages by acting as a DAMP[309]. It causes severe damage to myelin and loss of neurons in the rabbit brain, an event known as the Gordon phenomenon[310]. Possibly, a highly inverse association between *RNASE2* and lateral occipital cortical thickness in our FES patients may suggest that their thinner lateral occipital cortex may be particularly vulnerable to the neurotoxic effects of *RNASE2*, while the downregulation of *RNASE2* in patient group hints a self-protective response of host.

6.2.2 Association of immune DEGs with limbic structures and PSS score in FES (papers II, III)

In our results (paper II), ~25 % of blood immune developmental DEGs were significantly correlated negatively with PSS score but positively with the volume of right hippocampal fimbria. This reveals a close link between the immune and nervous systems that can be impacted by stress during development. Our results support the notion that early immune system maldevelopment combined with brain abnormality may contribute to schizophrenia[116,117]. The results also corroborate previous evidence on the association between childhood trauma and inflammatory phenotype in schizophrenia[172,173], indicating that immune alterations in patients may be due to stress hypersensitivity caused by early life adversities. Additionally, we found that *KCNQ1*, encoding a potassium channel and as a known risk gene for schizophrenia[311,312], was elevated in our FES patients and CUS+repMg-exposed animals. This upregulation is

possibly a compensational mechanism for stress adaptation in schizophrenia. Indeed, its correlation with both PSS score and fimbria volume implies it as a nexus between microglia and stress-regulation in schizophrenia. Overall, our results imply that reprogramed microglia in animals may recapitulate changes in myeloid developmental process shown in our FES patients, which may negatively impact hippocampal development.

In paper III, we surprisingly found that FES-hs patients who were more sensitive to stress did not show significant differences in amygdaloid size and PLXNB2 expression as compared to HCs. This suggests that the amygdala-dependent stress-coping neurobiological machinery used by this group of patients may be somewhat like the HCs. Nevertheless, they may still differentiate from the HCs in utilization of stress-coping machinery. Indeed, the other limbic structures, namely the caudate and thalamus, were significantly bigger in these patients than the HCs, indicative of the higher demand of energy for somatosensory processing needed for stress perception and handling in these patients. Corroboratively, their PANSS-G score was higher and their thalamic size was negatively correlated with the PANSS-G score, hence demonstrating the involvement of the thalamus in psychopathology in this group of patients. Of note, lower stress level and larger amygdaloid size were associated with higher *PLXNB2* mRNA level in the FES-hs patients.

By contrast, FES-ls patients who were less sensitive to stress even compared with the HCs, showed the smallest amygdala and the highest level of *PLXNB2* expression. Furthermore, no correlations of perceived stress with *PLXNB2* expression and amygdaloid size were found in them. These hint a different and perhaps more complicated psycho-neurobiological machinery was used by these patients, disengaging the amygdala with other limbic structures and furthermore dispensable with *PLXNB2*. Interestingly, their hippocampi were smaller than those of the FES-hs patients and were positively correlated with PANSS-N scores, hence indicative of impaired hippocampal connection with other limbic regions and irregular cognition-dependent emotional processes in this unique group of FES-ls patients.

6.3 Microglia in regulation of stress response

6.3.1 Microglial depletion and replenishment in stress context (paper II)

We found that after microglial depletion and replenishment, e.g., repMg, animals showed enhanced anxiety similarly as in CUS condition, and repMg couldn't rescue CUS-induced anxiety. As anxiety is the foundation for animals to survive and adapt to stress behaviorally, its reset due to repMg is understandable. Notably, CUS-triggered social withdrawal and depressive-like behavior were partially or fully recovered after microglial renewal in our experiments. Currently available studies have given mixed results, with some showing

harmful effect of microglial ablation or repopulation on psychiatric-like behaviors[226–228], while others showing no or beneficial effect[203,221–225,229,231,234] in various chronic stress models. This suggests an intricated brain immune environment in psychiatric conditions. Besides, only a few animal stress-modeling papers performed microglial repopulation experiment[221–223,226], while many studies did not arrange such approach[203,224,225,228,230,231,234]. Thus, our study filled the knowledge gap of how replenished microglia behave in CUS condition that is highly relevant to schizophrenia.

Our results on flow cytometry showed that mice of CUS+repMg group had a higher percentage of hippocampal microglia than those of repMg group, indicating that in CUS context, stressed microglia that survived the CSF1Ri-induced ablation may have been more sensitive to the loss of their peers in neighborhood and may have proliferated or migrated faster to fill the empty space. CUS-induced inflammatory environment may also have provided proliferative or migratory cues to replenishing microglia. Thus, microglial replenishment may be transiently accelerated by the CUS. It should however be pointed out that we only studied microglial replenishment after 14 days of recovery from ablation. It is unclear what would be the long-term effect of CUS on microglial recovery, which is worth addressing in the future. Other studies have shown that chronic stress could increase regional microglial density in IHC, possibly due to increased microglial proliferation and/or accumulation[313,314]. In the present study, we did not observe gross increase of microglia by CUS alone compared to Ctr, which suggests the effect may be dependent on stress model and duration, as has been pointed out by earlier studies[202,314].

6.3.2 Synaptic pruning of glia cells (paper II)

Friton et. al proposed the synaptic disconnection hypothesis in 1990s, specifically on the modulation of synaptic plasticity in those brain areas responsible for learning, memory, and emotion[154]. The latest synaptic hypothesis has postulated that specific synaptic loss contributes to certain psychotic and cognitive deficits in schizophrenia[4].

Exaggerated glia-dependent synaptic pruning is known to contribute to neurodevelopmental disorders including schizophrenia[149,150]. Among the molecular machineries for glia-mediated synaptic pruning, increased C4 copy number variants is genetically linked to schizophrenia [168]. Preclinical data also link stress to immune activation and synaptic loss. Microglia phagocytose neuronal elements and contribute to structural and functional remodeling of neurons in chronic stress [149,150]. Our result on RNA-seq of the PFC directed us to investigate microglial synaptic pruning by IHC and flow cytometry. In our CUS model, stressed microglia showed excessive engulfment of SYP and Vglut2 along with hyper-ramified morphology, which could be reversed by repopulated microglia. Remarkably, we found CUS also enhanced Vglut2 pruning of astrocytes and OPCs, both known important regulators of synaptic/axonal functions in psychiatric disorders[150]. Moreover, we found microglial repopulation restored

expression of brain developmental genes changed by CUS. Attenuation of astrocytic pruning by microglial repopulation after CUS could be due to dampened neuroinflammation, which helps restore glutamate metabolism in astrocytes, as has been suggested[149,150].

6.3.3 Stress and microglial hyper-ramification (papers II, III)

Hyper-ramification of microglia suggests exaggerated immune response[195,196] and synaptic loss[197]. Stress-induced over-ramification of microglia has been constantly observed by others and us[193,194]. Ramification of microglia usually indicates enhanced surveillance of the changing surrounding environment, such as changes in neurotransmission underlying anxiety behaviors[194,202]. In consistent with the previous studies, we observed CUS-conditioned microglia had a larger ramification index and longer total branch length, compared to Ctr (paper II). And no differences were found in the number of branches among the groups.

In our paper III, we found mAb102 injection in the AMG resulted in enhanced anxiety, amygdaloid enlargement, hyper-ramification of microglia, and decreased $MHCII^+$ microglia population in the AMG. It is plausible that mAb102 directly affected microglial Plxnb2, but whether it may also affect neurons, as Paldy et al. demonstrated [105], which then indirectly induce microglial morphological changes and anxiety behavior, is considerable. Besides, since astrocytes are also important for brain and behavior, dysfunctional astrocyte-microglia crosstalk contributes to microglial activation and neuroinflammation pertaining to pathogenesis in schizophrenia[150,151]. In this sense, although we did not observe overt changes in number and morphology of astrocytes by mAb102, we did find reduced $GFAP^+$ astrocytes. Therefore, the potential contribution of astrocytic Plxnb2 to schizophrenia and stress disorders is worth pursuing more carefully in the future.

6.3.4 Microglial Plxnb2 in stress regulation

In paper III, inhibition of Plxnb2 in the AMG induced anxiety in mice, which spent shorter time on open arms in EPM. Along with clinical data showing that *PLXNB2* expression was at the lowest level in FES-hs patients compared with FES-ls patients and HCs, this suggests that Plxnb2 could dampen stress and anxiety.

Plxnb2 was previously shown to regulate fear memory by mediating fear-induced hippocampal functional plasticity and dendritic and synaptic density in adult mice [105]. Moreover, deletion of *Plxnb2* dampened nociception induced by chronic inflammatory pain in mice[109], which is known to lead to stress and anxiety in animals, thereby implying a protective role of Plxnb2 in inflammatory pain. Altogether, these suggest the potential role of microglia and the myeloid receptor Plxnb2 in stress regulation in schizophrenia.

6.4 Limitations of our studies

It is essential to acknowledge several limitations in the current studies. Firstly, the cross-sectional nature and small sample size in our clinical cohorts in these papers limit the generalizability of the findings. Secondly, patient stratification based on their inflammatory profiles, which we missed in doing so, may better reveal the intricate relationships among stress, immune activation, and psychosis. Thus, this is worth pursuing in the future. Additionally, the transcriptomic changes identified in the studies were not exclusively attributed to specific cell types, prompting the need for more advanced approaches, such as single-cell RNA-seq, in the future. Consideration should be given to the possible anti-inflammatory role of antipsychotic medications, as most patients had short-term exposure, primarily to risperidone. Future studies, particularly those involving drug-naïve patients, should explore the impact of antipsychotic medications on peripheral inflammatory cytokines. Lastly, paper III lacked an mAb control group, and depiction of potential neuronal and other glial changes in animal experiments was not fully performed. These limitations underscore the need for caution in interpreting the results and highlight areas for improvement in future research endeavors.

CONCLUSIONS

I. This study aimed to address how monocytic subsets regulated brain and cognition in human subjects. We showed that (1) Nonclassical monocytes were decreased and monocyte-related transcriptomic profiles showed significant changes in FES, especially for intermediate and nonclassical monocytic subsets, with the most outstanding alterations being downregulated S100A and upregulated IFITM family members belonging to the intermediate and nonclassical monocytes, respectively; (2) Inverse inter-relationships of monocytic DEGs with cortical thicknesses and cognition existed in HCs, which was ameliorated in FES patients; meanwhile, the percentage of nonclassical monocytes was negatively associated with the thicknesses of multiple brain cortical regions in FES patients; (3) The lateral occipital cortex fully mediated a negative effect of a classical monocytic gene *RNASE2*, encoding an eosinophil-derived neurotoxin, on visual learning and memory in the FES patients.

II. This study aimed to address how microglia may benefit the brain and psychiatric behaviors in a stressful context after they were reprogrammed in animals and whether this may recapitulate immune mechanism underlying FES. Our main findings include: (1) Microglial renewal partially rescued CUS-triggered deficits in behavior and brain developmental processes such as axonal/synaptic formation, which is modulated by glial cells; (2) FES patients showed higher stress sensitivity along with smaller hippocampal structures and changed expressions of blood genes involved in immune development.

III. This study aimed to address how microglia mediated stress-induced neuroinflammation and the modulatory role of glial Plxnb2 in animals and FES patients. Our main findings include: (1) In FES-hs patients, lower stress level and larger amygdaloid size were associated with higher PLXNB2 mRNA level; (2) CUS induced a downregulation of Plxnb2 expression in the mouse brain, and inhibition of Plxnb2 induced anxiety as well as amygdaloid enlargement and microglial ramification in mice.

These findings suggest that subsets of monocytes, representing circulatory counterparts of brain-residential microglia, as well as monocytic subset genes, may be detrimental for brain and cognition in healthy controls, but they may develop an (mal)adaptive inflammation-related mechanism while trying to alleviate brain and cognitive dysfunction in FES. Inside the brain, microglial reprogramming may benefit animals in stress response through modulating biological processes underlying the development of the PFC and HPC. Furthermore, amygdaloid microglial activation may contribute to stress and anxiety, which may be leveraged by Plxnb2, as a novel cellular and molecular mechanism in stress regulation of individuals of schizophrenia with different stress traits (**Fig. 21**). Overall, these findings provide valuable insights into the intri-

cate connections between stress, monocytic/microglial functions, and symptomatic outcomes in schizophrenia, offering potential new avenues for further research and therapeutic interventions in tackling this disorder.

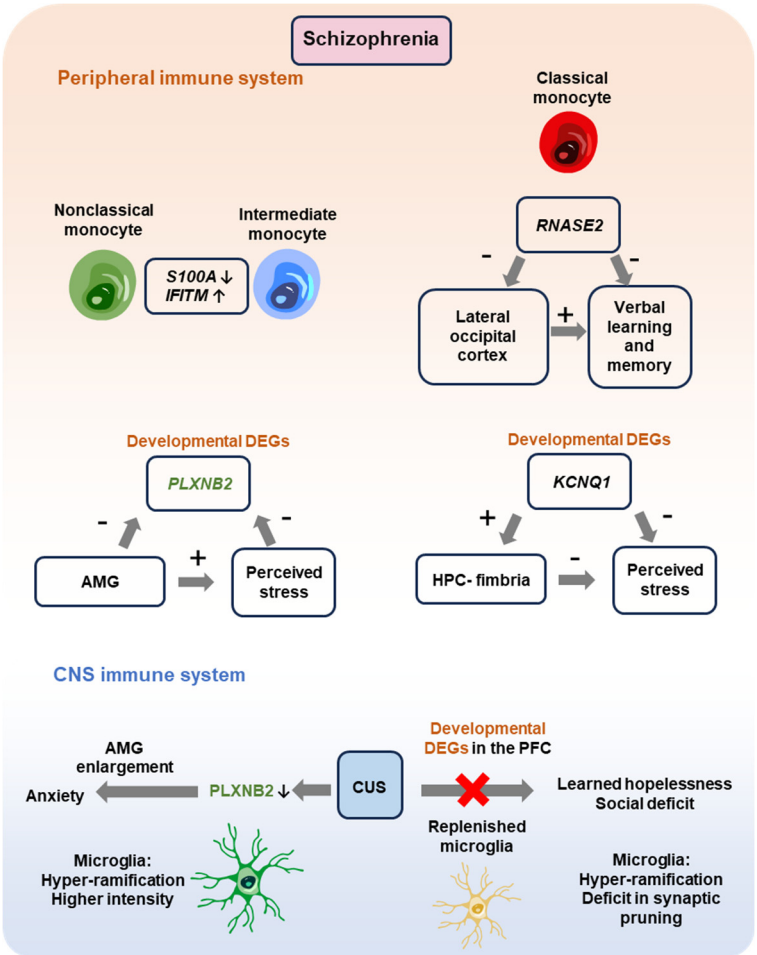

Fig. 21. Monocytic and microglial modulators in stress-associated brain and cognitive deficits in schizophrenia. In the periphery, blood nonclassical/intermediate monocytic DEGs, such as *S100A* and *IFITM*, were altered in FES patients, and the classical monocytic DEG *RNASE2* expression was correlated negatively with the thickness of the lateral occipital cortex and verbal learning and memory. Furthermore, immune developmental DEGs including *PLXNB2* and *KCNQ1* were involved in the associations of the AMG and the HPC with perceived stress, respectively. In the CNS, CUS dampened the expression of Plxnb2 in microglia and astrocytes along with AMG enlargement and microglial activation, which ultimately contributed to enhanced anxiety in mice. Moreover, replenished microglia rescued CUS-induced depressive-like behaviors via modulating expressions of developmental DEGs as well as microglial hyper-ramification and synaptic pruning in the PFC of mice. AMG: amygdala; CNS: central nervous system; CUS: chronic unpredictable stress; HPC: hippocampus.

REFERENCES

1. McCutcheon, R.A., Marques, T.R. & Howes, O.D. Schizophrenia-An Overview. *Jama Psychiatry* **77**, 201–210 (2020).
2. Stepnicki, P., Kondej, M. & Kaczor, A.A. Current Concepts and Treatments of Schizophrenia. *Molecules* **23** (2018).
3. Gomes, F.V., Zhu, X. & Grace, A.A. Stress during critical periods of development and risk for schizophrenia. *Schizophr Res* **213**, 107–113 (2019).
4. Howes, O.D. & Onwordi, E.C. The synaptic hypothesis of schizophrenia version III: A master mechanism. *Mol Psychiatry* **28**, 1843–1856 (2023).
5. Muller, N. Inflammation in schizophrenia: Pathogenetic aspects and therapeutic considerations. *Schizophr Bull* **44**, 973–982 (2018).
6. Horvath, S. & Mirnics, K. Immune system disturbances in schizophrenia. *Biol Psychiatry* **75**, 316–323 (2014).
7. Ermakov, E.A., Melamud, M.M., Buneva, V.N. & Ivanova, S.A. Immune system abnormalities in schizophrenia: An integrative view and translational perspectives. *Front Psychiatry* **13**, 880568 (2022).
8. Zhuo, C.*, et al.* Microglia and cognitive impairment in schizophrenia: translating scientific progress into novel therapeutic interventions. *Schizophrenia (Heidelb)* **9**, 42 (2023).
9. Woodburn, S.C., Bollinger, J.L. & Wohleb, E.S. The semantics of microglia activation: Neuroinflammation, homeostasis, and stress. *J Neuroinflammation* **18**, 258 (2021).
10. Amorim, A.*, et al.* IFN gamma and GM-CSF control complementary differentiation programs in the monocyte-to-phagocyte transition during neuroinflammation. *Nat Immunol* **23**, 217–228 (2022).
11. Thion, M.S., Ginhoux, F. & Garel, S. Microglia and early brain development: An intimate journey. *Science* **362**, 185–189 (2018).
12. Niraula, A., Witcher, K.G., Sheridan, J.F. & Godbout, J.P. Interleukin-6 induced by social stress promotes a unique transcriptional signature in the monocytes that facilitate anxiety. *Biol Psychiatry* **85**, 679–689 (2019).
13. Jauhar, S., Johnstone, M. & McKenna, P.J. Schizophrenia. *Lancet* **399**, 473–486 (2022).
14. Haijma, S.V.*, et al.* Brain volumes in schizophrenia: A meta-analysis in over 18 000 subjects. *Schizophr Bull* **39**, 1129–1138 (2013).
15. White, T.*, et al.* Limbic structures and networks in children and adolescents with schizophrenia. *Schizophr Bull* **34**, 18–29 (2008).
16. van Erp, T.G.M.*, et al.* Cortical brain abnormalities in 4474 individuals with schizophrenia and 5098 control subjects via the enhancing neuro imaging genetics through meta analysis (ENIGMA) consortium. *Biol Psychiatry* **84**, 644–654 (2018).
17. Warland, A., Kendall, K.M., Rees, E., Kirov, G. & Caseras, X. Schizophrenia-associated genomic copy number variants and subcortical brain volumes in the UK Biobank. *Mol Psychiatry* **25**, 854–862 (2020).
18. Dong, D.B., Wang, Y.L., Chang, X.B., Luo, C. & Yao, D.Z. Dysfunction of large-scale brain networks in schizophrenia: A meta-analysis of resting-state functional connectivity. *Schizophr Bull* **44**, 168–181 (2018).

19. Paquin, V., Lapierre, M., Veru, F. & King, S. Early environmental upheaval and the risk for schizophrenia. in *Annual Review of Clinical Psychology, Vol 17, 2021* 285–311 (2021).
20. Dinzeo, T.J., Cohen, A.S., Nienow, T.M. & Docherty, N.M. Stress and arousability in schizophrenia. *Schizophr Res* **71**, 127–135 (2004).
21. Bob, P. Stress, Dissociation and Schizophrenia. in *Handbook of schizophrenia spectrum disorders, Vol Ii: Phenotypic and endophenotypic presentations* 75–87 (2011).
22. Zhou, Y.*, et al.* Allostatic load effects on cortical and cognitive deficits in essentially normotensive, normoweight patients with schizophrenia. *Schizophr Bull* **47**, 1048–1057 (2021).
23. Pani, L., Porcella, A. & Gessa, G.L. The role of stress in the pathophysiology of the dopaminergic system. *Mol Psychiatry* **5**, 14–21 (2000).
24. Belujon, P. & Grace, A.A. Regulation of dopamine system responsivity and its adaptive and pathological response to stress. *Proc Royal Soc B* **282**, 2014–2516 (2015).
25. Javitt, D.C. Glutamatergic theories of schizophrenia. *Isr J Psychiatry Relat Sci* **47**, 4–16 (2010).
26. Gaspar, P.A., Bustamante, M.L., Silva, H. & Aboitiz, F. Molecular mechanisms underlying glutamatergic dysfunction in schizophrenia: therapeutic implications. *J Neurochem* **111**, 891–900 (2009).
27. Wei, J.*, et al.* Estrogen protects against the detrimental effects of repeated stress on glutamatergic transmission and cognition. *Mol Psychiatry* **19**, 588–598 (2014).
28. Nakahara, T.*, et al.* Glutamatergic and GABAergic metabolite levels in schizophrenia-spectrum disorders: a meta-analysis of (1)H-magnetic resonance spectroscopy studies. *Mol Psychiatry* **27**, 744–757 (2022).
29. Chiappelli, J.*, et al.* Glutamatergic response to heat pain stress in schizophrenia. *Schizophr Bull* **44**, 886–895 (2018).
30. Esterlis, I., Holmes, S.E., Sharma, P., Krystal, J.H. & DeLorenzo, C. Metabotropic glutamatergic receptor 5 and stress disorders: Knowledge gained from receptor imaging studies. *Biol Psychiatry* **84**, 95–105 (2018).
31. Shepard, R. & Coutellier, L. Changes in the prefrontal glutamatergic and parvalbumin systems of mice exposed to unpredictable chronic stress. *Mol Neurobiol* **55**, 2591–2602 (2018).
32. Jia, T., Chen, J., Wang, Y.D., Xiao, C. & Zhou, C.Y. A subthalamo-parabrachial glutamatergic pathway is involved in stress-induced self-grooming in mice. *Acta Pharmacol Sin* **44**, 2169–2183 (2023).
33. Willner, P. The chronic mild stress (CMS) model of depression: History, evaluation and usage. *Neurobiol Stress* **6**, 78–93 (2017).
34. Antoniuk, S., Bijata, M., Ponimaskin, E. & Wlodarczyk, J. Chronic unpredictable mild stress for modeling depression in rodents: Meta-analysis of model reliability. *Neurosci Biobehav Rev* **99**, 101–116 (2019).
35. Katz, R.J., Roth, K.A. & Carroll, B.J. Acute and chronic stress effects on open field activity in the rat: Implications for a model of depression. *Neurosci Biobehav Rev* **5**, 247–251 (1981).
36. Qiao, H.*, et al.* Dendritic spines in depression: What we Learned from animal models. *Neural Plast* **2016**, 8056370 (2016).

37. Ang, M.J., Lee, S., Kim, J.C., Kim, S.H. & Moon, C. Behavioral tasks evaluating schizophrenia-like symptoms in animal models: A recent update. *Curr Neuropharmacol* **19**, 641–664 (2021).
38. Hollis, F., Isgor, C. & Kabbaj, M. The consequences of adolescent chronic unpredictable stress exposure on brain and behavior. *Neuroscience* **249**, 232–241 (2013).
39. Chaby, L.E., Cavigelli, S.A., Hirrlinger, A.M., Caruso, M.J. & Braithwaite, V.A. Chronic unpredictable stress during adolescence causes long-term anxiety. *Behav Brain Res* **278**, 492–495 (2015).
40. Samant, N.P. & Gupta, G.L. Gossypetin- based therapeutics for cognitive dysfunction in chronic unpredictable stress- exposed mice. *Metab Brain Dis* **37**, 1527–1539 (2022).
41. Liu, D.*, et al.* Histone acetylation and expression of mono-aminergic transmitters synthetases involved in CUS-induced depressive rats. *Exp Biol Med* **239**, 330–336 (2014).
42. Palumbo, M.C., Dominguez, S. & Dong, H.X. Sex differences in hypothalamic-pituitary-adrenal axis regulation after chronic unpredictable stress. *Brain Behav* **10**, e01586 (2020).
43. Sandi, C.*, et al.* Chronic stress-induced alterations in amygdala responsiveness and behavior - modulation by trait anxiety and corticotropin-releasing factor systems. *Eur J Neurosci* **28**, 1836–1848 (2008).
44. Meng, F.T.*, et al.* Brain-derived neurotrophic factor in 5-HT neurons regulates susceptibility to depression-related behaviors induced by subchronic unpredictable stress. *J Psychiatr Res* **126**, 55–66 (2020).
45. Parul*, et al.* Chronic unpredictable stress negatively regulates hippocampal neurogenesis and promote anxious depression-like behavior via upregulating apoptosis and inflammatory signals in adult rats. *Brain Res Bull* **172**, 164–179 (2021).
46. Liang, X.*, et al.* Exercise more efficiently regulates the maturation of newborn neurons and synaptic plasticity than fluoxetine in a CUS-induced depression mouse model. *Exp Neurol* **354**, 114103 (2022).
47. Yue, N.*, et al.* Activation of P2X7 receptor and NLRP3 inflammasome assembly in hippocampal glial cells mediates chronic stress-induced depressive-like behaviors. *J Neuroinflammation* **14**, 102 (2017).
48. Patel, A.A., Ginhoux, F. & Yona, S. Monocytes, macrophages, dendritic cells and neutrophils: an update on lifespan kinetics in health and disease. *Immunology* **163**, 250–261 (2021).
49. Ziegler-Heitbrock, L.*, et al.* Nomenclature of monocytes and dendritic cells in blood. *Blood* **116**, e74–80 (2010).
50. Wong, K.L.*, et al.* Gene expression profiling reveals the defining features of the classical, intermediate, and nonclassical human monocyte subsets. *Blood* **118**, e16–31 (2011).
51. Patel, A.A.*, et al.* The fate and lifespan of human monocyte subsets in steady state and systemic inflammation. *J Exp Med* **214**, 1913–1923 (2017).
52. Schmidl, C.*, et al.* Transcription and enhancer profiling in human monocyte subsets. *Blood* **123**, e90–99 (2014).
53. Kapellos, T.S.*, et al.* Human monocyte subsets and phenotypes in major chronic inflammatory diseases. *Front Immunol* **10**, 2035 (2019).
54. Narasimhan, P.B., Marcovecchio, P., Hamers, A.A.J. & Hedrick, C.C. Nonclassical monocytes in health and disease. *Annu Rev Immunol* **37**, 439–456 (2019).

55. Ong, S.M.*, et al.* The pro-inflammatory phenotype of the human non-classical monocyte subset is attributed to senescence. *Cell Death Dis* **9**, 266 (2018).
56. Yona, S.*, et al.* Fate mapping reveals origins and dynamics of monocytes and tissue macrophages under homeostasis. *Immunity* **38**, 79–91 (2013).
57. Rogacev, K.S.*, et al.* CD14++CD16+ monocytes independently predict cardiovascular events: a cohort study of 951 patients referred for elective coronary angiography. *J Am Coll Cardiol* **60**, 1512–1520 (2012).
58. Passos, S.*, et al.* Intermediate monocytes contribute to pathologic immune response in Leishmania braziliensis infections. *J Infect Dis* **211**, 274–282 (2015).
59. Ginhoux, F.*, et al.* Fate mapping analysis reveals that adult microglia derive from primitive macrophages. *Science* **330**, 841–845 (2010).
60. Paolicelli, R.C.*, et al.* Microglia states and nomenclature: A field at its crossroads. *Neuron* **110**, 3458–3483 (2022).
61. Greter, M. & Merad, M. Regulation of microglia development and homeostasis. *Glia* **61**, 121–127 (2013).
62. Bottcher, C.*, et al.* Human microglia regional heterogeneity and phenotypes determined by multiplexed single-cell mass cytometry. *Nat Neurosci* **22**, 78–90 (2019).
63. Masuda, T., Sankowski, R., Staszewski, O. & Prinz, M. Microglia heterogeneity in the single-cell era. *Cell Rep* **30**, 1271–1281 (2020).
64. Masuda, T.*, et al.* Spatial and temporal heterogeneity of mouse and human microglia at single-cell resolution. *Nature* **566**, 388–392 (2019).
65. Li, Q.Y.*, et al.* Developmental heterogeneity of microglia and brain myeloid cells revealed by deep single-cell RNA sequencing. *Neuron* **101**, 207–223 (2019).
66. Mosser, C.A., Baptista, S., Arnoux, I. & Audinat, E. Microglia in CNS development: Shaping the brain for the future. *Prog Neurobiol* **149–150**, 1–20 (2017).
67. Stremmel, C.*, et al.* Yolk sac macrophage progenitors traffic to the embryo during defined stages of development. *Nat Commun* **9**, 75 (2018).
68. Reemst, K., Noctor, S.C., Lucassen, P.J. & Hol, E.M. The indispensable roles of microglia and astrocytes during brain development. *Front Hum Neurosci* **10**, 566 (2016).
69. Smolders, S.M.*, et al.* Microglia: Brain cells on the move. *Prog Neurobiol* **178**, 101612 (2019).
70. Bennett, M.L. & Bennett, F.C. The influence of environment and origin on brain resident macrophages and implications for therapy. *Nat Neurosci* **23**, 157–166 (2020).
71. Spittau, B., Dokalis, N. & Prinz, M. The role of TGFβ signaling in microglia maturation and activation. *Trends Immunol* **41**, 836–848 (2020).
72. Elmore, M.R.P.*, et al.* Colony-stimulating factor 1 receptor signaling is necessary for microglia viability, unmasking a microglia progenitor cell in the adult brain. *Neuron* **82**, 380–397 (2014).
73. Olmos-Alonso, A.*, et al.* Pharmacological targeting of CSF1R inhibits microglial proliferation and prevents the progression of Alzheimer's-like pathology. *Brain* **139**, 891–907 (2016).
74. Cuadros, M.A., Martin, C., Coltey, P., Almendros, A. & Navascues, J. First appearance, distribution, and origin of macrophages in the early development of the avian central nervous system. *J Comp Neurol* **330**, 113–129 (1993).
75. Monier, A.*, et al.* Entry and distribution of microglial cells in human embryonic and fetal cerebral cortex. *J Neuropathol Exp Neurol* **66**, 372–382 (2007).

76. Squarzoni, P.*, et al.* Microglia modulate wiring of the embryonic forebrain. *Cell Rep* **8**, 1271–1279 (2014).
77. Ashwell, K. The distribution of microglia and cell death in the fetal rat forebrain. *Brain Res Dev Brain Res* **58**, 1–12 (1991).
78. Dalmau, I., Finsen, B., Zimmer, J., Gonzalez, B. & Castellano, B. Development of microglia in the postnatal rat hippocampus. *Hippocampus* **8**, 458–474 (1998).
79. Swinnen, N.*, et al.* Complex invasion pattern of the cerebral cortex bymicroglial cells during development of the mouse embryo. *Glia* **61**, 150–163 (2013).
80. Menassa, D.A. & Gomez-Nicola, D. Microglial dynamics during human brain development. *Front Immunol* **9**, 1014 (2018).
81. Hume, D.A.*, et al.* Phenotypic impacts of CSF1R deficiencies in humans and model organisms. *J Leukoc Biol* **107**, 205–219 (2020).
82. Cahoy, J.D.*, et al.* A transcriptome database for astrocytes, neurons, and oligodendrocytes: a new resource for understanding brain development and function. *J Neurosci* **28**, 264–278 (2008).
83. Konno, T.*, et al.* Haploinsufficiency of CSF-1R and clinicopathologic characterization in patients with HDLS. *Neurology* **82**, 139–148 (2014).
84. Xun, Q.J., Wang, Z., Hu, X.L., Ding, K. & Lu, X.Y. Small-molecule CSF1R inhibitors as anticancer agents. *Curr Med Chem* **27**, 3944–3966 (2020).
85. Denny, W.A. & Flanagan, J.U. Small-molecule CSF1R kinase inhibitors; review of patents 2015-present. *Expert Opin Ther Pat* **31**, 107–117 (2021).
86. Cannarile, M.A.*, et al.* Colony-stimulating factor 1 receptor (CSF1R) inhibitors in cancer therapy. *J Immunother Cancer* **5**, 53 (2017).
87. Cangalaya, C., Stoyanov, S., Fischer, K.D. & Dityatev, A. Light-induced engagement of microglia to focally remodel synapses in the adult brain. *Elife* **9**, e58435 (2020).
88. Jongbloets, B.C. & Pasterkamp, R.J. Semaphorin signalling during development. *Development* **141**, 3292–3297 (2014).
89. Hota, P.K. & Buck, M. Plexin structures are coming: Opportunities for multilevel investigations of semaphorin guidance receptors, their cell signaling mechanisms, and functions. *Cell Mol Life Sci* **69**, 3765–3805 (2012).
90. Yu, W.*, et al.* Plexin-B2 mediates physiologic and pathologic functions of angiogenin. *Cell* **171**, 849–864.e825 (2017).
91. Kumanogoh, A. & Kikutani, H. Immunological functions of the neuropilins and plexins as receptors for semaphorins. *Nat Rev Immunol* **13**, 802–814 (2013).
92. Hirschberg, A.*, et al.* Gene deletion mutants reveal a role for semaphorin receptors of the Plexin-B family in mechanisms underlying corticogenesis. *Mol Cell Neurosci* **30**, 764–780 (2010).
93. Limoni, G., Murthy, S., Jabaudon, D., Dayer, A. & Niquille, M. PlexinA4-Semaphorin3A-mediated crosstalk between main cortical interneuron classes is required for superficial interneuron lamination. *Cell Rep* **34**, 108644 (2021).
94. Okada, A. & Tomooka, Y. Possible roles of Plexin-A4 in positioning of oligodendrocyte precursor cells in developing cerebral cortex. *Neurosci Lett* **516**, 259–264 (2012).
95. Xiang, X., Zhang, X. & Huang, Q.L. Plexin A3 is involved in semaphorin 3F-mediated oligodendrocyte precursor cell migration. *Neurosci Lett* **530**, 127–132 (2012).

96. Deng, S.H.*, et al.* Plexin-B2, but not Plexin-B1, critically modulates neuronal migration and patterning of the developing nervous system in vivo. *Neurosci J* **27**, 6333–6347 (2007).
97. Maier, V.*, et al.* Semaphorin 4C and 4G are ligands of Plexin-B2 required in cerebellar development. *Mol Cell Neurosci* **46**, 419–431 (2011).
98. Azzarelli, R.*, et al.* An antagonistic interaction between PlexinB2 and Rnd3 controls RhoA activity and cortical neuron migration. *Nat Commun* **5**, 3405 (2014).
99. Li, D.*, et al.* Cleavage of semaphorin 4 C interferes with the neuroprotective effect of the semaphorin 4 C/Plexin B2 pathway on experimental intracerebral hemorrhage in rats. *J Chem Neuroanat* **132**, 102318 (2023).
100. Suto, F.*, et al.* Interactions between plexin-A2, plexin-A4, and semaphorin 6A control lamina-restricted projection of hippocampal mossy fibers. *Neuron* **53**, 535–547 (2007).
101. Lin, X.Z.*, et al.* Sema4D-plexin-B1 implicated in regulation of dendritic spine density through RhoA/ROCK pathway. *Neurosci Lett* **428**, 1–6 (2007).
102. Pecho-Vrieseling, E., Sigrist, M., Yoshida, Y., Jessell, T.M. & Arber, S. Specificity of sensory-motor connections encoded by Sema3e-Plxnd1 recognition. *Nature* **459**, 842–846 (2009).
103. Ding, J.B., Oh, W.J., Sabatini, B.L. & Gu, C.H. Semaphorin 3E-Plexin-D1 signaling controls pathway-specific synapse formation in the striatum. *Nat Neurosci* **15**, 215–223 (2012).
104. McDermott, J.E., Goldblatt, D. & Paradis, S. Class 4 Semaphorins and Plexin-B receptors regulate GABAergic and glutamatergic synapse development in the mammalian hippocampus. *Mol Cell Neurosci* **92**, 50–66 (2018).
105. Simonetti, M.*, et al.* The impact of Semaphorin 4C/Plexin-B2 signaling on fear memory via remodeling of neuronal and synaptic morphology. *Mol Psychiatry* **26**, 1376–1398 (2021).
106. Khdour, H.Y.*, et al.* Neuropilin 2/Plexin-A3 receptors regulate the functional connectivity and the excitability in the layers 4 and 5 of the cerebral cortex. *Neurosci J* **42**, 4828–4840 (2022).
107. Kim, J., Oh, W.J., Gaiano, N., Yoshida, Y. & Gu, C.H. Semaphorin 3E-Plexin-D1 signaling regulates VEGF function in developmental angiogenesis via a feedback mechanism. *Genes Dev* **25**, 1399–1411 (2011).
108. Kang, S.J.*, et al.* Semaphorin 6D reverse signaling controls macrophage lipid metabolism and anti-inflammatory polarization. *Nat Immunol* **19**, 561–570 (2018).
109. Paldy, E.*, et al.* Semaphorin 4C Plexin-B2 signaling in peripheral sensory neurons is pronociceptive in a model of inflammatory pain. *Nat Commun* **8**, 176 (2017).
110. Yan, H.*, et al.* Plexin B2 and Semaphorin 4C guide T cell recruitment and function in the germinal center. *Cell Rep* **19**, 995–1007 (2017).
111. Zhang, C.*, et al.* CD100-Plexin-B2 promotes the inflammation in psoriasis by activating NF-kappa B and the inflammasome in keratinocytes. *J Invest Dermatol* **138**, 375–383 (2018).
112. He, Y.*, et al.* Interferon-α-enhanced CD100/Plexin-B1/B2 interactions promote natural killer cell functions in patients with chronic hepatitis C virus infection. *Front Immunol* **8**, 1435 (2017).
113. Ma, Y., Yang, S., He, Q., Zhang, D. & Chang, J. The role of immune cells in post-stroke angiogenesis and neuronal remodeling: The known and the unknown. *Front Immunol* **12**, 784098 (2021).

114. Kang, H.R., Lee, C.G., Homer, R.J. & Elias, J.A. Semaphorin 7A plays a critical role in TGF-β1-induced pulmonary fibrosis. *J Exp Med* **204**, 1083–1093 (2007).
115. Ueda, Y.*, et al.* Sema3e/Plexin D1 modulates immunological synapse and migration of thymocytes by Rap1 inhibition. *J Immunol* **196**, 3019–3031 (2016).
116. Anders, S. & Kinney, D.K. Abnormal immune system development and function in schizophrenia helps reconcile diverse findings and suggests new treatment and prevention strategies. *Brain Res* **1617**, 93–112 (2015).
117. Zengeler, K.E. & Lukens, J.R. Innate immunity at the crossroads of healthy brain maturation and neurodevelopmental disorders. *Nat Rev Immunol* **21**, 454–468 (2021).
118. Haddad, F.L., Patel, S.V. & Schmid, S. Maternal immune activation by poly I:C as a preclinical model for neurodevelopmental disorders: A focus on autism and schizophrenia. *Neurosci Biobehav Rev* **113**, 546–567 (2020).
119. Kępińska, A.P.*, et al.* Schizophrenia and influenza at the centenary of the 1918–1919 spanish influenza pandemic: Mechanisms of psychosis risk. *Front Psychiatry* **11**, 72 (2020).
120. Luo, C.*, et al.* Subtypes of schizophrenia identified by multi-omic measures associated with dysregulated immune function. *Mol Psychiatry* **26**, 6926–6936 (2021).
121. Sæther, L.S.*, et al.* Inflammation and cognition in severe mental illness: patterns of covariation and subgroups. *Mol Psychiatry* **28**, 1284–1292 (2023).
122. Enrico, P.*, et al.* A machine learning approach on whole blood immunomarkers to identify an inflammation-associated psychosis onset subgroup. *Mol Psychiatry* **28**, 1190–1200 (2023).
123. Lizano, P.*, et al.* Peripheral inflammatory subgroup differences in anterior Default Mode network and multiplex functional network topology are associated with cognition in psychosis. *Brain Behav Immun* **114**, 3–15 (2023).
124. Halstead, S.*, et al.* Alteration patterns of peripheral concentrations of cytokines and associated inflammatory proteins in acute and chronic stages of schizophrenia: A systematic review and network meta-analysis. *Lancet Psychiatry* **10**, 260–271 (2023).
125. Leirer, D.J.*, et al.* Differential gene expression analysis in blood of first episode psychosis patients. *Schizophr Res* **209**, 88–97 (2019).
126. Lanz, T.A.*, et al.* Postmortem transcriptional profiling reveals widespread increase in inflammation in schizophrenia: a comparison of prefrontal cortex, striatum, and hippocampus among matched tetrads of controls with subjects diagnosed with schizophrenia, bipolar or major depressive disorder. *Transl Psychiatry* **9**, 151 (2019).
127. Kathuria, A.*, et al.* Transcriptomic landscape and functional characterization of induced pluripotent stem cell-derived cerebral organoids in schizophrenia. *Jama Psychiatry* **77**, 745–754 (2020).
128. Hwang, Y.*, et al.* Gene expression profiling by mRNA sequencing reveals increased expression of immune/inflammation-related genes in the hippocampus of individuals with schizophrenia. *Transl Psychiatry* **3**, e321 (2013).
129. Siegel, B.I., Sengupta, E.J., Edelson, J.R., Lewis, D.A. & Volk, D.W. Elevated viral restriction factor levels in cortical blood vessels in schizophrenia. *Biol Psychiatry* **76**, 160–167 (2014).
130. Volk, D.W.*, et al.* Molecular mechanisms and timing of cortical immune activation in schizophrenia. *Am J Psychiatry* **172**, 1112–1121 (2015).

131. Trépanier, M.O., Hopperton, K.E., Mizrahi, R., Mechawar, N. & Bazinet, R.P. Postmortem evidence of cerebral inflammation in schizophrenia: a systematic review. *Mol Psychiatry* **21**, 1009–1026 (2016).
132. Pérez-Santiago, J.*, et al.* A combined analysis of microarray gene expression studies of the human prefrontal cortex identifies genes implicated in schizophrenia. *J Psychiatr Res* **46**, 1464–1474 (2012).
133. Gardiner, E.J.*, et al.* Gene expression analysis reveals schizophrenia-associated dysregulation of immune pathways in peripheral blood mononuclear cells. *J Psychiatr Res* **47**, 425–437 (2013).
134. Fillman, S.G.*, et al.* Increased inflammatory markers identified in the dorsolateral prefrontal cortex of individuals with schizophrenia. *Mol Psychiatry* **18**, 206–214 (2013).
135. Wang, C.Y., Aleksic, B. & Ozaki, N. Glia-related genes and their contribution to schizophrenia. *Psychiatry Clin Neurosci* **69**, 448–461 (2015).
136. Orhan, F.*, et al.* Increased number of monocytes and plasma levels of MCP-1 and YKL-40 in first-episode psychosis. *Acta Psychiatr Scand* **138**, 432–440 (2018).
137. Mazza, M.G.*, et al.* Monocyte count in schizophrenia and related disorders: a systematic review and meta-analysis. *Acta Neuropsychiatr* **32**, 229–236 (2020).
138. Melbourne, J.K., Rosen, C., Chase, K.A., Feiner, B. & Sharma, R.P. Monocyte transcriptional profiling highlights a shift in immune signatures over the course of illness in schizophrenia. *Front Psychiatry* **12** (2021).
139. Sahpolat, M., Ayar, D., Ari, M. & Karaman, M.A. Elevated monocyte to high-density lipoprotein ratios as an inflammation markers for schizophrenia patients. *Clin Psychopharmacol Neurosci* **19**, 112–116 (2021).
140. Kowalski, J., Blada, P., Kucia, K., Madej, A. & Herman, Z.S. Neuroleptics normalize increased release of interleukin-1 beta and tumor necrosis factor-alpha from monocytes in schizophrenia. *Schizophr Res* **50**, 169–175 (2001).
141. Krause, D.L.*, et al.* Intracellular monocytic cytokine levels in schizophrenia show an alteration of IL-6. *Eur Arch Psychiatry Clin Neurosci* **262**, 393–401 (2012).
142. Uranova, N.A., Bonartsev, P.D., Androsova, L.V., Rakhmanova, V.I. & Kaleda, V.G. Impaired monocyte activation in schizophrenia: Ultrastructural abnormalities and increased IL-1 beta production. *Eur Arch Psychiatry Clin Neurosci* **267**, 417–426 (2017).
143. Kuebler, R., Ormel, P.R., Sommer, I.E.C., Kahn, R.S. & de Witte, L.D. Gene expression profiling of monocytes in recent-onset schizophrenia. *Brain Behav Immun* **111**, 334–342 (2023).
144. Shimamoto-Mitsuyama, C.*, et al.* Lipid pathology of the corpus callosum in schizophrenia and the potential role of abnormal gene regulatory networks with reduced microglial marker expression. *Cereb Cortex* **31**, 448–462 (2021).
145. Pruenster, M., Vogl, T., Roth, J. & Sperandio, M. S100A8/A9: From basic science to clinical application. *Pharmacol Ther* **167**, 120–131 (2016).
146. Muller, N.*, et al.* Impaired monocyte activation in schizophrenia. *Psychiatry Res* **198**, 341–346 (2012).
147. Chen, S.*, et al.* More dampened monocytic toll-like receptor 4 response to lipopolysaccharide and its association with cognitive function in Chinese Han first-episode patients with schizophrenia. *Schizophr Res* **206**, 300–306 (2019).
148. Hu, H.L., Yang, X., He, Y.Q., Duan, C.H. & Sun, N.N. Psychological stress induces depressive-like behavior associated with bone marrow-derived monocyte

infiltration into the hippocampus independent of blood-brain barrier disruption. *J Neuroinflammation* **19** (2022).
149. Neniskyte, U. & Gross, C.T. Errant gardeners: Glial-cell-dependent synaptic pruning and neurodevelopmental disorders. *Nat Rev Neurosci* **18**, 658–670 (2017).
150. Dietz, A.G., Goldman, S.A. & Nedergaard, M. Glial cells in schizophrenia: A unified hypothesis. *Lancet Psychiatry* **7**, 272–281 (2020).
151. de Oliveira Figueiredo, E.C., Calì, C., Petrelli, F. & Bezzi, P. Emerging evidence for astrocyte dysfunction in schizophrenia. *Glia* **70**, 1585–1604 (2022).
152. Furuyashiki, T. & Kitaoka, S. Neural mechanisms underlying adaptive and maladaptive consequences of stress: Roles of dopaminergic and inflammatory responses. *Psychiatry Clin Neurosci* **73**, 669–675 (2019).
153. Müller, N. & Ackenheil, M. Psychoneuroimmunology and the cytokine action in the CNS: Implications for psychiatric disorders. *Prog Neuropsychopharmacol Biol Psychiatry* **22**, 1–33 (1998).
154. Friston, K.J. Schizophrenia and the disconnection hypothesis. *Acta Psychiatr Scand* **99**, 68–79 (1999).
155. Steiner, J.*, et al.* Distribution of HLA-DR-positive microglia in schizophrenia reflects impaired cerebral lateralization. *Acta Neuropathol* **112**, 305–316 (2006).
156. Bloomfield, P.S.*, et al.* Microglial activity in people at ultra high risk of psychosis and in schizophrenia: An [C-11]PBR28 PET brain imaging study. *Am J Psychiatry* **173**, 44–52 (2016).
157. Lopez-Gonzalez, I.*, et al.* Neuroinflammation in the dorsolateral prefrontal cortex in elderly chronic schizophrenia. *Eur Neuropsychopharmacol* **29**, 384–396 (2019).
158. Marques, T.R.*, et al.* Neuroinflammation in schizophrenia: Meta-analysis of in vivo microglial imaging studies. *Psychol Med* **49**, 2186–2196 (2019).
159. Corley, E.*, et al.* Microglial-expressed genetic risk variants, cognitive function and brain volume in patients with schizophrenia and healthy controls. *Transl Psychiatry* **11**, 490 (2021).
160. Beumer, W.*, et al.* The immune theory of psychiatric diseases: A key role for activated microglia and circulating monocytes. *J Leukoc Biol* **92**, 959–975 (2012).
161. Sellgren, C.M.*, et al.* Increased synapse elimination by microglia in schizophrenia patient-derived models of synaptic pruning. *Nat Neurosci* **22**, 374–385 (2019).
162. Conen, S.*, et al.* Neuroinflammation as measured by positron emission tomography in patients with recent onset and established schizophrenia: Implications for immune pathogenesis. *Mol Psychiatry* **26**, 5398–5406 (2021).
163. Rahimian, R., Wakid, M., O'Leary, L.A. & Mechawar, N. The emerging tale of microglia in psychiatric disorders. *Neurosci Biobehav Rev* **131**, 1–29 (2021).
164. Gober, R.*, et al.* Microglia activation in postmortem brains with schizophrenia demonstrates distinct morphological changes between brain regions. *Brain Pathol* **32**, e13003 (2022).
165. Basilico, B.*, et al.* Microglia control glutamatergic synapses in the adult mouse hippocampus. *Glia* **70**, 173–195 (2022).
166. Hogenaar, J.T.T. & van Bokhoven, H. Schizophrenia: Complement cleaning or killing. *Genes (Basel)* **12**, 259 (2021).
167. Rey, R.*, et al.* Overexpression of complement component C4 in the dorsolateral prefrontal cortex, parietal cortex, superior temporal gyrus and associative striatum of patients with schizophrenia. *Brain Behav Immun* **90**, 216–225 (2020).
168. Sager, R.E.H.*, et al.* Trajectory of change in brain complement factors from neonatal to young adult humans. *J Neurochem* **157**, 479–493 (2021).

169. Sellgren, C.M.*, et al.* Patient-specific models of microglia-mediated engulfment of synapses and neural progenitors. *Mol Psychiatry* **22**, 170–177 (2017).
170. Yilmaz, M.*, et al.* Overexpression of schizophrenia susceptibility factor human complement C4A promotes excessive synaptic loss and behavioral changes in mice. *Nat Neurosci* **24**, 214–224 (2021).
171. Ren, M.*, et al.* KCNH2–3.1 mediates aberrant complement activation and impaired hippocampal-medial prefrontal circuitry associated with working memory deficits. *Mol Psychiatry* **25**, 206–229 (2020).
172. Dennison, U., McKernan, D., Cryan, J. & Dinan, T. Schizophrenia patients with a history of childhood trauma have a pro-inflammatory phenotype. *Psychol Med* **42**, 1865–1871 (2012).
173. Chase, K.A.*, et al.* Traumagenics: At the intersect of childhood trauma, immunity and psychosis. *Psychiatry Res* **273**, 369–377 (2019).
174. van de Wouw, M.*, et al.* Acute stress increases monocyte levels and modulates receptor expression in healthy females. *Brain Behav Immun* **94**, 463–468 (2021).
175. Miller, G.E.*, et al.* Greater inflammatory activity and blunted glucocorticoid signaling in monocytes of chronically stressed caregivers. *Brain Behav Immun* **41**, 191–199 (2014).
176. Irwin, M.R. & Cole, S.W. Reciprocal regulation of the neural and innate immune systems. *Nat Rev Immunol* **11**, 625–632 (2011).
177. Beis, D.*, et al.* The Role of norepinephrine and -adrenergic receptors in acute stress-induced changes in granulocytes and monocytes. *Psychosom Med* **80**, 649–658 (2018).
178. Casaletto, K.B.*, et al.* Perceived stress is associated with accelerated monocyte/ macrophage aging trajectories in clinically normal adults. *Am J Geriatr Psychiatry* **26**, 952–963 (2018).
179. McDonald, L.T.*, et al.* Early blood profile of C57BL/6 mice exposed to chronic unpredictable stress. *Front Psychiatry* **10**, 230 (2019).
180. Götz, A.A., Wittlinger, S. & Stefanski, V. Maternal social stress during pregnancy alters immune function and immune cell numbers in adult male Long-Evans rat offspring during stressful life-events. *J Neuroimmunol* **185**, 95–102 (2007).
181. Wohleb, E.S.*, et al.* Re-establishment of anxiety in stress-sensitized mice Is caused by monocyte trafficking from the spleen to the brain. *Biol Psychiatry* **75**, 970–981 (2014).
182. Ménard, C., Pfau, M.L., Hodes, G.E. & Russo, S.J. Immune and neuroendocrine mechanisms of stress vulnerability and resilience. *Neuropsychopharmacol* **42**, 62–80 (2017).
183. Pfau, M.L.*, et al.* Role of monocyte-derived microRNA106b~25 in resilience to social stress. *Biol Psychiatry* **86**, 474–482 (2019).
184. Jonsdottir, I.H., Hägg, D.A., Glise, K. & Ekman, R. Monocyte chemotactic protein-1 (MCP-1) and growth factors called into question as markers of prolonged psychosocial stress. *PLoS One* **4**, e7659 (2009).
185. Orso, R.*, et al.* A systematic review and multilevel meta-analysis of the prenatal and early life stress effects on rodent microglia, astrocyte, and oligodendrocyte density and morphology. *Neurosci Biobehav Rev* **150**, 105202 (2023).
186. Cattane, N.*, et al.* Preclinical animal models of mental illnesses to translate findings from the bench to the bedside: Molecular brain mechanisms and peripheral biomarkers associated to early life stress or immune challenges. *Eur Neuropsychopharmacol* **58**, 55–79 (2022).

187. Fan, Y., Chen, Z.L., Pathak, J.L., Carneiro, A.M.D. & Chung, C.Y. Differential regulation of adhesion and phagocytosis of resting and activated microglia by dopamine. *Front Cell Neurosci* **12**, 309 (2018).
188. Sugama, S. & Kakinuma, Y. Noradrenaline as a key neurotransmitter in modulating microglial activation in stress response. *Neurochem Int* **143**, 104943 (2021).
189. Yu, Z.Q.*, et al.* Contextual fear conditioning regulates synapse-related gene transcription in mouse microglia. *Brain Res Bull* **189**, 57–68 (2022).
190. Ronaldson, P.T. & Davis, T.P. Regulation of blood-brain barrier integrity by microglia in health and disease: A therapeutic opportunity. *J Cereb Blood Flow Metab* **40**, S6-S24 (2020).
191. Serna-Rodríguez, M.F., Bernal-Vega, S., de la Barquera, J., Camacho-Morales, A. & Pérez-Maya, A.A. *J Neuroimmunol* **371**, 577951 (2022).
192. Zhang, S.T.*, et al.* HMGB1/RAGE axis mediates stress-induced RVLM neuroinflammation in mice via impairing mitophagy flux in microglia. *J Neuroinflammation* **17**, 15 (2020).
193. Piirainen, S.*, et al.* Microglia contribute to social behavioral adaptation to chronic stress. *Glia* **69**, 2459–2473 (2021).
194. Cathomas, F.*, et al.* Beyond the neuron: Role of non-neuronal cells in stress disorders. *Neuron* **110**, 1116–1138 (2022).
195. Gouweleeuw, L.*, et al.* Effects of selective TNFR1 inhibition or TNFR2 stimulation, compared to non-selective TNF inhibition, on (neuro)inflammation and behavior after myocardial infarction in male mice. *Brain Behav Immun* **93**, 156–171 (2021).
196. Zhang, Y.*, et al.* Microglia-specific transcriptional repression of interferon-regulated genes after prolonged stress in mice. *Neurobiol Stress* **21**, 100495 (2022).
197. Smith, K.L.*, et al.* Microglial cell hyper-ramification and neuronal dendritic spine loss in the hippocampus and medial prefrontal cortex in a mouse model of PTSD. *Brain Behav Immun* **80**, 889–899 (2019).
198. Damani, M.R.*, et al.* Age-related alterations in the dynamic behavior of microglia. *Aging Cell* **10**, 263–276 (2011).
199. Aires, V.*, et al.* CD22 blockage restores age-related impairments of microglia surveillance capacity. *Front Immunol* **12**, 684430 (2021).
200. De Luca, S.N.*, et al.* Conditional microglial depletion in rats leads to reversible anorexia and weight loss by disrupting gustatory circuitry. *Brain Behav Immun* **77**, 77–91 (2019).
201. Wang, Y.L.*, et al.* Microglial activation mediates chronic mild stress-induced depressive- and anxiety-like behavior in adult rats. *J Neuroinflammation* **15**, 21 (2018).
202. Koo, J.W. & Wohleb, E.S. How stress shapes neuroimmune function: Implications for the neurobiology of psychiatric disorders. *Biol Psychiatry* **90**, 74–84 (2021).
203. McKim, D.B.*, et al.* Microglial recruitment of IL-1β-producing monocytes to brain endothelium causes stress-induced anxiety. *Mol Psychiatry* **23**, 1421–1431 (2018).
204. Bolton, J.L.*, et al.* Early stress-induced impaired microglial pruning of excitatory synapses on immature CRH-expressing neurons provokes aberrant adult stress responses. *Cell Rep* **38** (2022).
205. Hellwig, S.*, et al.* Altered microglia morphology and higher resilience to stress-induced depression-like behavior in CX3CR1-deficient mice. *Brain Behav Immun* **55**, 126–137 (2016).

206. Rogers, J.T.*, et al.* CX3CR1 deficiency leads to impairment of hippocampal cognitive function and synaptic plasticity. *J Neurosci* **31**, 16241–16250 (2011).
207. Rimmerman, N., Schottlender, N., Reshef, R., Dan-Goor, N. & Yirmiya, R. The hippocampal transcriptomic signature of stress resilience in mice with microglial fractalkine receptor (CX3CR1) deficiency. *Brain Behav Immun* **61**, 184–196 (2017).
208. Antony, J.M. Grooming and growing with microglia. *Science Signaling* **3**, jc8 (2010).
209. Tränkner, D.*, et al.* A microglia sublineage protects from sex-linked anxiety symptoms and obsessive compulsion. *Cell Rep* **29**, 791–799 (2019).
210. Nagarajan, N. & Capecchi, M.R. Optogenetic stimulation of mouse Hoxb8 microglia in specific regions of the brain induces anxiety, grooming, or both. *Mol Psychiatry*, Epub ahead of print (2023).
211. Liu, M.C.*, et al.* Microglia activation regulates GluR1 phosphorylation in chronic unpredictable stress-induced cognitive dysfunction. *Stress* **18**, 96–106 (2015).
212. Xiao, K.*, et al.* Beneficial effects of running exercise on hippocampal microglia and neuroinflammation in chronic unpredictable stress-induced depression model rats. *Transl Psychiatry* **11**, 461 (2021).
213. Milior, G.*, et al.* Fractalkine receptor deficiency impairs microglial and neuronal responsiveness to chronic stress. *Brain Behav Immun* **55**, 114–125 (2016).
214. Liu, Y.*, et al.* Involvement of CX3CL1/CX3CR1 in depression and cognitive impairment induced by chronic unpredictable stress and relevant underlying mechanism. *Behav Brain Res* **381**, 112371 (2020).
215. Horchar, M.J. & Wohleb, E.S. Glucocorticoid receptor antagonism prevents microglia-mediated neuronal remodeling and behavioral despair following chronic unpredictable stress. *Brain Behav Immun* **81**, 329–340 (2019).
216. Picard, K.*, et al.* Microglial-glucocorticoid receptor depletion alters the response of hippocampal microglia and neurons in a chronic unpredictable mild stress paradigm in female mice. *Brain Behav Immun* **97**, 423–439 (2021).
217. Woodburn, S.C.*, et al.* Depletion of microglial BDNF increases susceptibility to the behavioral and synaptic effects of chronic unpredictable stress. *Brain Behav Immun* **109**, 127–138 (2023).
218. Wohleb, E.S., Terwilliger, R., Duman, C.H. & Duman, R.S. Stress-induced neuronal colony stimulating factor 1 provokes microglia-mediated neuronal remodeling and depressive-like behavior. *Biol Psychiatry* **83**, 38–49 (2018).
219. Yan, L.*, et al.* CSF1R regulates schizophrenia-related stress response and vascular association of microglia/macrophages. *BMC Med* **21**, 286 (2023).
220. Han, J., Zhu, K., Zhang, X.M. & Harris, R.A. Enforced microglial depletion and repopulation as a promising strategy for the treatment of neurological disorders. *Glia* **67**, 217–231 (2019).
221. Elmore, M.R., Lee, R.J., West, B.L. & Green, K.N. Characterizing newly repopulated microglia in the adult mouse: impacts on animal behavior, cell morphology, and neuroinflammation. *PLoS One* **10**, e0122912 (2015).
222. Lehmann, M.L., Weigel, T.K., Poffenberger, C.N. & Herkenham, M. The behavioral sequelae of social defeat require microglia and are driven by oxidative stress in mice. *J Neurosci* **39**, 5594–5605 (2019).
223. Weber, M.D.*, et al.* The influence of microglial elimination and repopulation on stress sensitization induced by repeated social defeat. *Biol Psychiatry* **85**, 667–678 (2019).

224. Ikezu, S.*, et al.* Inhibition of colony stimulating factor 1 receptor corrects maternal inflammation-induced microglial and synaptic dysfunction and behavioral abnormalities. *Mol Psychiatry* **26**, 1808–1831 (2021).
225. Li, C.H.*, et al.* Neuronal-microglial liver X receptor β activating decrease neuro-inflammation and chronic stress-induced depression-related behavior in mice. *Brain Res* **1797** (2022).
226. Torres, L.*, et al.* Dynamic microglial modulation of spatial learning and social behavior. *Brain Behav Immun* **55**, 6–16 (2016).
227. Rosin, J.M., Vora, S.R. & Kurrasch, D.M. Depletion of embryonic microglia using the CSF1R inhibitor PLX5622 has adverse sex-specific effects on mice, including accelerated weight gain, hyperactivity and anxiolytic-like behaviour. *Brain Behav Immun* **73**, 682–697 (2018).
228. Worthen, R.J., Zighelboim, S.S.G., Jaramillo, C.S.T. & Beurel, E. Anti-inflammatory IL-10 administration rescues depression-associated learning and memory deficits in mice. *J Neuroinflammation* **17**, 246 (2020).
229. Wang, L.F.*, et al.* Pexidartinib (PLX3397) through restoring hippocampal synaptic plasticity ameliorates social isolation-induced mood disorders. *Int Immunopharmacol* **113**, 109436 (2022).
230. Wang, J.*, et al.* Microglial activation contributes to depressive-like behavior in dopamine D3 receptor knockout mice. *Brain Behav Immun* **83**, 226–238 (2020).
231. Torres-Rodriguez, O.*, et al.* Sex-dependent effects of microglial reduction on impaired fear extinction induced by single prolonged stress. *Front Behav Neurosci* **16**, 148112 (2023).
232. Ni, R.J.*, et al.* Depletion of microglia with PLX3397 attenuates MK-801-induced hyperactivity associated with regulating inflammation-related genes in the brain. *Zool Res* **44**, 543–555 (2023).
233. Wu, C.M. & Lai, T.W.T. Microglia depletion by PLX3397 has no effect on cocaine-induced behavioral sensitization in male mice. *Brain Res* **1761**, 147391 (2021).
234. Grant, C.V.*, et al.* Microglia are implicated in the development of paclitaxel chemotherapy-associated cognitive impairment in female mice. *Brain Behav Immun* **108**, 221–232 (2023).
235. Gao, M.H.*, et al.* Identification of a microglial activation-dependent antidepressant effect of amphotericin B liposome. *Neuropsychopharmacol* **151**, 33–44 (2019).
236. Ye, T.*, et al.* Antidepressive properties of macrophage-colony stimulating factor in a mouse model of depression induced by chronic unpredictable stress. *Neuropsychopharmacol* **172**, 108132 (2020).
237. Zheng, M.*, et al.* Intranasal Monophosphoryl Lipid a Administration Ameliorates depression-like Behavior in Chronically Stressed Mice Through Stimulation of Microglia. *Neurochem Res* **48**, 3160–3176 (2023).
238. Gu, Y.*, et al.* Tolerance-inducing effect and properties of innate immune stimulation on chronic stress-induced behavioral abnormalities in mice. *Brain Behav Immun* **91**, 451–471 (2021).
239. Huang, C.*, et al.* Intranasal administration of lipopolysaccharide reverses chronic stress-induced depression-like behavior in mice by microglial stimulation. *Int Immunopharmacol* **120**, 110347 (2023).
240. Vichaya, E.G.*, et al.* Microglia depletion fails to abrogate inflammation-induced sickness in mice and rats. *J Neuroinflammation* **17**, 172 (2020).

241. Weber, M.D.*, et al.* The Influence of Microglial Elimination and Repopulation on Stress Sensitization Induced by Repeated Social Defeat. *Biol Psychiatry* **85**, 667–678 (2019).
242. Rimmerman, N.*, et al.* Microglia and their LAG3 checkpoint underlie the anti-depressant and neurogenesis-enhancing effects of electroconvulsive stimulation. *Mol Psychiatry* **27**, 1120–1135 (2022).
243. Chung, S.*, et al.* Plexin-A4 mediates amyloid-β-induced tau pathology in Alzheimer's disease animal model. *Prog Neurobiol* **203**, 102075 (2021).
244. Matrone, C. & Ferretti, G. Semaphorin 3A influences neuronal processes that are altered in patients with autism spectrum disorder: Potential diagnostic and therapeutic implications. *Neurosci Biobehav Rev* **153**, 105338 (2023).
245. Goteson, A.*, et al.* Cerebrospinal fluid proteomics targeted for central nervous system processes in bipolar disorder. *Mol Psychiatry* **26**, 7446–7453 (2021).
246. Yang, G.*, et al.* Neurite outgrowth deficits caused by rare PLXNB1 mutation in pediatric bipolar disorder. *Mol Psychiatry* **28**, 2525–2539 (2023).
247. Eastwood, S.L., Law, A.J., Everall, I.P. & Harrison, P.J. The axonal chemorepellant semaphorin 3A is increased in the cerebellum in schizophrenia and may contribute to its synaptic pathology. *Mol Psychiatry* **8**, 148–155 (2003).
248. Mah, S.*, et al.* Identification of the semaphorin receptor PLXNA2 as a candidate for susceptibility to schizophrenia. *Mol Psychiatry* **11**, 471–478 (2006).
249. Fujii, T.*, et al.* Possible association of the semaphorin 3D gene (SEMA3D) with schizophrenia. *J Psychiatr Res* **45**, 47–53 (2011).
250. Gilabert-Juan, J.*, et al.* Semaphorin and plexin gene expression is altered in the prefrontal cortex of schizophrenia patients with and without auditory hallucinations. *Psychiatry Res* **229**, 850–857 (2015).
251. Zhao, X.F.*, et al.* PlexinA2 forward signaling through Rap1 GTPases regulates dentate gyrus development and schizophrenia-like behaviors. *Cell Rep* **22**, 456–470 (2018).
252. Wray, N.R.*, et al.* Anxiety and comorbid measures associated with PLXNA2. *Arch gen psychiatry* **64**, 318–326 (2007).
253. Jahan, M.S.*, et al.* PlexinA1 deficiency in BALB/cAJ mice leads to excessive self-grooming and reduced prepulse inhibition. *IBRO Rep* **9**, 276–289 (2020).
254. Ferretti, G.*, et al.* An increase in Semaphorin 3A biases the axonal direction and induces an aberrant dendritic arborization in an in vitro model of human neural progenitor differentiation. *Cell Biosci* **12**, 182 (2022).
255. Costa, C.*, et al.* Expression of semaphorin 3A, semaphorin 7A and their receptors in multiple sclerosis lesions. *Mult Scler J* **21**, 1632–1643 (2015).
256. Jagadapillai, R.*, et al.* Potential cross talk between autism risk genes and neurovascular molecules: A pilot study on impact of blood brain barrier integrity. *Cells* **11**, 2211 (2022).
257. Paldy, E.*, et al.* Semaphorin 4C Plexin-B2 signaling in peripheral sensory neurons is pronociceptive in a model of inflammatory pain. *Nat. Commun.* **8**, 176 (2017).
258. Gong, L.L.*, et al.* Spatiotemporal dynamics of the molecular expression pattern and intercellular interactions in the glial scar response to spinal cord injury. *Neurosci Bull* **39**, 213–244 (2023).
259. Jeppesen, R.*, et al.* Efficacy and safety of anti-inflammatory agents in treatment of psychotic disorders - A comprehensive systematic review and meta-analysis. *Brain Behav Immun* **90**, 364–380 (2020).

260. Fond, G., Lançon, C., Korchia, T., Auquier, P. & Boyer, L. The role of inflammation in the treatment of schizophrenia. *Front Psychiatry* **11**, 160 (2020).
261. Mattei, D.*, et al.* Minocycline rescues decrease in neurogenesis, increase in microglia cytokines and deficits in sensorimotor gating in an animal model of schizophrenia. *Brain Behav Immun* **38**, 175–184 (2014).
262. Zhang, L.L. & Zhao, J.P. Profile of minocycline and its potential in the treatment of schizophrenia. *Neuropsychiatr Dis Treat* **10**, 1103–1111 (2014).
263. Cortez, I.L., da Silva, N.R., Guimaraes, F.S. & Gomes, F.V. Are CB2 receptors a new target for schizophrenia treatment? *Front Psychiatry* **11**, 587154 (2020).
264. Giridharan, V.V.*, et al.* Clozapine prevents poly (I:C) induced inflammation by modulating NLRP3 pathway in microglial cells. *Cells* **9**, 577 (2020).
265. Yu, X.L.*, et al.* Fingolimod ameliorates schizophrenia-like cognitive impairments induced by phencyclidine in male rats. *Br J Pharmacol* **180**, 161–173 (2023).
266. Limoa, E.*, et al.* Electroconvulsive shock attenuated microgliosis and astrogliosis in the hippocampus and ameliorated schizophrenia-like behavior of Gunn rat. *J Neuroinflammation* **13**, 230 (2016).
267. First, M., Spitzer, R.L., Gibbon, M.L. & Williams, J. Structured clinical interview for DSM-IV-TR Axis I Disorders, Research Version, Non-patient Edition. (2002).
268. Phillips, M. & Xh, L. *Translated and adapted Chinese version of User's Guide for Structured Clinical Interview for DSM-IV-TR Axis I Disorders (Research Version) by Michael B. First, Robert L. Spitzer, Miriam Gibbon, and Janet B.W. Williams* (2011).
269. Shi, C.*, et al.* The MATRICS Consensus Cognitive Battery (MCCB): Co-norming and standardization in China. *Schizophr Res* **169**, 109–115 (2015).
270. Zou, Y.*, et al.* Clinical reliability and validity of the Chinese version of measurement and treatment research to improve cognition in schizophrenia consensus cognitive battery. *Chin J Psychiatry* **42**, 29–33 (2009).
271. Bernstein, D.P.*, et al.* Development and validation of a brief screening version of the Childhood Trauma Questionnaire. *Child Abuse Negl* **27**, 169–190 (2003).
272. Jiang, W.J.*, et al.* Reliability and validity of the Chinese version of the childhood trauma questionnaire-short form for inpatients with schizophrenia. *PLoS One* **13**, e0208779 (2018).
273. Cohen, S., Kamarck, T. & Mermelstein, R. A global measure of perceived stress. *J Health Soc Behav* **24**, 385–396 (1983).
274. Lee, E.H. Review of the psychometric evidence of the perceived stress scale. *Asian Nurs Res (Korean Soc Nurs Sci)* **6**, 121–127 (2012).
275. Kay, S.R., Fiszbein, A. & Opler, L.A. The positive and negative syndrome scale (PANSS) for schizophrenia. *Schizophr Bull* **13**, 261–276 (1987).
276. Fischl, B.*, et al.* Whole brain segmentation: Automated labeling of neuroanatomical structures in the human brain. *Neuron* **33**, 341–355 (2002).
277. Zhou, G.*, et al.* NetworkAnalyst 3.0: A visual analytics platform for comprehensive gene expression profiling and meta-analysis. *Nucleic Acids Res* **47**, W234-W241 (2019).
278. Zawada, A.M.*, et al.* SuperSAGE evidence for CD14++CD16+ monocytes as a third monocyte subset. *Blood* **118**, e50–61 (2011).
279. Villani, A.C.*, et al.* Single-cell RNA-seq reveals new types of human blood dendritic cells, monocytes, and progenitors. *Science* **356**, eaah4573 (2017).

280. Zilionis, R.*, et al.* Single-cell transcriptomics of human and mouse lung cancers reveals conserved myeloid populations across individuals and species. *Immunity* **50**, 1317–1334 (2019).
281. Heger, L.*, et al.* Subsets of CD1c(+) DCs: Dendritic cell versus monocyte lineage. *Front Immunol* **11**, 559166 (2020).
282. Schindelin, J.*, et al.* Fiji: an open-source platform for biological-image analysis. *Nat Methods* **9**, 676–682 (2012).
283. Chithanathan, K., Xuan, F.L., Hickey, M.A. & Tian, L. Enhanced anxiety and olfactory microglial activation in early-stage familial Alzheimer's disease mouse model. *Biology (Basel)* **11**, 938 (2022).
284. Thion, M.S.*, et al.* Microbiome influences prenatal and adult microglia in a sex-specific manner. *Cell* **172**, 500–516 (2018).
285. Barrera García, A.*, et al.* Infiltrating CD16(+) are associated with a reduction in peripheral CD14(+)CD16(++) monocytes and severe forms of lupus nephritis. *Autoimmune Dis* **2016**, 9324315 (2016).
286. Nguyen, T.T.*, et al.* Abnormal levels of vascular endothelial biomarkers in schizophrenia. *Eur Arch Psychiatry Clin Neurosci* **268**, 849–860 (2018).
287. Salminen, A. Activation of immunosuppressive network in the aging process. *Ageing Res Rev* **57**, 100998 (2020).
288. Desai, T.M.*, et al.* IFITM3 restricts influenza A virus entry by blocking the formation of fusion pores following virus-endosome hemifusion. *PLoS Pathog* **10**, e1004048 (2014).
289. Ashley, C.L., Abendroth, A., McSharry, B.P. & Slobedman, B. Interferon-independent innate responses to cytomegalovirus. *Front Immunol* **10**, 2751 (2019).
290. Krause, D.*, et al.* The association of infectious agents and schizophrenia. *World J Biol Psychiatry* **11**, 739–743 (2010).
291. Kebir, O.*, et al.* Methylomic changes during conversion to psychosis. *Mol Psychiatry* **22**, 512–518 (2017).
292. DeKoter, R.P. & Singh, H. Regulation of B lymphocyte and macrophage development by graded expression of PU.1. *Science* **288**, 1439–1441 (2000).
293. Deng, Y.*, et al.* Zbtb14 regulates monocyte and macrophage development through inhibiting *pu.1* expression in zebrafish. *Elife* **11**, e80760 (2022).
294. Jacobsen, M.*, et al.* A point mutation in *PTPRC* is associated with the development of multiple sclerosis. *Nat Genet* **26**, 495–499 (2000).
295. Riise, R.E.*, et al.* TLR-stimulated neutrophils instruct NK cells to trigger dendritic cell maturation and promote adaptive T cell responses. *J Immunol* **195**, 1121–1128 (2015).
296. Alard, J.E., Dueymes, M., Youinou, P. & Jamin, C. Modulation of endothelial cell damages by anti-Hsp60 autoantibodies in systemic autoimmune diseases. *Autoimmun Rev* **6**, 438–443 (2007).
297. Pouget, J.G.*, et al.* Genome-wide association studies suggest limited immune gene enrichment in schizophrenia compared to 5 autoimmune diseases. *Schizophr Bull* **42**, 1176–1184 (2016).
298. Martin, F.M., Bydlon, G. & Friedman, J.S. SOD2-deficiency sideroblastic anemia and red blood cell oxidative stress. *Antioxid Redox Signal* **8**, 1217–1225 (2006).
299. Burnett, A.K.*, et al.* Arsenic trioxide and all-trans retinoic acid treatment for acute promyelocytic leukaemia in all risk groups (AML17): Results of a randomised, controlled, phase 3 trial. *Lancet Oncology* **16**, 1295–1305 (2015).

300. Neves, H., Ramos, C., da Silva, M.G., Parreira, A. & Parreira, L. The nuclear topography of ABL, BCR, PML, and RARα genes: Evidence for gene proximity in specific phases of the cell cycle and stages of hematopoietic differentiation. *Blood* **93**, 1197–1207 (1999).
301. Gu, F., Wang, J., Fu, L. & Ma, Y.J. Co-culture with microglia promotes neural stem cells differentiation into astrocytes. *Chin Med J* **124**, 3394–3398 (2011).
302. Garey, L. When cortical development goes wrong: Schizophrenia as a neuro-developmental disease of microcircuits. *J Anat* **217**, 324–333 (2010).
303. Wannan, C.M.J.*, et al.* Evidence for network-based cortical thickness reductions in schizophrenia. *Am J Psychiatry* **176**, 552–563 (2019).
304. Kamkwalala, A.R.*, et al.* Brief report: Higher peripheral monocyte activation markers are associated with smaller frontal and temporal cortical volumes in women with HIV. *J Acquir Immune Defic Syndr* **84**, 54–59 (2020).
305. Veenstra, M.*, et al.* CCR2 on peripheral blood CD14(+)CD16(+) monocytes correlates with neuronal damage, HIV-associated neurocognitive disorders, and peripheral HIV DNA: Reseeding of CNS reservoirs? *J Neuroimmune Pharmacol* **14**, 120–133 (2019).
306. Keren-Shaul, H.*, et al.* A unique microglia type associated with restricting development of Alzheimer's disease. *Cell* **169**, 1276–1290 (2017).
307. Olah, M.*, et al.* Single cell RNA sequencing of human microglia uncovers a subset associated with Alzheimer's disease. *Nat Commun* **11**, 6129 (2020).
308. Cabinio, M.*, et al.* Association between hippocampal shape, neuroinflammation, and cognitive decline in Alzheimer's disease. *J Alzheimers Dis* **66**, 1131–1144 (2018).
309. Rosenberg, H.F. Eosinophil-derived neurotoxin (EDN/RNase 2) and the mouse eosinophil-associated RNases (mEars): Expanding roles in promoting host defense. *Int J Mol Sci* **16**, 15442–15455 (2015).
310. Durack, D.T., Ackerman, S.J., Loegering, D.A. & Gleich, G.J. Purification of human eosinophil-derived neurotoxin. *Proc Natl Acad Sci U S A* **78**, 5165–5169 (1981).
311. Rannals, M.D.*, et al.* Psychiatric risk gene transcription factor 4 regulates intrinsic excitability of prefrontal neurons via repression of SCN10a and KCNQ1. *Neuron* **90**, 43–55 (2016).
312. Bruce, H.A.*, et al.* Potassium channel gene associations with joint processing speed and white matter impairments in schizophrenia. *Genes Brain Behav* **16**, 515–521 (2017).
313. Tynan, R.J.*, et al.* Chronic stress alters the density and morphology of microglia in a subset of stress-responsive brain regions. *Brain Behav Immun* **24**, 1058–1068 (2010).
314. Kreisel, T.*, et al.* Dynamic microglial alterations underlie stress-induced depressive-like behavior and suppressed neurogenesis. *Mol Psychiatry* **19**, 699–709 (2014).

SUMMARY IN ESTONIAN

Stressivastuse reguleerimine skisofreenia esimese episoodi korral monotsüütide ja mikrogliia poolt

Skisofreenia, keeruline neuropsühhiaatriline häire, mõjutab ligikaudu 1% maailma elanikkonnast ja esitab olulisi väljakutseid selle patobioloogiliste mehhanismide mõistmisel. Käesolev väitekiri keskendub monotsüütide ja mikroglia rolli lahtiharutamisele neuroinflammatoorsetes protsessides skisofreenias, eriti stressi kontekstis. Meie uurimused keskendusid esimese episoodi skisofreeniaga (FES) patsientidele ja loomade stressimudelitele, et selgitada välja nende immuunrakkude vahendatud molekulaarsed mehhanismid. FES patsientidel leiti muutusi monotsüütidega seotud transkriptoomiprofiilides, eriti mitteklassikaliste ja vahepealsete monotsüütide alamrühmades. Lisaks leiti, et suurema stressitundlikkusega FES patsientidel olid väiksemad hipokampuse struktuurid ja muutunud geeniexpressioon, mis oli seotud immuunarenguga. Mikroglia uuenemine leevendas osaliselt kroonilise ettearvamatu stressi (CUS) poolt hiirtel esile kutsutud psühhiaatrilisi käitumishäireid, mõjutades aju transkriptoomikat, mis on seotud arenguprotsessidega nagu aksionaalne ja sünaptiline moodustumine. Veelgi enam, madalama stressi tunnustega FES patsientidel olid väiksemad amügdalad ja kõrgem PLXNB2 ekspressioon, mis oli negatiivselt seotud tajutava stressi raskusega. Hiirtel põhjustas CUS Plxnb2 ekspressiooni languse ja Plxnb2 blokeerimine tekitas ärevust, amügdaloidset suurenemist ja mikroglia hargnemist. Need leiud viitavad sellele, et kuigi monotsüütide alamrühmad ja nende geenid võivad olla tervetel inimestel kahjulikud aju funktsioonile ja kognitsioonile, võivad nad arendada kohanemisvastaseid põletikuga seotud mehhanisme, et leevendada aju- ja kognitiivseid defitsiite FES-is. Mikroglia ümberprogrammeerimine võib pakkuda eeliseid skisofreenias, eriti stressitaju osas. Peale selle toob amügdaloidse mikroglia aktivatsioon, mida võib potentsiaalselt modulleerida Plxnb2, esile uue rakulise ja molekulaarse mehhanismi, mis on seotud skisofreeniaga seotud erinevate stressiomadustega. See uurimus pakub väärtuslikke teadmisi keerulise seose kohta stressi, monotsüütide/mikroglia funktsiooni ja neuronite tulemuste vahel skisofreenias, sillutades teed tulevastele uuringutele ja potentsiaalsetele terapeutilistele sekkumistele.

ACKNOWLEDGEMENTS

I am filled with immense gratitude towards numerous individuals who have contributed significantly to my academic journey. First and foremost, I wish to express my deep appreciation to Professor Li Tian, my main supervisor. Her invaluable expertise, insightful feedback, and extensive knowledge have been a guiding light in exploring intriguing research topics. She has consistently offered a broad and insightful perspective on our work. I am particularly moved by her exceptional patience and unwavering support in helping me navigate through all challenges.

I am also immensely thankful to my co-supervisors, Professors Claudio Rivera and Eero Vasar, and Dr. Kersti Lilleväli, for their support throughout my studies. Professor Claudio assisted me with technical matters at the project's inception, while Professor Eero Vasar consistently stood by my side, ready to provide support in the face of any obstacle. Kersti Lilleväli provided crucial guidance on developmental biology.

My gratitude extends to the medical staff and students at Beijing Huilongguan Hospital, whose dedication to participant recruitment and clinical investigations has been instrumental in shaping my thesis work. I am also deeply appreciative of all my co-authors, whose contributions have been integral in crafting our research narratives.

Special thanks go to Dr. Ling Yan, Keerthana Chithanathan, and Dr. Mohan Jayaram for their unwavering commitment, friendship, and enthusiasm. They were not only invaluable collaborators but also a constant source of warmth throughout this four-year journey.

I must also acknowledge Professor Anti Kalda, who generously shared his knowledge and provided crucial support in introducing me to cranial microinjection. Dr. Malle Kuum's assistance in optimizing live imaging protocols and Sami Piirainen's aid in microglial morphology analysis are greatly appreciated. I am grateful to my colleagues in the Department of Physiology for creating a welcoming and supportive atmosphere. Their camaraderie and support have enriched my research experience, making it an unforgettable journey.

I would like to express my gratitude to all volunteers who participated in clinical studies and laboratory mice that were sacrificed in preclinical studies. Their contribution was indispensable to the project.

I would also like to express my appreciation to the peer reviewers Liina Haring and Kalle Kilk, who invested their valuable time in providing suggestions for this thesis. Likewise, I am genuinely grateful to my opponent, Pentti Tienari, for assisting me in finalizing this academic chapter.

Last but certainly not least, my family and friends deserve sincere thanks for their unwavering support, understanding, and encouragement throughout my entire academic pursuit.

PUBLICATIONS

CURRICULUM VITAE

Name: Fangling Xuan
Date of Birth: May 29, 1992, China
Address: Ravila 14b, 50411, Tartu, Estonia
E-mail: xuanfl529@gmail.com

Education:

2019–present	**PhD.** in Neurosciences, University of Tartu, Faculty of Medicine, Estonia
2016–2019	**MSc.** in Physiology, Yanbian University, Institute of Medicine, China
2011–2015	**BSc.** in Bioengineering, Dalian Nationalities University, Institute of Life Science, China

Main fields of research: Neuroimmunology and neuroinflammation in schizophrenia

Research in neuroinflammation focuses on unraveling the complex interplay between immune activation in the central nervous system and its implications for brain function in schizophrenia. Investigations delve into the impact of neuroinflammation on stress perception, stress response, and cognitive impairments observed in individuals with schizophrenia. Through a comprehensive approach, novel insights are sought into the mechanisms underlying schizophrenia pathophysiology, with the ultimate goal of identifying potential therapeutic targets and biomarkers for improved diagnosis and treatment outcomes.

Professional Courses and Conferences

2023 Competence course in laboratory animal science, Tartu
2022 MIND & BRAIN – 61st International Neuropsychiatric Congress, online
2021 MIND & BRAIN – 60st International Neuropsychiatric Congress, online
2017 The 12th National Academic Conference of Young Physiologists of the Chinese Physiological Society, China

Research Publication

1. **Xuan FL**, Yan L, Li Y, Fan F, Deng H, Gou M, Chithanathan K, Heinla I, Yuan L, Seppa K, Zharkovsky A, Kalda A, Hong LE, Hu GF, Tan Y, Tian L. Glial receptor PLXNB2 regulates schizophrenia-related stress perception via the amygdala. Front Immunol. 2022 Oct 17;13:1005067. doi: 10.3389/fimmu.2022.1005067.
2. Yan L, **Xuan FL**, Chen S, Gou M, Chen W, Li Y, Wang Z, Wang L, Xie T, Fan F, Zharkovsky A, Tan Y, Tian L. Replenished microglia partially rescue schizophrenia-related stress response. Front Cell Neurosci. 2023 Sep 12;17:1254923. doi: 10.3389/fncel.2023.1254923.

3. Chen S, Fan F, **Xuan FL**, Yan L, Xiu M, Fan H, Cui Y, Zhang P, Yu T, Yang F, Tian B, Hong LE, Tan Y, Tian L. Monocytic Subsets Impact Cerebral Cortex and Cognition: Differences Between Healthy Subjects and Patients With First-Episode Schizophrenia. Front Immunol. 2022 Jul 11;13:900284. doi: 10.3389/fimmu.2022.900284.
4. Pan S, Zhou Y, Yan L, **Xuan F**, Tong J, Li Y, Huang J, Feng W, Chen S, Cui Y, Yang F, Tan S, Wang Z, Tian B, Hong LE, Tan YL, Tian L. TGF-β1 is associated with deficits in cognition and cerebral cortical thickness in first-episode schizophrenia. J Psychiatry Neurosci. 2022 Mar 17;47(2):E86-E98. doi: 10.1503/jpn.210121.
5. Chithanathan K, **Xuan FL**, Hickey MA, Tian L. Enhanced Anxiety and Olfactory Microglial Activation in Early-Stage Familial Alzheimer's Disease Mouse Model. Biology (Basel). 2022 Jun 20;11(6):938. doi: 10.3390/biology11060938.
6. **Xuan FL**, Chithanathan K, Lilleväli K, Yuan X, Tian L. Differences of Microglia in the Brain and the Spinal Cord. Front Cell Neurosci. 2019 Nov 14;13:504. doi: 10.3389/fncel.2019.00504.
7. **Xuan FL**, Wang HW, Cao LX, Bing YH, Chu CP, Jin R, Qiu DL. Propofol Inhibits Cerebellar Parallel Fiber-Purkinje Cell Synaptic Transmission via Activation of Presynaptic GABAB Receptors in vitro in Mice. Front Neurosci. 2018 Dec 6;12:922. doi: 10.3389/fnins.2018.00922.
8. Dong WW, **Xuan FL**, Zhong FL, Jiang J, Wu S, Li D, Quan LH. Comparative Analysis of the Rats' Gut Microbiota Composition in Animals with Different Ginsenosides Metabolizing Activity. J Agric Food Chem. 2017 Jan 18;65(2):327–337. doi: 10.1021/acs.jafc.6b04848.

ELULOOKIRJELDUS

Nimi: Fangling Xuan
Sünniaeg: 29. mai 1992, Hiina
Aadress: Ravila 14b, 50411, Tartu, Eesti
E-post: xuanfl529@gmail.com

Haridus:

2019–praegune	Doktorikraad neuroteadustes, Tartu Ülikool, Arstiteaduskond, Eesti
2016–2019	MSc füsioloogias, Yanbiani ülikool, meditsiiniinstituut, Hiina
2011–2015	Bioinseneri bakalaureuseõpe, Daliani rahvusülikool, bioteaduste instituut, Hiina

Peamised uurimisvaldkonnad: Neuroimmunoloogia ja neuroinflammatsioon skisofreenia korral

Neuropõletiku alased uuringud keskenduvad kesknärvisüsteemi immuunaktivatsiooni ja selle mõju ajufunktsioonile skisofreenia korral keeruka koosmõju lahtiharutamisele. Uuringutes uuritakse neuropõletiku mõju stressitajule, stressireaktsioonile ja skisofreeniahaigetel täheldatud kognitiivsetele häiretele. Tervikliku lähenemisviisi kaudu otsitakse uudseid teadmisi skisofreenia patofüsioloogia aluseks olevate mehhanismide kohta, mille lõppeesmärk on tuvastada võimalikud terapeutilised sihtmärgid ja biomarkerid, et parandada diagnoosimist ja ravi tulemusi.

Professionaalsed kursused ja konverentsid

2023 Laboriloomateaduse pädevuskursus, Tartu
2022 MIND & BRAIN – 61. rahvusvaheline neuropsühhiaatriakongress, võrgus
2021 MIND & BRAIN – 60. rahvusvaheline neuropsühhiaatriakongress, võrgus
2017 Hiina Füsioloogiaühingu noorte füsioloogide 12. riiklik akadeemiline konverents, Hiina

Publikatsioonid

1. **Xuan FL**, Yan L, Li Y, Fan F, Deng H, Gou M, Chithanathan K, Heinla I, Yuan L, Seppa K, Zharkovsky A, Kalda A, Hong LE, Hu GF, Tan Y, Tian L. Glial receptor PLXNB2 regulates schizophrenia-related stress perception via the amygdala. Front Immunol. 2022 Oct 17;13:1005067. doi: 10.3389/fimmu.2022.1005067.
2. Yan L, **Xuan FL**, Chen S, Gou M, Chen W, Li Y, Wang Z, Wang L, Xie T, Fan F, Zharkovsky A, Tan Y, Tian L. Replenished microglia partially rescue schizophrenia-related stress response. Front Cell Neurosci. 2023 Sep 12;17:1254923. doi: 10.3389/fncel.2023.1254923.
3. Chen S, Fan F, **Xuan FL**, Yan L, Xiu M, Fan H, Cui Y, Zhang P, Yu T, Yang F, Tian B, Hong LE, Tan Y, Tian L. Monocytic Subsets Impact

Cerebral Cortex and Cognition: Differences Between Healthy Subjects and Patients With First-Episode Schizophrenia. Front Immunol. 2022 Jul 11;13: 900284. doi: 10.3389/fimmu.2022.900284.

4. Pan S, Zhou Y, Yan L, **Xuan F**, Tong J, Li Y, Huang J, Feng W, Chen S, Cui Y, Yang F, Tan S, Wang Z, Tian B, Hong LE, Tan YL, Tian L. TGF-β1 is associated with deficits in cognition and cerebral cortical thickness in first-episode schizophrenia. J Psychiatry Neurosci. 2022 Mar 17;47(2):E86-E98. doi: 10.1503/jpn.210121.
5. Chithanathan K, **Xuan FL**, Hickey MA, Tian L. Enhanced Anxiety and Olfactory Microglial Activation in Early-Stage Familial Alzheimer's Disease Mouse Model. Biology (Basel). 2022 Jun 20;11(6):938. doi: 10.3390/biology11060938.
6. **Xuan FL**, Chithanathan K, Lilleväli K, Yuan X, Tian L. Differences of Microglia in the Brain and the Spinal Cord. Front Cell Neurosci. 2019 Nov 14;13:504. doi: 10.3389/fncel.2019.00504.
7. **Xuan FL**, Wang HW, Cao LX, Bing YH, Chu CP, Jin R, Qiu DL. Propofol Inhibits Cerebellar Parallel Fiber-Purkinje Cell Synaptic Transmission via Activation of Presynaptic GABAB Receptors in vitro in Mice. Front Neurosci. 2018 Dec 6;12:922. doi: 10.3389/fnins.2018.00922.
8. Dong WW, **Xuan FL**, Zhong FL, Jiang J, Wu S, Li D, Quan LH. Comparative Analysis of the Rats' Gut Microbiota Composition in Animals with Different Ginsenosides Metabolizing Activity. J Agric Food Chem. 2017 Jan 18;65(2):327–337. doi: 10.1021/acs.jafc.6b04848.

DISSERTATIONES NEUROSCIENTIAE UNIVERSITATIS TARTUENSIS

1. **Sirli Raud.** Cholecystokinin$_2$ receptor deficient mice: changes in function of GABA-ergic system. Tartu, 2005.
2. **Kati Koido.** Single-nucleotide polymorphism profiling of 22 candidate genes in mood and anxiety disorders. Tartu, 2005.
3. **Dzhamilja Safiulina.** The studies of mitochondria in cultured cerebellar granule neurons: characterization of mitochondrial function, volume homeostasis and interaction with neurosteroids. Tartu, 2006.
4. **Tarmo Areda.** Behavioural and neurogenetic study of mechanisms related to cat odour induced anxiety in rodents. Tartu, 2006.
5. **Aleksei Nelovkov.** Behavioural and neurogenetic study of molecular mechanisms involved in regulation of exploratory behaviour in rodents. Tartu, 2006.
6. **Annika Vaarmann**. The studies on cystatin B deficient mice: neurochemical and behavioural alterations in animal model of progressive myoclonus epilepsy of Unverricht-Lundborg type. Tartu, 2007.
7. **Urho Abramov.** Sex and environmental factors determine the behavioural phenotype of mice lacking CCK_2 receptors: implications for the behavioural studies in transgenic lines. Tartu, 2008.
8. **Hendrik Luuk.** Distribution and behavioral effects of WFS1 protein in the central nervous system. Tartu, 2009.
9. **Anne Must.** Studies on molecular genetics of male completed suicide in Estonian population. Tartu, 2009.
10. **Kaido Kurrikoff**. Involvement of cholecystokinin in chronic pain mechanisms and endogenous antinociception. Tartu, 2009.
11. **Anu Aonurm-Helm.** Depression-like phenotype and altered intracellular signalling in neural cell adhesion molecule (NCAM)-deficient mice. Tartu, 2010.
12. **Silva Sütt.** Role of endocannabinoid system and *Wfs1* in regulation of emotional behaviour: behavioural, pharmacological and genetic studies. Tartu, 2010.
13. **Mari-Anne Philips.** Characterization of *Myg1* gene and protein: expression patterns, subcellular localization, gene deficient mouse and functional polymorphisms in human. Tartu, 2010.
14. **Ranno Rätsep.** Genetics of psoriasis and vitiligo, focus on IL10 family cytokines. Tartu, 2010.
15. **Kairit Joost.** Selective screening of metabolic diseases in Estonia: the application of new diagnostic methods. Tartu, 2012, 143 p.
16. **Monika Jürgenson.** A complex phenotype in mice with partial or complete deficiency of the NCAM protein. Tartu, 2012, 117 p.
17. **Ene Reimann.** Description of the cytokines and cutaneous neuroendocrine system in the development of vitiligo. Tartu, 2012, 117 p.

18. **Jürgen Innos.** Behavioural, pharmacological and neurochemical characterisation of limbic system-associated membrane protein (LSAMP) deficient mice. Tartu, 2013, 113 p.
19. **Kaili Anier.** The role of DNA methylation in the development of cocaine-induced behavioural sensitisation. Tartu, 2013, 147 p.
20. **Maarika Liik.** Cognitive functioning, perceived cognition, subjective complaints and symptoms of depression in patients with epilepsy: neuropsychological assessment and spet brain imaging study. Tartu, 2014, 124 p.
21. **Sten Ilmjärv.** Estimating differential expression from multiple indicators. Tartu, 2015, 125 p.
22. **Paula Reemann.** The effects of microenvironment on skin cells. Tartu, 2015, 146 p.
23. **Tanel Visnapuu.** Pharmacological and behavioral characterization of the monoaminergic and GABA-ergic systems of Wfs1-deficient mice. Tartu, 2015, 107 p.
24. **Indrek Heinla.** Behavioural and genetic comparison of B6 and 129Sv mouse lines focusing on the anxiety profile and the expression of *Lsamp* gene. Tartu, 2016, 115 p.
25. **Liina Haring.** Cognitive functioning after first psychotic episode. Tartu, 2017, 146 p.
26. **Triin Tekko.** Neurodevelopmental Approach in the Study of the Function of *Wfs1* and *Lsamp*, Potential Targets in the Regulation of Emotional Behaviour. Tartu, 2018, 194 p.
27. **Alina Altpere.** Targeting of mechanisms of elevated anxiety in female Wfs1-deficient mice. Tartu, 2018, 98 p.
28. **Maarja Toots.** Pharmacological challenge in rodent models of Wolfram syndrome with emphasis on diabetic phenotype. Tartu, 2018, 114 p.
29. **Katyayani Singh.** Neuropsychiatric endophenotypes – focusing on IgLON adhesion molecules in the mouse brain. Tartu, 2019, 148 p.
30. **Kattri-Liis Eskla.** Therapeutic strategies for ischemia reperfusion injury. Tartu, 2019, 138 p.
31. **Hardo Lilleväli**. Hyperphenylalaninaemias and neurophysiological disorders associated with the condition. Tartu, 2020, 134 p.
32. **Roman Balõtšev**. Interaction between the immune and metabolic systems in different stages of schizophrenia spectrum disorders. Tartu, 2020, 164 p.
33. **Mari Urb**. DNA methylation in the predisposition, expression and abstinence of cocaine addiction. Tartu, 2020, 147 p.
34. **Liisa Leppik.** Alterations in metabolomic profile of lipids, amino acids and biogenic amines in the early course of schizophrenia spectrum disorders. Tartu, 2021, 173 p.
35. **Kadri Seppa.** The neuroprotective effect of GLP-1 receptor agonist liraglutide in a rat model of Wolfram syndrome. Tartu, 2021, 154 p.
36. **Akbar Zeb.** The novel mechanisms of Parkin-dependent mitophagy. Tartu, 2022, 146 p.

37. **Aleksandr Bregin.** Alterations of emotional behaviour induced by the genetic invalidation of the limbic system associated membrane protein (Lsamp) – potential implications for neuropsychiatric disorders. Tartu, 2022, 176 p.
38. **Jane Varul.** Different stress coping strategies of 129Sv and C57/Bl6 mouse strains – evidence from behavioural, pharmacological, metabolomics and gene expression studies. Tartu, 2022, 177 p.
39. **Maria Kaare.** The involvement of NEGR1 and LSAMP in the psychiatric disorders are mediated through monoaminergic neurotransmission and changes in the systemic metabolism. Tartu, 2023, 164 p.
40. **Maria Piirsalu.** Effects of inflammation and diet on the metabolic profile and selected genetic parameters of Bl6 and 129Sv mouse lines. Tartu, 2023, 183 p.
41. **Taavi Vanaveski.** Modelling the quantitative nature of neuropsychiatric disorders in animal models: metabolic, behavioural, and genetic profiles. Tartu, 2023, 165 p.
42. **Keiu Heinla.** Effects of GLP-1 receptor agonists on pituitary and adrenal hormones. Tartu, 2023, 119 p.
43. **Ling Yan.** Stress-associated immune mechanisms of schizophrenia: the importance of region-specific microglia-neurovascular interaction. Tartu, 2023, 206 p.